This document was prepared for the ETI by third parties under contract to the ETI. The ETI is making these documents and data available to the public to inform the debate on low carbon energy innovation and deployment.

Programme Area: Marine

Project: PerAWAT

Title: Report on Non-Linear Analysis of Single and Arrays of Free Floating Devices

Abstract:

This report presents and discusses the results of fully nonlinear potential flow simulations of the regular wave interactions involving a single truncated cylinder and an array of four truncated cylinders. The key objectives of this study are to compare the results of fully nonlinear simulations to weakly nonlinear results, in particular in the case of the single cylinder, and to investigate the cylinder excitation forces and cylinder responses in an array of four cylinders subject to regular incident waves. The report outlines how these objectives have been met and describes any issues arising from their completion. The similarities and differences between the fully nonlinear time-domain solutions and the linear frequency domain solutions are considered in detail. A number of validation studies were also conducted in parallel with and as preparation for the completion of the main aims of the deliverable. These case studies contain independent verifications of the fully nonlinear potential flow solver and are included in the report to illustrate the full capabilities of the fully nonlinear approach.

Context:

The Performance Assessment of Wave and Tidal Array Systems (PerAWaT) project, launched in October 2009 with £8m of ETI investment. The project delivered validated, commercial software tools capable of significantly reducing the levels of uncertainty associated with predicting the energy yield of major wave and tidal stream energy arrays. It also produced information that will help reduce commercial risk of future large scale wave and tidal array developments.

Energy Technologies Institute

PerAWaT MA1003

WG1 WP1 D9: Report on non-linear analysis of single and arrays of free floating devices

Author: C. Fitzgerald

Checked by: P. H. Taylor and R. Eatock Taylor

Date: 30th November 2011

Version 1.0

CONTEXT

This report (WG1 WP1 D9) presents and discusses the results of fully nonlinear potential flow simulations of the regular wave interactions involving a single truncated cylinder and an array of four truncated cylinders. The context and frame of reference for the discussion and analysis of the fully nonlinear results is provided by the linear and weakly nonlinear results presented in WG1 WP1 D8. The fully nonlinear hydrodynamic model and the numerical method to solve nonlinear wave-structure interactions are described in the previous deliverable (WG1 WP1 D7) from Oxford University.

The key objectives of this study are to compare the results of the fully nonlinear simulations to the weakly nonlinear results, in particular in the case of the single cylinder, and to investigate the cylinder excitation forces and cylinder responses in an array of four cylinders subject to regular incident waves. This report outlines how these objectives have been met and describes any issues arising from the completion of these objectives. The similarities and differences between the fully nonlinear time-domain solutions and the linear frequency domain solutions are considered in detail. A number of validation studies were also conducted in parallel with and as preparation for the completion of the main aims of the deliverable. These case studies contain independent verifications of the fully nonlinear potential flow solver and are included in the report to illustrate the full capabilities of the fully nonlinear approach.

TABLE OF CONTENTS

LIST OF FIGURES

1 INTRODUCTION

1.1 Outline of the report

The fully nonlinear potential flow solver, referred to here as OXPOT, is a powerful tool for the analysis of fully nonlinear hydrodynamic interactions. This report details how OXPOT is utilised to obtain fully nonlinear simulations of single cylinder and multiple cylinder interactions with regular incident waves. Comparisons with the linear and weakly nonlinear results from WG1 WP1 D8 form a significant proportion of the discussion and analysis of these results, particularly for the single cylinder interaction problem.

The report is divided into six main sections and is structured so that the initial sections analyse relatively simple interaction problems (e.g. the wavemaker problem, single cylinder interaction problems) and the later sections relate to the more complex hydrodynamic interactions involving arrays of up to four cylinders. In section 2, a summary of the description of the higher order boundary element method provided in WG1 WP1 D7 is presented. In that deliverable some simulation results were presented in order to illustrate the capabilities of OXPOT and these are also highlighted in section 2 thus providing a useful background to the validation studies which follow in the subsequent sections. The method for generating the regular incident waves in the OXPOT simulations is described in section 3 and a comparison with linear analytical results is also made for a simple test case and for the four incident waves identified as key comparison cases in WG1 WP1 D8.

The simulations of the interactions between regular incident waves and a single truncated cylinder are presented in section 4. A test cylinder with a standard geometry taken from the frequency-domain analysis of (Matsui & Tamaki, 1981) is first considered for the purposes of independent verification and to understand any issues that might arise when comparing OXPOT results to linear frequency-domain data. Radiation and diffraction problems and the problem of a freely heaving cylinder in regular waves are all simulated and the comparisons with the linear theory are presented. An analysis of the linearised OXPOT results of the simulations involving the particular truncated cylinder geometry identified in D8 is presented in this section and a full set of comparisons to the results of D8 are provided. In section 5, the uncertainties arising from the comparison of the second order component of the OXPOT results to the second-order results from WG1 WP1 D8 are outlined. Independent verifications of the OXPOT second-order force computations obtained through the simulation of diffraction interactions are described in section 5 including a successful comparison with an experimental case study.

In section 6 and 7 fully nonlinear interaction simulations for multiple cylinders are described. The emphasis in section 6 is on independently verifying the multiple cylinder interaction results from OXPOT with existing frequency-domain data from the literature on array interactions. Diffraction and radiation problems are both considered for the purposes of verification. In section 7, the fully nonlinear interactions between arrays of four truncated cylinders and regular incident waves are described both for the case of fixed cylinders and for the case of cylinders free to respond to the incident waves in heave. Comparisons with the four body results from WG1 WP1 D8 are also made.

Summaries of the most important sections are provided in the body of the report; however, a final summary and discussion of future work is also presented in in section 8 in addition to a discussion of lessons learned and a description of how progress is to continuewith the fully nonlinear analysis.

1.2 WG1 WP1 D9 acceptance criteria

The acceptance criteria as listed in the Second Amendent to the Technology Contract are as follows:

> *"Results will be calculated and presented for fully nonlinear responses of an array of four uncontrolled axisymmetric devices in regular waves. In so far as it is possible prior to validation, findings will be discussed and applications and limitations of this approach will be described, including any lessons learned on methodology. A comparison will be made with the 2nd order analysis on a single body as reported inWG1 WP1 D8."*

In the variation request form it was also stated that:

> *"GH's report will highlight the key comparisons that still need to be made between fully nonlinear and linear models by Oxford in WG1 WP1 D9."*

The sections addressing these acceptance criteria are sections 4 and 5 for the comparisons of linear and second order forces and responses for a single cylinder. Section 7 contains the fully nonlinear analysis of the response of an array of four cylinders in regular waves.

1.3 Details of computational work

The OXPOT code was compiled and run on both a Windows platform using the Salford FT95 Fortran compiler for Win32 and on a Linux platform using the Intel Fortran compiler for a 64-bit Linux OS. Most of the computations were run on the Linux platform both on a desktop computer and on single nodes of the Oxford Supercomputing Centre cluster. The desktop computer has an Intel Xeon 3.20GHz processor with 6.00GB of available RAM while the nodes in the cluster have 8 processors (2 quad-core Intel Xeon 2.66GHz processors) with 16GB DDR2 memory. No significant difference in run-times were observed between executions on the Linux desktop platform and on a single supercomputer node. If parallelisation of the OXPOT code is achieved then significant improvements in computational run-times on the supercomputer are expected.

2 BRIEF INTRODUCTION TO THE FULLY NONLINEAR POTENTIAL FLOW SOLVER

The fully nonlinear potential flow solver developed in Oxford in recent years was previously described in WG1 WP1 D7. In that deliverable the mathematical formulation of the fully nonlinear hydrodynamic model is presented to provide a context for the numerical method for time-domain simulations of fully nonlinear wave interactions. The main theoretical aspects of the higher order boundary element method, adopted as part of the Mixed Eulerian-Lagrangian (MEL) time-stepping technique, are described in detail along with the numerical implementation of some performance related aspects of the method. The description of OXPOT in WG1 WP1 D7 provides a comprehensive summary of the OXPOT code; however, for a full account of the development of this fully nonlinear potential flow tool upon which OXPOT is based it is necessary to refer to the work of (Bai & Eatock Taylor, 2006), (Bai & Eatock Taylor, 2007) and (Bai & Eatock Taylor, 2009).

In the MEL technique, the fully nonlinear boundary conditions can be satisfied on the instantaneous free water and body surfaces using a higher order boundary element method. The unknowns (potential or normal velocity) are distributed on the discretised computational boundary and a system of linear equations must be solved at every time step given that the boundary changes in time due to the fully nonlinear boundary conditions. The boundary integral equation method and the details of the higher order parameterisation of the discrete boundary elements are described in WG WP1 D7 and the system of linear equations solved at every time-step are also presented. Furthermore, a brief summary of the auxiliary function method, as used by (Wu & Eatock Taylor, 1996), to compute the hydrodynamic forces is given also. The implementation of some important aspects of the numerical simulation method is presented, including: the mesh generation algorithm, the artificial damping layer, the time stepping integration approach and also the domain decomposition method

Illustrations of the capabilities of the code are also presented in WG1 WP1 D7 and include the propagation of impulse waves, regular waves and focussed waves and also the interaction of focussed waves with a bottom mounted cylinder. The convergence of the numerical solutions is analysed and in addition the effect of nonlinearity on the free-surface elevations and wave forces are discussed. Comparisons to existing experimental data are also made to illustrate the effectiveness of the code in describing complex interactions. To augment these investigations, some standard frequency domain test problems solved using OXPOT are compared to existing analytical and numerical *linear* solutions in the following section in order to further verify the code. The waves generated in these simulations are chosen to be very small relative to the incident wavelength so that nonlinear components are negligible thus enabling straightforward comparisons between OXPOT results and linear frequency-domain results. The first problem to be considered is the piston wave-maker problem; thereafter, simple radiation, diffraction and interaction problems involving a truncated cylinder are also considered for validation purposes. These investigations are particularly relevant to the investigations into the fully nonlinear response of the truncated cylinder for which a weakly nonlinear frequency domain analysis was conducted for WG1 WP1 D8.

3 FULLY NONLINEAR SOLUTION OF WAVE PROPAGATION PROBLEMS

3.1 Verification of linear component of OXPOT computations

The wave-maker problem is a classical water-wave problem with a simple analytical frequency-domain solution. Given that we seek to generate regular waves, the frequency-domain solution provides a suitable point of comparison for the time-domain solution after the initial transient wave front has passed. The problem is posed as follows: consider a semi-infinite tank of fluid occupying $x > -L,\ z \in (-h, 0)$ where h is the constant finite depth of the fluid. On $x = -L$ there is a piston wave-maker that oscillates with a specified velocity at an angular frequency ω and hence generates waves that propagate towards large positive x. If the velocity potential is denoted $\Phi(x, z, t)$ then the wave-maker boundary condition can be expressed as

$$\frac{\partial \Phi}{\partial x} = a_p\, \omega \sin(\omega t)\ \ on\ \ x = -L\,, \tag{1}$$

where a_p is the displacement amplitude of the piston and this condition holds for all $z \in (-h, 0)$. If the frequency-domain assumption that all motions have settled to steady state is adopted then $\Phi = \mathrm{Re}(\phi e^{-i\omega t})$ and by removing the time-dependence the frequency-domain form of the problem can be obtained. The frequency-domain equations are

$$\Delta\phi = 0 \tag{2}$$

$$\frac{\partial \phi}{\partial x} = i a_p \omega\ on\ x = -L \tag{3}$$

$$\frac{\partial \phi}{\partial z} = 0\ on\ z = -h \tag{4}$$

and these must be augmented with a radiation condition

$$\frac{\partial \phi}{\partial x} - ik\phi \to 0\ \ as\ \ x \to \infty \tag{5}$$

which specifies that only right travelling waves are present in the domain. The solution to this problem is obtained by expanding the potential in terms of vertical eigenfunctions. Of most interest is the propagating mode (corresponding to the $n = 0$ eigenfunction) because beyond more than a couple of wavelengths from the wave-maker the evanescent modes ($n \geq 1$) will have decayed. This mode has the following form

$$\phi_0(x, z) = \frac{4 a_p \omega}{k} \frac{\sinh(kh)}{2kh + \sinh(2kh)} \cosh\big(k(z + h)\big)\, e^{ik(x+L)} \tag{6}$$

and in terms of the free-surface elevation it is

$$\eta_0(x) = 2 a_p \tanh(kh) \frac{\sinh(2kh)}{2kh + \sinh(2kh)}\, i e^{ik(x+L)}\,. \tag{7}$$

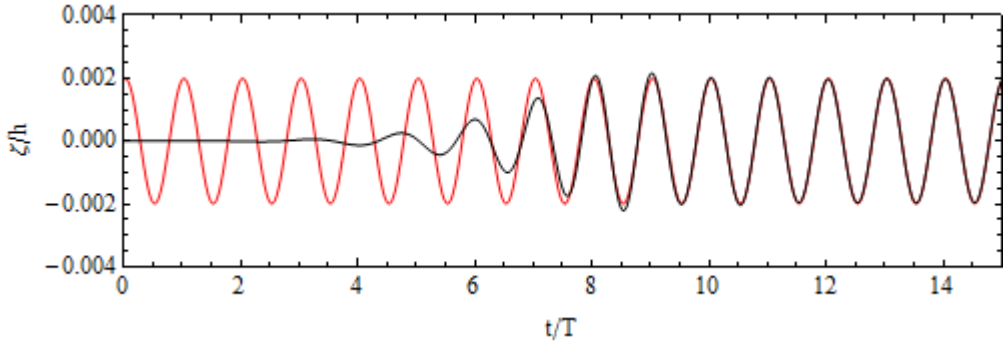

Figure 1: Free-surface elevation at $x = 0$ as computed by OXPOT (black) and as predicted by the linear theory (red).

Therefore, given the piston displacement amplitude, the frequency of oscillation, the piston location and the water depth it is straightforward to compute the free-surface elevation at any position x where the evanescent modes have decayed. Similarly, with these inputs it is straightforward using OXPOT to fully simulate the development of a regular propagating wave train, generated using a full-draft piston wave-maker, with the fluid initially at rest. By choosing a sufficiently small piston displacement amplitude the generated wave train had a negligible nonlinear component. However, it should be noted that in the OXPOT simulation the position of the wavemaker changes in time and so the boundary condition is not the same as the linear condition (1) which always holds at $x = -L$.

In a non-dimensional simulation with the acceleration due to gravity g, the water density ρ and the tank depth h chosen to be unity (effectively non-dimensionalising the problem) the waves were generated by a piston displacement amplitude of $0.001h$ and with an oscillation amplitude of $\omega = 2.0$. The wave tank was specified to have a total tank length of $L_T = 7.5h$ and a width W=1.0 with the undisturbed wavemaker position at $x = -4.375h$. The free-surface elevation was then measured at the centre line of the tank at $x = 0.0$. In figure 1, the free-surface elevation as computed in OXPOT was compared to the linear prediction defined by (7). The average free-surface elevation amplitude over 7 periods was calculated to be 1.985×10^{-3} compared to a predicted linear value of 1.989×10^{-3}. The corresponding steepness of this wave is $H/\lambda = 0.0025$ which is very weakly nonlinear.

Clearly, the fully non-linear solver predicts the linear component successfully for extremely small wave-maker oscillation amplitudes. However, it is important for the generation of more non-linear waves that the linear component as computed by OXPOT is still correct so that comparisons to linear theory are valid. Therefore, it was decided that the waves listed in Table 1 (taken from WG1 WP1 D8) should be generated using an oscillatory piston motion and the resultant free-surface wave elevation compared to that predicted by the linear theory at various points in the tank.

The steepness's of these waves are considerably larger than the test case presented above and so to extract the linear amplitude it was necessary to employ a Stokes' expansion approach to separate odd and even harmonic contributions to the total wave elevation. This approach is described by (Jonathan & Taylor, 1997) and (Zang, et al., 2010) among others and will be used throughout this report in the analysis of the OXPOT results for both free-surface elevations and hydrodynamic forces in order to isolate the linear and second order contributions. (In OXPOT, the total hydrodynamic

quantities are computed not the separate first, second and higher order components.) If the fully nonlinear hydrodynamic quantity f can be expressed as a Stoke's expansion with dominant first and second order contributions then it will obey

$$f(t) = f^{(0)} + \varepsilon f^{(1)}(t) + \varepsilon^2 f^{(2)}(t) + O(\varepsilon^3), \quad (8)$$

where $f^{(1)}$ is the first order component, $f^{(2)}$ the second and ε is a small parameter dependent on the wave amplitude. By solving the same interaction problem (in this case a wave propagation problem) but with incident waves that are π out of phase with the original incident waves then it is possible to extract the first and second order components. For a $\sin(\omega t)$ wavemaker velocity profile, the wave quantities are given the suffix C to denote waves with a crest at some reference point x_0 on the free-surface and the inverse/negated waves ($-\sin(\omega t)$ profile) are given the suffix T denoting waves with a trough at x_0. The free-surface elevations at x_0 is given by

$$\eta_C(x_0, t) = \eta^{(0)}(x_0) + A\eta^{(1)}(x_0, t) + A^2\eta^{(2)}(x_0, t) + O(A^3), \quad (9)$$

$$\eta_T(x_0, t) = \eta^{(0)}(x_0) - A\eta^{(1)}(x_0, t) + A^2\eta^{(2)}(x_0, t) - O(A^3), \quad (10)$$

for the two incident waves and, therefore, the first order component is obtained from the difference of the signals $A\eta^{(1)}(t) = (\eta_C(t) - \eta_T(t))/2$ and the second order sum frequency component from the sum $A^2\eta^{(2)}(t) = (\eta_C(t) + \eta_T(t))/2 - \eta^{(0)}$ where $\eta^{(0)}$ is the second order difference frequency mean set-up or set-down. It is important to note that the higher order contributions are neglected – the difference term actually includes third and higher order odd components and similarly for the sum term with respect to fourth and higher order even components.

Period (T) [s]	Height (H) [m]	Wavelength (λ) [m]	Steepness (H/λ)
5.0	1.0	39.0	0.0256273
7.0	2.0	76.5	0.0261505
9.0	4.0	126.4	0.0316609
10.25	6.0	163.3	0.0367442

Table 1: Wave periods and heights of the regular waves considered for the comparison between weakly non-linear and fully non-linear hydrodynamic quantities.

3.2 Propagation simulations and comparisons

In order to generate a suitable mesh for the propagation problem, it was necessary to refer to the investigation by (Bai & Eatock Taylor, 2007) into the convergence characteristics of the solutions for different meshes in the case of regular wave and focussed wave diffraction. By choosing a mesh with a resolution similar to the finest mesh chosen by (Bai & Eatock Taylor, 2007) it was assumed the results had converged and would have satisfactory accuracy. (Bai & Eatock Taylor, 2009) utilised this convergence study when specifying the mesh for floating body simulations and the domain and element sizes specified here are adopted directly from this investigation. In the later simulations, where bodies are present in the computational domain, the convergence of the solution will be tested by solving the interaction problem using even finer meshes but it was considered sufficient for the propagation problem to appropriate the findings of (Bai & Eatock Taylor, 2009).

The standard mesh configuration consisted of a regular mesh of quadrilateral panels on the wall boundaries of the subdomains (side walls and interfaces between subdomains) combined with an unstructured mesh of triangular elements on the free surface. The latter allows localized refinement around any bodies introduced into the domain. Eight and six nodes are placed on each quadrilateral and triangular element respectively. A typical mesh for a domain divided into six subdomains is shown in Figure 2. In a non-dimensional problem, for a wave of frequency of approximately $\omega = 2.0$ ($\lambda \simeq 1.57$), the domain was chosen to be of length $L_T = 7.5h \simeq 5\lambda$ and was divided into 6 subdomains. The wave tank was given a width $W = 0.625$ corresponding to half the length of a sub-domain. In accordance with (Bai & Eatock Taylor, 2009), the elements dimensions Δx and Δy were set to be approximately 0.125 **(**$\simeq \lambda/12$) and the number of vertical elements was set to be 6, a standard configuration from both (Bai & Eatock Taylor, 2009) and (Bai & Eatock Taylor, 2007).

The exact specifications for the simulation featuring waves of period $T = 9s$ ($\omega = 1.993$ in non-dimensional terms) and height $H = 4m$ were as follows; the length-wise subdomain walls were divided into $n_z = 6$ vertical intervals and $n_x = 12$ horizontal intervals; the end-walls and interfaces were divided into 6 vertical intervals and $n_y = 6$ horizontal intervals and the free-surface consisted of 134 triangular free-surface elements. Therefore, there were a total of 144 quadrilateral elements and 134 triangular elements per subdomain – in total the boundary mesh comprised 1668 elements and 4944 nodes. For each wave specified in Table 1, the meshing details remain approximately the same with the length and width of the domain varying proportionally with the wavelength. Of course when a structure is present the discretisation must be modified to match the size of the device relative to the waves. Furthermore, the width of the domain and the effects of reflections of diffracted waves from the side-wall must be taken into account also. Nevertheless, in this instance the meshing is straightforward and is almost identical in each case – only the domain size changes.

As stated previously, the motivation for the wave propagation investigation was to ensure the waves generated by the piston wavemaker boundary condition were of suitable amplitude for the diffraction and coupled response simulations that were to follow. Table 3 presents the linear prediction for the non-dimensional free-surface elevation amplitude ($H/2h$) for each wave and compares it to the average linear value obtained from the OXPOT simulations where the elevation is measured at 5 different locations in the tank. Each of these locations is more than a wavelength away from the wave-maker and so the effect of the evanescent modes should be negligible. For each regular wave the predicted free-surface elevation evolution at particular locations on the free-surface was compared to the linear component of the fully nonlinear numerical solution in a similar manner to Figure 1. In general, the agreement was satisfactory although on average in all cases the linear component of the generated waves is less than the linear frequency-domain amplitude. Furthermore, there was some variation in the mean amplitude from location to location. At some points on the free-surface the wave amplitude was found to be less than predicted while at other points the amplitude was greater. Therefore, an error is associated with the average of the amplitudes as measured over four or five locations in the domain. The agreement is reasonably good for all the incident waves although for the highest frequency the computed amplitude is 2.4% lower than the linear analytical amplitude – the largest discrepancy observed. The variation in the measured amplitude across the domain is also most significant in this case. These variations are most likely due to the fact that the high frequency propagation simulation is the most numerically problematic for OXPOT. In fact, the time-step in this case had to be reduced from $0.02T$ to $0.01T$ to

ensure the computation remained stable. Furthermore, the mesh regeneration techniques that are typically implemented in fully nonlinear codes involve a degree of numerical damping to ensure the stability of highly nonlinear waves and it is possible that this has an effect on even moderately nonlinear waves. Nevertheless, the agreement was considered sufficiently satisfactory to start simulating the interactions of the propagating waves with structures.

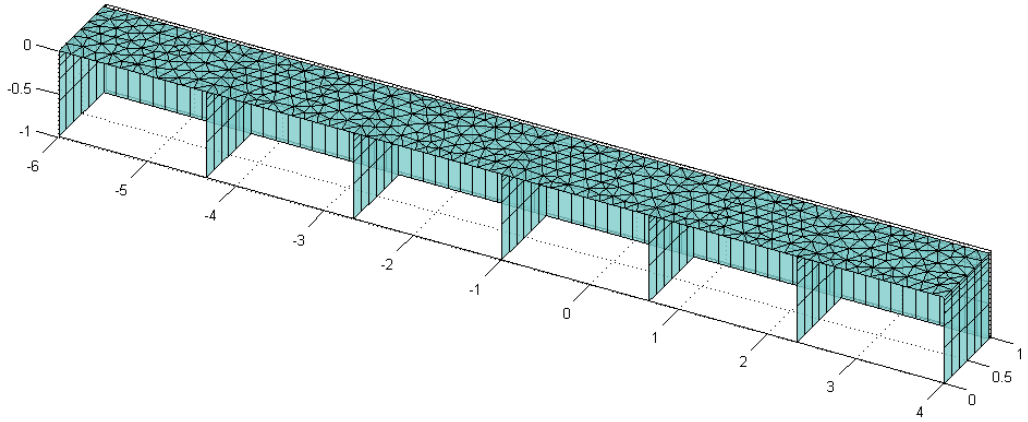

Figure 2: Typical boundary mesh for a computational domain divided into six subdomains.

Wave (T [s],H [m])	Left wall x_L	Right wall x_R	Total length	Width	Wavelength λ/h	Subdomains
(5, 1)	-1.3125	0.9375	2.25	0.1875	0.488	6
(7, 2)	-2.625	1.875	4.5	0.375	0.956	6
(9, 4)	-4.375	3.125	7.5	0.625	1.579	6
(10,6)	-6.0	4.0	10.0	0.95	2.05	6

Table 2: Geometrical specifications for the numerical wave tanks involved in the wave propagation investigations.

Incident wave (T [s], H [m])	Analytical linear amplitude η/h	Average computed amplitude η/h	Percentage Error
(5, 1)	0.00625	0.0061 ± 0.0002	-2.4%
(7, 2)	0.0125	0.0123 ± 0.0003	-1.6%
(9, 4)	0.0250	0.0249 ± 0.0002	-0.4%
(10,6)	0.0375	0.0371 ± 0.0003	-1.0%

Table 3: Comparison of the analytical free-surface elevation amplitude predicted by the linear theory and the linear component of the fully nonlinear free-surface elevation computed by OXPOT.

Property	SI unit	Dimensionless value
Water depth	$80m$	1.0
Cylinder Diameter	$20m$	0.25
Cylinder Draft	$20m$	0.25
Volume of displaced water	$6.28 \times 10^3\ m^3$	1.227×10^{-2}
Cylinder Mass	$6.44 \times 10^6\ kg$	1.227×10^{-2}
Position of centre of mass (x_{CM}, y_{CM}, z_{CM})	$(0.0,0.0,-14.59m)$	$(0.0,0.0,-0.182375)$
Inertia matrix (I_{11}, I_{22}, I_{33})	$(2.38, 2.38,1.82) \times 10^8 kgm^2$	$(7.10, 7.10,5.43) \times 10^{-5}$

Table 4: Main geometric properties associated with the cylinder.

4 SINGLE TRUNCATED CYLINDER SIMULATIONS – A LINEAR ANALYSIS

In deliverable D8, the first and second order hydrodynamic forces and unconstrained motions associated with a single truncated cylinder were computed over a total of 45 regular waves with different periods with a particular focus on the four wave frequencies and wave heights shown in Table 1. The main properties of the cylinder are presented in Table 1 in WG1 WP1 D8. The position of the centre of mass is given in terms of the global Cartesian coordinate system which is defined to have a right-handed orientation, is located in an inertial frame of reference and has the z axis pointing vertically and the origin in the mean free-surface. This coordinate system and the body fixed coordinate system whose axis is coincident with the global system when in an undisturbed position are depicted in figure 1 of WG1 WP1 D8. Here, we reproduce the properties of the cylinder in non-dimensional form in Table 4 as these are the inputs used for the OXPOT simulations where lengths are scaled by the water depth of 80 metres and densities by 1025 kg/m^3.

4.1 Test Cylinder

However, prior to simulating the interaction of waves with the truncated cylinder whose geometry is given in Table 4 a preliminary investigation of another cylinder was conducted. The reason for this preliminary investigation was that radiation and diffraction force data and also body motion data existed for this particular truncated cylinder for the case of a single cylinder in isolation and also within a two body array. Therefore, verifications of radiation, diffraction and coupled motion simulations for both single cylinder and multi-cylinder arrays were possible. Furthermore, the single cylinder simulations were useful to understand the mesh and domain configurations needed for accurate results for the later multiple cylinder investigations. The truncated cylinder is that described by (Matsui & Tamaki, 1981) – it has a radius of $a = 0.2$ and a draft of $0.5a$ in water of a depth $10a$. Prior to verifying the two-cylinder results presented by (Matsui & Tamaki, 1981), a comparison between the OXPOT simulations and the single cylinder results from (Matsui & Tamaki, 1981) were sought in order to understand the degree of agreement to be expected in the multiple cylinder case. To obtain phase information, existing data generated from a frequency domain code developed at Oxford (referred to as DIFFRACT) was used. A slight difference existed in that this data corresponded to a water depth equalling $5a$. For higher frequency waves, the interactions were essentially deep water interactions and the results from (Matsui & Tamaki, 1981) and DIFFRACT were almost identical.

Three different comparisons were made: firstly, the radiation forces on the oscillating cylinder were compared to the added mass and damping coefficients for a given frequency; secondly, the excitation forces on the cylinder in an incident wave field of a specified wave frequency were compared to the frequency-domain values; lastly, the unconstrained heave motions were compared. This necessitated the execution of three different OXPOT simulations with the free-surface mesh identical in the diffraction and unconstrained heave motion cases. The most straightforward simulation was the radiation problem because of the presence of a damping zone to absorb most of the outgoing wave energy. This simulation will be considered first and compared to the corresponding frequency-domain results.

4.1.1 Radiation Problem

In the radiation problem, the cylinder was positioned at the centre of a circular domain with an artificial damping layer imposed on the free-surface forming an outer annulus of the cylindrical domain. The radius of the cylindrical domain is denoted R and was chosen to be approximately twice the radiated wavelength. The artificial damping layer was chosen to extend one wavelength in the radial direction and so lies in the region from $r = R - \lambda$ to $r = R$. The details of the damping layer are described in WG1 WP1 D7. The oscillatory frequency was chosen so that $ka = 0.8$ corresponding to a non-dimensional frequency of $\omega = \sqrt{\mathrm{k}\tanh(k)} \simeq 1.993$, a wavelength $\lambda = \pi/2$ and a period $T = 2\pi/\omega \simeq \pi$. Only half of the wave tank is considered in this and subsequent simulations due to symmetry of the computational domain and solution. There are six boundary elements in the vertical direction on the outer boundary and body surfaces. The outer boundary in the half-plane is divided into 30 intervals in the circumferential direction and the half-circumference of the body is divided into 12 intervals. Including 97 triangular elements on the truncated cylinder surface and 1070 elements on the free surface, there are a total of 1419 elements distributed on the computational boundary corresponding to 3293 nodes. The simulation duration was typically between 8 and 10 periods with the time step equalling $0.025T$. Computational times ranged from 8 to 12 hours which is relatively modest compared to computational times for subsequent simulations.

In the radiation simulations, the cylinder was forced to oscillate in the i^{th} mode with a displacement and velocity of the centre of mass given by

$$\xi_i = -a_b \cos \omega t, \tag{11}$$
$$v_i = a_b \omega \sin \omega t, \tag{12}$$

in a fluid initially at rest. The motion of the cylinder was ramped from zero to purely sinusoidal oscillations over a specified number of periods using some ramping function $f(t)$; however, after this start-up time interval the motion was purely sinusoidal of the form given above. The heave force on the body was computed and compared to frequency-domain results. The added mass and damping coefficients, from which the total radiation force can be constructed, for a truncated cylinder are widely available – the data can be extracted from (Matsui & Tamaki, 1981) or computed using the method of (Yeung, 1981). The steady state force on the body in direction j is given by

$$\mathcal{F}_j(t) = Re\{ F_j \, e^{-i\omega t} \}, \tag{13}$$

where

$$F_j = i\rho\omega\, u_i \iint_{S_B} \phi_i\, n_j\, dS$$

with ϕ_i being the radiation potential corresponding to unit velocity amplitude in the i^{th} direction and u_i is the velocity amplitude. Since the added mass and damping coefficients are defined as

$$a_{ij} + \frac{ib_{ij}}{\omega} = \rho \iint_{S_B} \phi_i n_j\, dS \tag{14}$$

and with the velocity amplitude $u_i = ia_b\omega\delta_{ij}$ it is straightforward to show that the amplitude of the radiation force is

$$F_j = -a_b\omega^2\delta_{ij}\left(a_{ij} + \frac{ib_{ij}}{\omega}\right). \tag{15}$$

It is assumed that the forced motion occurs in a single mode only.

In the first simulation, the body was forced to move in heave according to equation (11) with the body displacement $a_b = 0.001$ so that nonlinear effects would be negligible. In OXPOT, the total vertical force on the body was computed, including the buoyancy, not the radiation force. Therefore, to extract the radiation force it was necessary to subtract the buoyancy force from the total force computed. Therefore, the vertical radiation force in OXPOT was calculated from

$$F_3^R(t) = F_3^T(t) - \rho g\, \pi a^2(d + a_b f(t)\cos\omega t), \tag{16}$$

where $f(t)$ is the ramp function for the body motion. The comparison of the radiation force from OXPOT to the frequency domain force as computed from the method of (Yeung, 1981) is shown in Figure 3. In a similar manner, the surge radiation force due to the surge motion of the body can be computed using the same computational domain specifications as in the heave problem. In fact, the surge comparison is a little more straightforward as there is no need to account for buoyancy – the total surge force is the radiation surge force. The OXPOT and frequency domain comparison for the surge radiation problem is shown in Figure 4. It is clear that the single body radiation force computations in OXPOT are accurate and comparison of the radiation force amplitude computed from the OXPOT results and the DIFFRACT radiation force results reveals a difference of less than 1%.

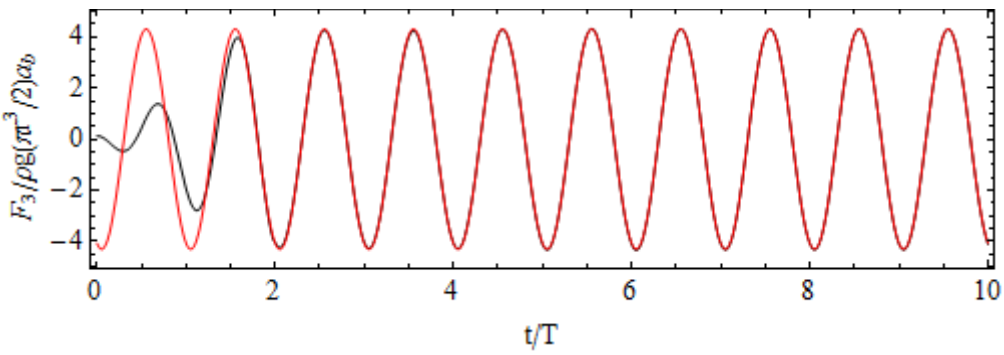

Figure 3: Comparison of heave radiation force computed by OXPOT (black) and frequency-domain result (red).

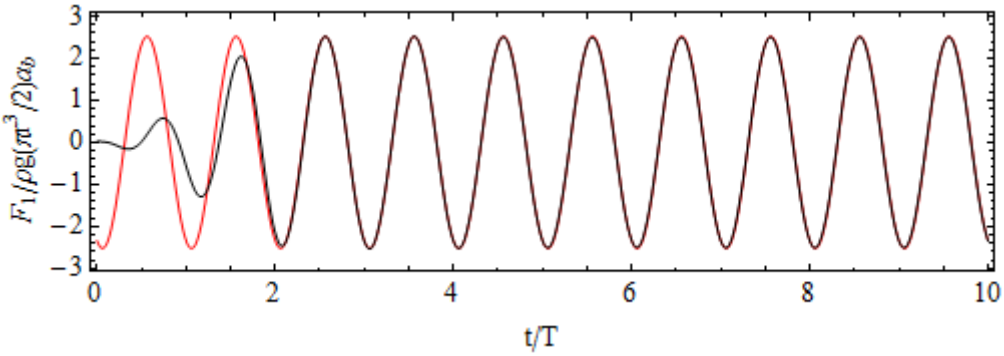

Figure 4: Comparison of the surge radiation force as computed by OXPOT (black) and from the frequency domain hydrodynamic coefficients

4.1.2 Diffraction Problem

The diffraction problem is a more difficult problem to simulate in OXPOT because the domain must be sufficiently long and wide to allow a wave train to interact with the cylinder and for the interaction to arrive at a steady state without reflections from the wave-maker and side walls interfering. However, with computational time having a quadratic dependence on the number of nodes in each subdomain it is not possible to arbitrarily increase the domain size – a balance between computational time and simulation accuracy must be struck. Thus, the following description of the diffraction problem involving a fixed truncated cylinder must be considered in the context of this trade-off between the desired accuracy and computational time.

The geometry of the truncated cylinder involved in the diffraction problem is identical to the one used in the radiation problem simulation. Initially, we adopted the same discretisation of the cylinder: 6 elements in the vertical direction, 12 on the half-circumference and 97 triangular elements on the truncated surface. The computational domain was rectangular in shape with a depth of $h = 1.0$ (corresponding to 5 radii) with a length of $L_T = 7.5$ and a half-width of 1.0 and it was divided into six subdomains of equal length. The wavemaker was a distance 4.375 units from the centre of the cylinder and the rightmost end-wall a distance 3.125 units from the centre of the cylinder. This asymmetry was used to prevent reflections from the cylinder interfering with the interaction occurring early in the simulation. (However, as will be explained shortly, the reflections from the side wall arise in the early stages of the interaction). The domain walls and sub-domain interfaces have six elements in the vertical direction with the meshing becoming finer near the free surface. The side walls were set to have 10 elements in the horizontal direction whereas the end walls and interfaces have 8 elements along the y-direction. A plot of this computational domain is shown in Figure 5. The dimensionless frequency of the incident wave was chosen to be $\omega = 2.0$ corresponding to a wavelength of $\lambda \simeq 1.57$. Therefore, the domain was less than one wavelength in width. The total simulation time was $15\,T$, T being the period of the incident wave, and the time-step was chosen to be $0.025T$. As mentioned previously, most of these simulation specifications were taken from (Bai & Eatock Taylor, 2009).

The wave force was measured in the surge, heave and pitch modes for an incident wave generated by a piston displacement amplitude of $a_p = 0.001$. The frequency-domain excitation forces used for comparison were obtained from (Matsui & Tamaki, 1981) and also through DIFFRACT computations.

The forces (or moments) computed by OXPOT and those obtained from the frequency-domain solutions are scaled by the term $\rho g a^2 A$ (or $\rho g a^3 A$), where A is the linear wave amplitude, and the time coordinate is scaled by $T = 2\pi/\omega$ for the purposes of non-dimensionalisation. The surge, heave and pitch excitation forces as computed by OXPOT are compared to the DIFFRACT computations in Figure 6. Clearly, both the surge and pitch forces computed by OXPOT agree very well with the frequency-domain prediction. However, there is a significant discrepancy (greater than 10%) in the heave forces which must be accounted for.

To understand this discrepancy some changes to the mesh and computational domain are necessary. To this end, two separate investigations were conducted. Firstly, the width of the domain was held constant and the mesh resolution on the body and on the free-surface was increased considerably. Secondly, the mesh fineness from the original simulation was preserved and the width of the domain doubled. In this way, the effect of mesh fineness and domain width could be assessed independently.

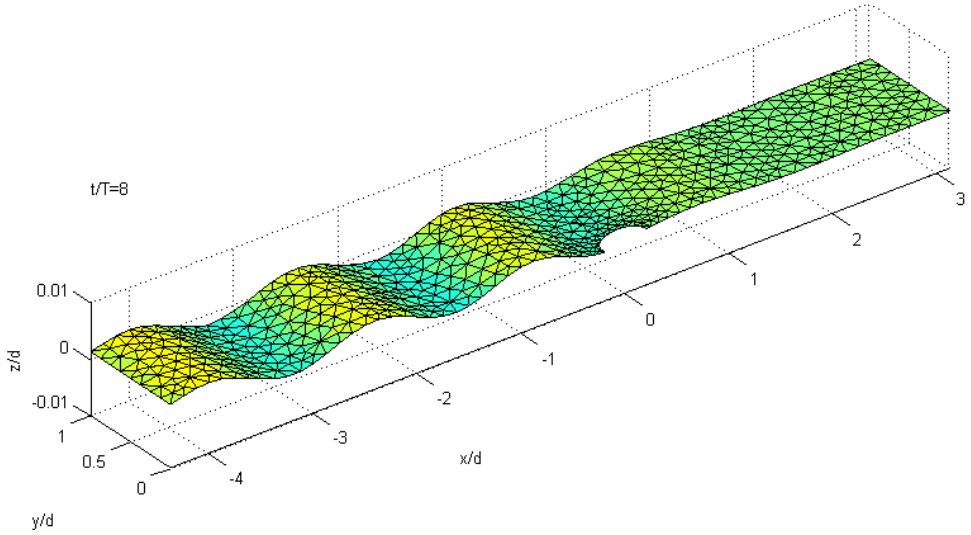

Figure 5: Computational domain for diffraction problem of width W=1.0 and with a standard mesh.

In the first case, the number of elements on the body was increased as follows. The number of intervals on the circumference on the body was increased from 12 to 20, the number of vertical elements from 6 to 10 and the number of elements on the truncated surface from 107 to 190. Around the body, the fineness of the mesh was also increased to match the increase in the fineness of the mesh on the body. The total number of elements and nodes in this simulation are compared to the corresponding totals from the first simulation in Table 5 and the changes in the body mesh are also highlighted in this table. Furthermore, the average heave and surge forces computed during the steady state section of the simulation are presented with reference to the DIFFRACT result. A comparison of these force results for the simulations reveals very little change due the increase in fineness. The difference between the surge and heave force measurements has a maximum value of approximately 0.025 in both cases which is approximately 1.8% of the overall force. Therefore, a large increase in the mesh resolution on the body and on the surrounding free-surface does not yield a significant improvement in the heave force results.

In the wide-domain simulation, the half-width of the domain increased from $W = 1.0$ to $W = 2.0$ (so that the domain half-width is larger than one incident wavelength) while the fineness of the body mesh is the same as the first simulation. A plot of the heave force computational results, with DIFFRACT results present for comparison, is shown in Figure 7. It is clear that the increase in the width of the domain yields a substantial improvement in the agreement between the DIFFRACT and OXPOT heave force results – in Table 5 it can be observed that the mean heave force decreases from approximately 1.4 to 1.2. The surge and pitch comparisons remain quite similar to those presented in Figure 6. Due to the increase in the free-surface area and hence in the number of triangular elements forming the free-surface mesh there is a substantial increase in the computational time.

The reason for the large difference between the heave force results measured in a narrow and wide domain (with little or no difference in the surge force results) is the reflections from the side walls of the computational domain. These reflection effects are manifest only in the heave results and not the surge results because the reflected waves are symmetric about the sway (y) direction and hence no net force is exerted on the body in surge (x) direction. These reflected waves can however exert a force in the vertical direction and hence the heave force measurement is significantly affected by the reflection of these diffracted waves from the side walls. The effect of these reflected waves can be observed after 12 periods in the wide-domain simulation where the OXPOT heave force results begin to diverge from the DIFFRACT results. In fact, it should be possibly to estimate the time it takes for the first reflected waves of significant amplitudes to reach the body using the group velocity c_g of the wave-train. The group velocity is defined as

$$c_g = \frac{d\omega}{dk} = \frac{\omega}{2k}\left(1 + \frac{2kh}{\sinh 2kh}\right), \tag{17}$$

and is approximately 0.25 in this case. The first significant waves from the wavemaker arrive at $t/T \simeq 7.0$ and hence the reflected waves should arrive approximately $(2\,W/c_g\,)/T \simeq 5$ periods later. This prediction can be seen to be approximately correct from the heave force plot in Figure 7. The surge force results will not be affected by diffracted waves reflected from the wavemaker until a much longer time has elapsed (approximately 11 periods after the first significant waves reach the cylinder). Therefore, the side-wall reflections must be taken into account when assessing the accuracy of the OXPOT results relative to the DIFFRACT results.

To obtain results close to the open-water frequency-domain results the domain half-width should be sufficiently large so that several periods must elapse before diffracted waves return to the body – a reasonable requirement would be that the domain half-width be at least greater than one incident wavelength. However, this inevitably leads to longer computational times – the computational time for the first simulation (denoted number 1 in Table 5) was 24 hours, for simulation 2 with the finest mesh it was 40 hours and for simulation 3 featuring the widest domain it was 61 hours. The choice of the width of the domain and the fineness of the mesh must be made with the computational runtime in mind. It is useful to note that increasing the mesh fineness does not necessarily improve the first order solution once the mesh density is sufficiently high – however in the simulations where the second order forces are important the mesh fineness must be retained even if the first order forces have already converged. One possibility for reducing computational times is to shorten the length of the domain. In the current domain configuration, it will take approximately 11 periods after the first significant wave reaches the cylinder for the surge results to be affected by the

reflected waves. Since less than 6 regular wave periods are simulated after the wave front arrives then reducing this distance will not affect the results significantly.

Simulation	Half-width	Boundary intervals		Body specification		Total # of elements/nodes		Force/$(\rho g\, a^2 A)$		
	W	n_x	n_y	n_{CIRC}	N_{TRUNC}	N_E	N_N	F_1	F_3	F_5
1	1.0	10	8	12	107	2281	6407	1.38	1.39	0.423
2	1.0	10	8	20	190	3014	8382	1.37	1.39	0.420
3	2.0	10	16	12	107	3891	10477	1.37	1.20	0.419
DIFFRACT								1.37	1.17	0.411

Table 5: Comparison of the computational boundary meshes and resulting force measurements for three different domains.

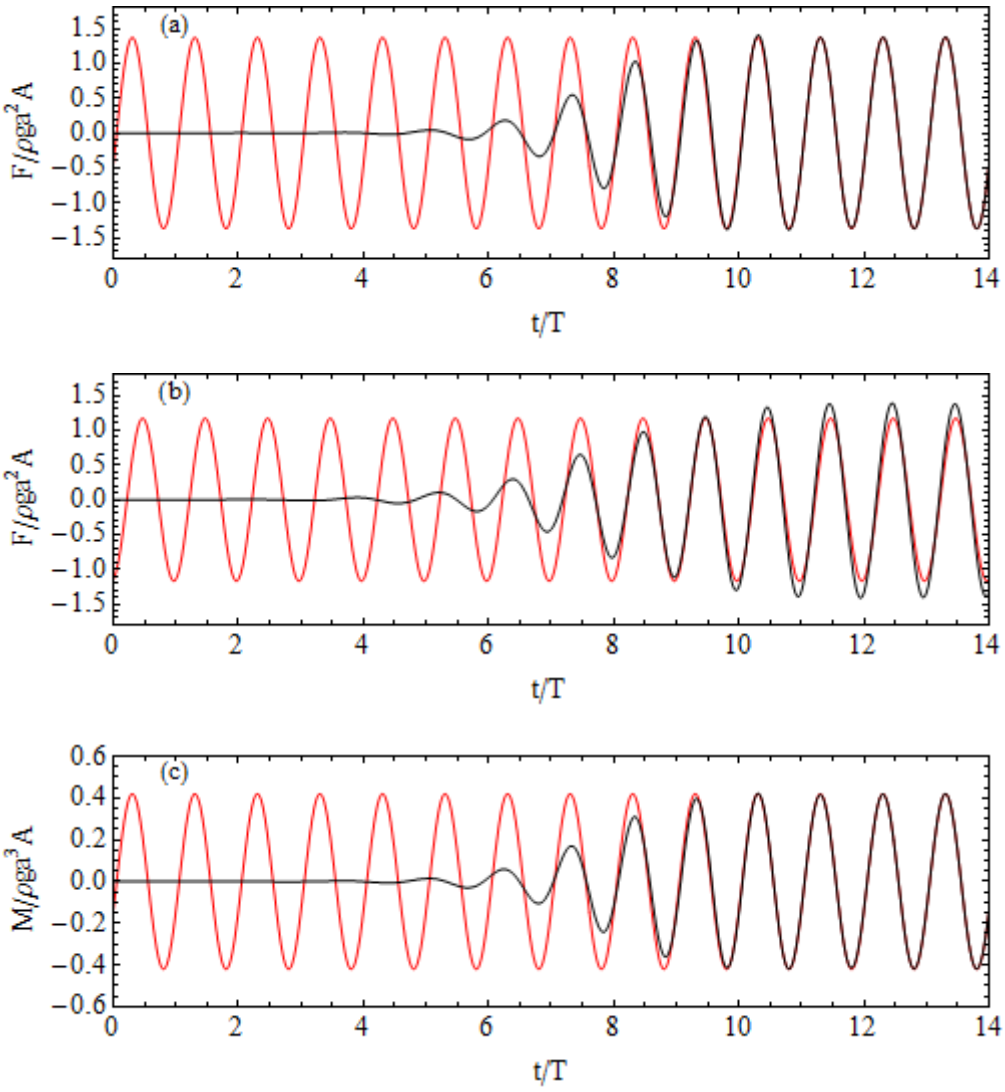

Figure 6: Surge (a), heave (b) and pitch (c) excitation forces on the truncated cylinder as computed by OXPOT (black) and DIFFRACT (red).

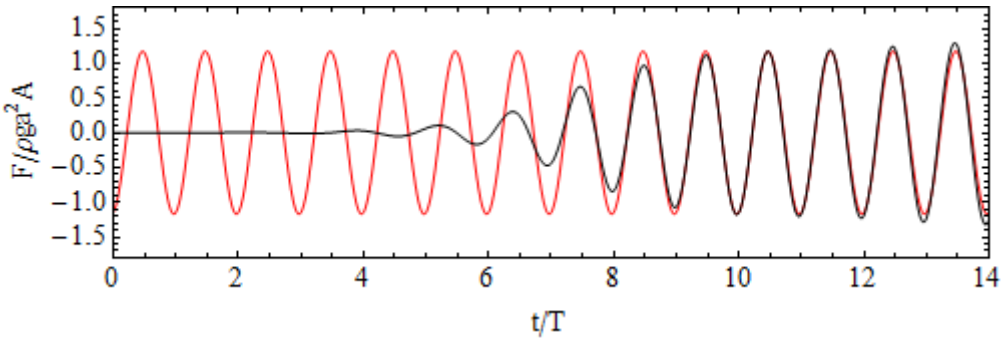

Figure 7: Heave excitation force on the truncated cylinder in a wide domain as computed by OXPOT (black) and DIFFRACT (red).

4.1.3 Unconstrained heave motion

Given that the radiation and diffraction problems have both been successfully simulated (for approximately linear interactions at least) the next problem to consider is that of a floating body free to respond to incident waves in the heave mode. The time-domain approach requires that the coupled problem involving the motion of both the body (in heave) and the fluid motion be solved for all time. Therefore, the heave displacement $x_3(t)$ of the body must be solved with the equation of motion

$$M\ddot{x}_3(t) = -\rho \iint_\Gamma \frac{\partial \Phi}{\partial t} n_3 dS - \rho g W_A x_3(t), \tag{18}$$

where W_A is the water plane area and M is the mass of the body, while simultaneously solving the motion of the fluid $\Phi(\boldsymbol{x}, t)$ throughout the fluid domain at each time t. In the frequency domain, the heave displacement amplitude ξ_3 can be obtained directly from the frequency-domain equation of motion which can be rearranged to give

$$\xi_3(\omega) = \frac{X_3(\omega)}{\rho g\, W_A - \omega^2(a_{33}(\omega) + M + ib_{33}(\omega)/\omega)} \tag{19}$$

where $X_3(\omega)$ is the exciting force on the body. Therefore, given the radiation force coefficients, the excitation force and the body geometry, it is straightforward to compute the motion.

In the comparison of the time-domain solution for a floating body free to move in regular waves and the corresponding frequency-domain solution the most important difference is that the natural resonance of the body, assumed to have decayed in the frequency-domain problem (steady-state solution), will be present in the time-domain case. The importance of this transient motion will depend on the degree to which it is excited and the length of time it takes to decay. The natural resonance is the mode that body oscillates in when released from an initial displacement or given an initial velocity. In mathematical terms, all hydrodynamic quantities can be regarded as functions of complex frequency $\omega = \omega_r + i\omega_i$ then a resonance is associated with a singularity of the quantity at some complex frequency $\omega = \omega_0 - i\epsilon$. These singularities are known as complex resonances or scattering frequencies and their existence in freely floating problems has been investigated by (Ursell, 1964) and more recently by (McIver, 2005). The real part ω_0 of the singularity location

determines the resonant oscillation frequency and the imaginary part $\epsilon > 0$ governs the decay rate of the oscillation. A small value of ϵ corresponds to a weakly damped resonant mode.

The nature of this resonance, both the frequency and decay rate, depends on the geometry of the structure and the extent to which it is excited depends on the properties of the incident wave and the properties of the resonance. Therefore, if the incident wave frequency is close to the natural resonance then strong excitation will occur. Furthermore, if the incident wave consists of a range of frequency components then the broader the spectrum the more likely it is that excitation of significant resonant motion will occur. If the resonant mode is weakly damped and if it is excited significantly then a large number of oscillations must occur before the contribution to motion is negligible, i.e. the transient motion will persist – and steady state will not be reached – for a long time.

To compute the time-domain simulation using OXPOT the problem is set up identically to the diffraction problem with the body now allowed to move in heave only. The domain and boundary mesh configuration were adopted from the diffraction simulation featuring the widest domain and the same incident wave was generated. Since only vertical motions of the body occur the free-surface mesh remains quite similar to that in the diffraction problem and no instabilities are observed to arise. The heave motion of the body is shown in Figure 8 with the frequency domain solution included for comparison and it can be seen that the agreement is relatively good although the OXPOT displacement amplitude varies throughout the simulation because of the interference between the forced and resonant modes. The presence of the two modes is difficult to distinguish in the simulation as the two frequencies are quite similar; however, an unconstrained motion simulation was also conducted and the pitch motion, shown in Figure 9, also showed large variations in the amplitude corresponding to the interference between two modes of closely spaced frequency. To assess the behaviour more comprehensively it would be necessary to increase the simulation run time so that the transient resonant motion would become negligible. However, to understand how long this decay might take it is useful to investigate the resonance in isolation.

Therefore, the release of the body from an initial displacement $\xi_{3(0)} = A$ was simulated and the frequency and decay of the resultant oscillations were measured. The variation of the displacement amplitude in time and the Fourier transform of this signal are shown in Figure 10. The frequency of the oscillations was approximately $\omega = 2.25$ which corresponds to the peak at $\omega/\omega_I = 1.125$ in Figure 9. By measuring the positions of the displacement maxima and fitting an exponential decay function $e^{-\varepsilon t}$ to the resultant list of points it can be shown that the decay rate for the oscillations is approximately $\varepsilon = 0.168$. The exponential decay function $A\ exp(-\epsilon t)$ is also plotted in Figure 10 (a) to illustrate the goodness of fit. This is a relatively strong damping as it takes only $\tau = 1/\varepsilon \simeq 6$ time units for the displacement amplitude to decay by $1/\epsilon$ (which corresponds to just two periods $T = 2\pi/\omega$ when $\omega = 2.0$). In the coupled heave motion problem, four or five decay times τ must elapse before the resonant motion becomes sufficiently small. Given that the peak amplitude occurs around $t/T \simeq 10$ then the simulation should run to 20 periods.

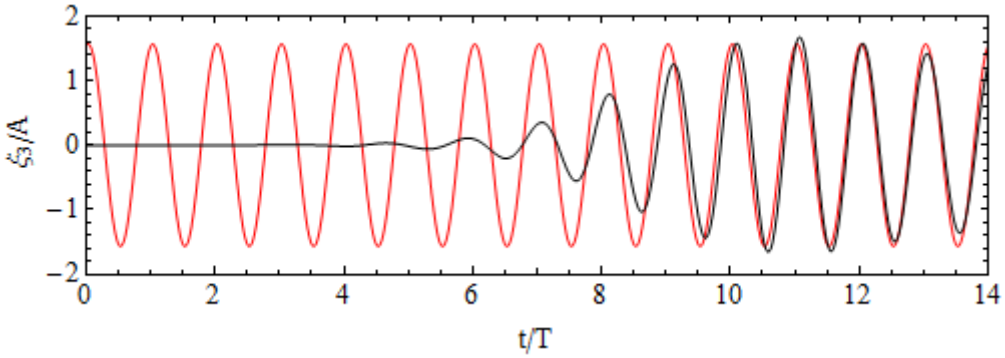

Figure 8: The heave displacement of the body as computed by OXPOT (black) and in the frequency domain (red).

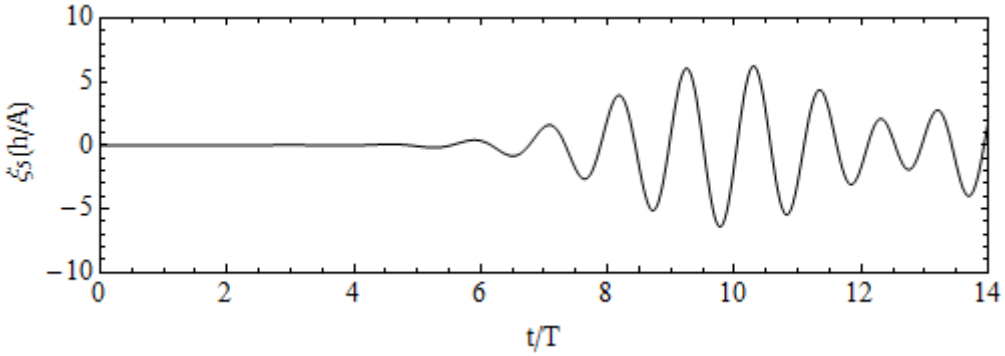

Figure 9: The pitch motion of the test cylinder as computed by OXPOT for the unconstrained response of a cylinder to incident waves.

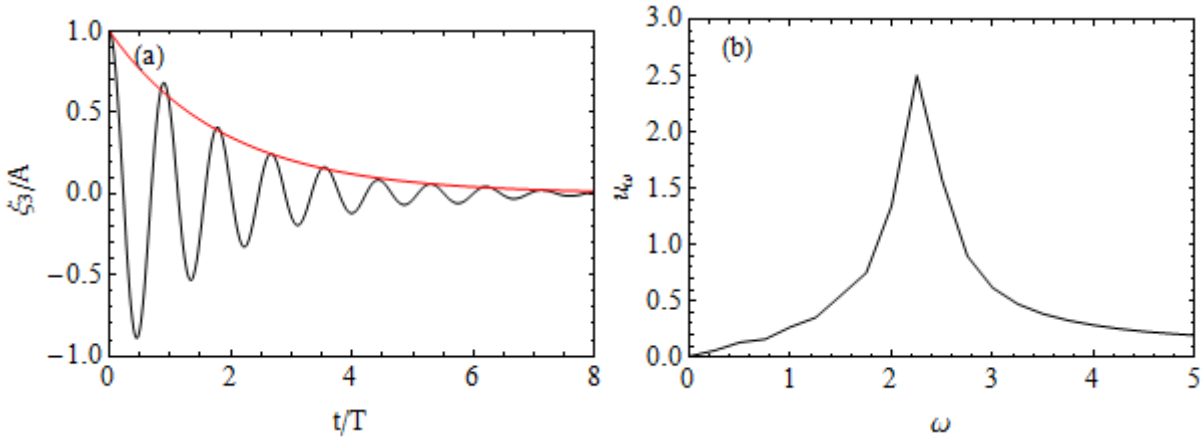

Figure 10: (a) Plot of the displacement of body in heave after release from an initial displacement (black) with an exponential decay function (red) shown for reference and (b) the discrete Fourier transform of this signal.

4.2 Vertical truncated cylinder from WG1 WP1 D8

The geometrical specifications of the cylinder for which the linear and second-order excitation forces and motions for incident waves of various frequencies must be compared to the frequency-domain results from D8 are presented in Table 4. The four different incident wave periods $(5s, 7s, 9s, 10.25s)$ have corresponding non-dimensional wavelengths of $(0.49, 0.95, 1.58, 2.05)$. The variation in wavelength is substantial so that it is important to mesh the cylinder and free-surface according to the specified incident wave and also to scale the width and length of the simulation domain depending on the wavelength (in a similar manner to the propagating wave simulations). Therefore, it was necessary to treat each simulation separately. Here, one incident wave case will be described in most depth while the other cases will be summarised. Unlike the test cylinder case, only the exciting force and unconstrained heave motion problems will be considered.

4.2.1 Diffraction problems – excitation forces

The first interaction to be simulated was the diffraction problem featuring the regular incident wave of period 9 seconds with a wave height of 4 metres. In these simulations the incident wave is generated in an identical manner to that described in section 3.2. The length of the domain is, as before, $L = 7.5$ with the wavemaker positioned at $x = -4.375$, the cylinder axis at $x = 0.0$ and the rightmost end wall at $x = 3.125$. The domain is divided into 6 subdomains of length $L_{SUB} = 1.25$ and the cylinder lies in the fourth subdomain from the left. The half-width of the solution domain is 1.25 in order to accommodate the cylinder and to allow the diffracted waves to dissipate somewhat. Nevertheless, it is quite a narrow domain: in relative terms the half-width is 10 radii in extent but, more importantly, this corresponds to less than one wavelength ($\lambda = 1.579$).

Each subdomain has a square free-surface boundary with a length of side of 1.25 and each side is divided into 12 boundary intervals. Both the structured mesh on the walls and the unstructured mesh on the free-surface use these intervals as a meshing basis – that is, each interval forms the side of a quadrilateral or triangular element on the side wall and free-surface respectively. The side walls and interfaces have 6 boundary elements in the vertical direction with the elements becoming finer near the free-surface. The free-surface has 246 triangular elements and there are a total of 462 elements (1300 nodes) in the subdomains without the cylinder. The curved surface of the cylinder is discretised by 12 intervals around the half-circumference and 6 elements in the vertical direction, thus generating a set of 72 quadrilateral elements. An unstructured mesh comprising 87 triangular elements discretises the bottom/truncated surface. In total, there are 3145 elements on the boundary of the computational domain with a corresponding set of 8689 nodes. The time step is chosen to be one fiftieth of a period $(0.02T)$ which was considered to be sufficiently small (simulations involving time steps of one-fortieth of a period were compared and the results differed only slightly).

The fineness of the mesh must be assessed relative to the incident linear and second-order wavelengths. For example, the horizontal extent of the free-surface elements away from the body is approximately $1.25/12 \simeq 0.10$ which is approximately 15 elements per incident wavelength. On the surface of the cylinder, the elements have lengths of $\pi r/12 = 0.033$ which corresponds to 48 elements per incident linear wavelength. In terms of the second order wavelength ($\lambda_2 \simeq 0.4$) there are approximately 12 elements per wavelength. These relative dimensions, although only calculated approximately, give an estimate of how fine the mesh is. In this case, it was considered that the mesh was sufficiently fine to accurately capture the second order dynamics.

Wave	Comp. Domain		Subdomain intervals			Body details		Total	
(T, H)	L	W	n_x	n_y	n_z	n_{CIRCUM}	n_{TRUNC}	Elements	Nodes
(5,1)	3.75	1.0	12	16	6	16	50	3564	9550
(7,2)	4.5	1.5	10	20	6	16	50	3944	11072
(9,4)	7.5	1.25	12	12	6	12	35	3145	8689
(10,6)	9.0	3.0	10	20	6	8	25	3887	10875

Table 6: Summary of the properties of the computational domain and mesh for the four wave cases featuring a single body.

The first order exciting force comparisons between OXPOT and WAMIT are shown Figure 11. The agreement between the two sets of results can be seen to be very good – to assess the error it is necessary to measure the amplitude of the force oscillations in the steady state part of the OXPOT simulation. In this case, the system seems to have settled to a steady state after $t = 90\ s$. Presented in Table 7 is a comparison of the frequency domain amplitudes as computed in WAMIT to the steady-state time-domain amplitudes – the relative error is also shown in this table. The uncertainty in the OXPOT values is included in the table although the mean value only is used for the relative error calculation $\Delta F/F = (F_{OX} - F_{WAM})/F_{WAM}$. The error is no greater than 4% which is a reasonably satisfactory agreement although there is certainly scope for improvement. The surge and pitch OXPOT results both underestimate the first order force predicted by WAMIT so it is possible that the linear component of the incident wave generated is slightly smaller than analytically predicted. On the other hand, the OXPOT heave force computations over-estimate the linear frequency-domain force. It is likely that the narrowness of the computational domain causes this because it would be expected that, in the absence of side wall reflections, the surge, heave and pitch results OXPOT would all either over- or under-estimate the WAMIT results. It has already been shown that side-wall reflections can increase the heave force relative to the open-water case. Therefore, it is possible that the waves generated are not quite as large as predicted – OXPOT uses a mesh regeneration technique to prevent saw-tooth instabilities occurring which can sometimes lead to numerical damping.

The details of the computational domain and mesh for the remaining simulations are summarised in Table 6. In the $(T, H) = (7\ s, 2\ m)$ case, the half-circumference of the body is initially discretised by 16 intervals before forming the mesh. The quadrilateral elements on the curved surface have a horizontal length $\pi r/16 \simeq 0.025$ which corresponds to approximately 40 elements per linear wavelength and 10 per second-order wavelength. This corresponds to a reduction in mesh resolution (relative to the wavelength) compared to the $(T, H) = (9\ s, 4\ m)$ case. This reduction is necessary to keep the computational times reasonable and to ensure the mesh is not too distorted. (Having very small intervals on the body and moderately large intervals on the side walls can cause distortion of the mesh unless a substantial number of triangular elements are inserted on the free-surface.) For the longest incident wave $(T, H) = (10.25\ s, 6\ m)$, the wavelength is approximately twice that of the $T = 7\ s$ case and hence the number of intervals on the half-circumference of the cylinder can be reduced to eight while preserving the quadrilateral element width-to-wavelength ratio. The linearised surge, heave and pitch force results for the four regular waves defined in Table

1 of section 3.1 are shown in Figure 12, 13 and 14 respectively. The forces are not shown over the entire simulation times in these figures, rather over a reduced time interval from when the incident wave begins to exert a force on the body until the interaction settles to a steady state. In general the agreement is satisfactory; however, the OXPOT computations give forces that are consistently very slightly smaller than the corresponding WAMIT computations. Furthermore for the $T = 7\ s$ period wave the heave results do not agree to the same extent as in the surge and pitch results. The discrepancy is significantly larger than in any of the other cases, apart from the corresponding heave computation for the 5 second period incident wave, as is evident from Table 7. Given that the width of the domain should be enough to preclude the occurrence of reflected waves in the early stages of the simulation (just after the initial build-up of the force) then the significant difference must be either due to issues with the wave generated by the piston wavemaker or else possibly the meshing of the truncated surface.

In the case of the ($T = 5\ s, H = 1\ m$) wave, there were difficulties in obtaining a stable simulation for very high mesh densities around the body. Therefore, it was decided to use a similar mesh to that for the incident wave of period 7 seconds. Given that the first-order wavelength of the incident wave for the wave of period 5 seconds is half that of the wave of period 7 seconds it is clear that convergence issues may exist in the case of the shorter wave. Nevertheless, the first-order wavelength to element length ratio for the wave of period 5 seconds was approximately 20 so it was expected that the linear analysis would yield good agreement. As is evident from Figure 12 and Figure 14 the linearised surge and pitch forces agree very well with the first-order WAMIT forces, in fact the error is less than 2% as is indicated in Table 7. However, in the case of the heave motions the error is close to 30% which implies the mesh density on the free-surface or on the cylinder boundary is not sufficiently high.

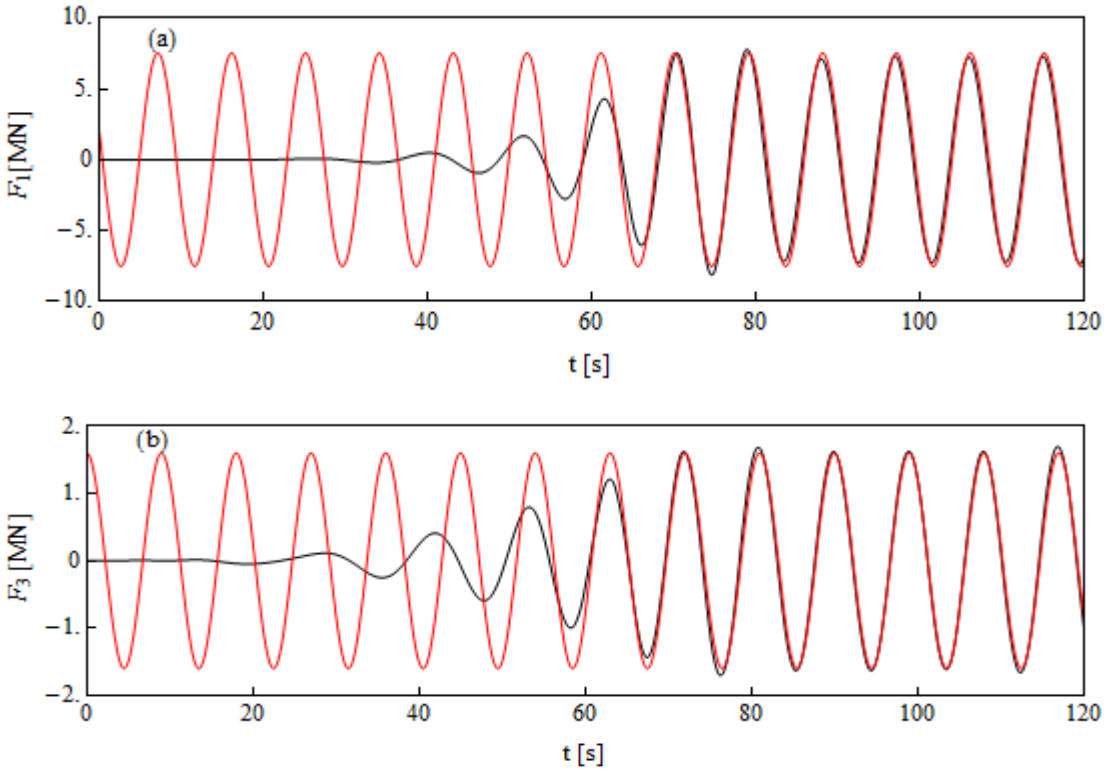

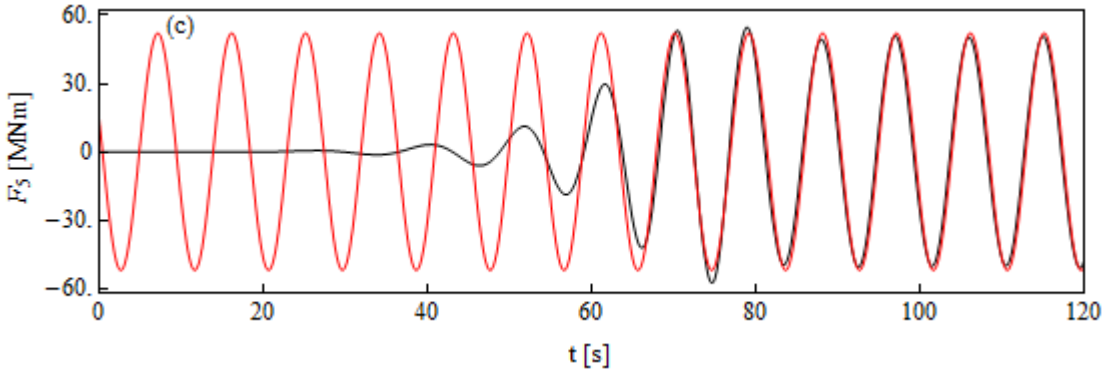

Figure 11: Comparison of OXPOT and WAMIT computations for the excitation forces in (a) surge, (b) heave and (c) pitch for incident wave of period T=9 seconds and height H=4m.

Incident wave	**Computational Method**	**Excitation forces amplitudes**		
		Surge ($F_1[M\ N]$)	**Heave ($F_3[M\ N]$)**	**Pitch ($F_5[M\ N]$)**
$T = 5\ s,$ $H = 1m$	WAMIT (F_{WAM})	1.15	0.0219	10.79
	OXPOT (F_{OX})	1.17 ± 0.01	0.029 ± 0.02	10.99 ± 0.01
	Relative Error ($\Delta F/F$)	1.7%	30%	1.9%
$T = 7\ s,$ $H = 2m$	WAMIT (F_{WAM})	4.07	0.332	31.2
	OXPOT (F_{OX})	3.83 ± 0.08	0.31 ± 0.02	29.9 ± 0.7
	Relative Error ($\Delta F/F$)	-5.8%	-8.0%	-4.2%
$T = 9\ s,$ $H = 4\ m$	WAMIT (F_{WAM})	7.54	1.60	52.0
	OXPOT (F_{OX})	7.33 ± 0.06	1.66 ± 0.03	51.0 ± 0.5
	Relative Error ($\Delta F/F$)	-2.7%	3.6%	-2.2%
$T = 10.25\ s,$ $H = 6\ m$	WAMIT (F_{WAM})	9.68	3.30	64.3
	OXPOT (F_{OX})	9.38 ± 0.07	3.26 ± 0.03	62.7 ± 0.8
	Relative Error ($\Delta F/F$)	-2.2%	-1.3%	-2.4%

Table 7: Comparison of excitation force amplitudes as computed by OXPOT and WAMIT for the four key regular incident waves.

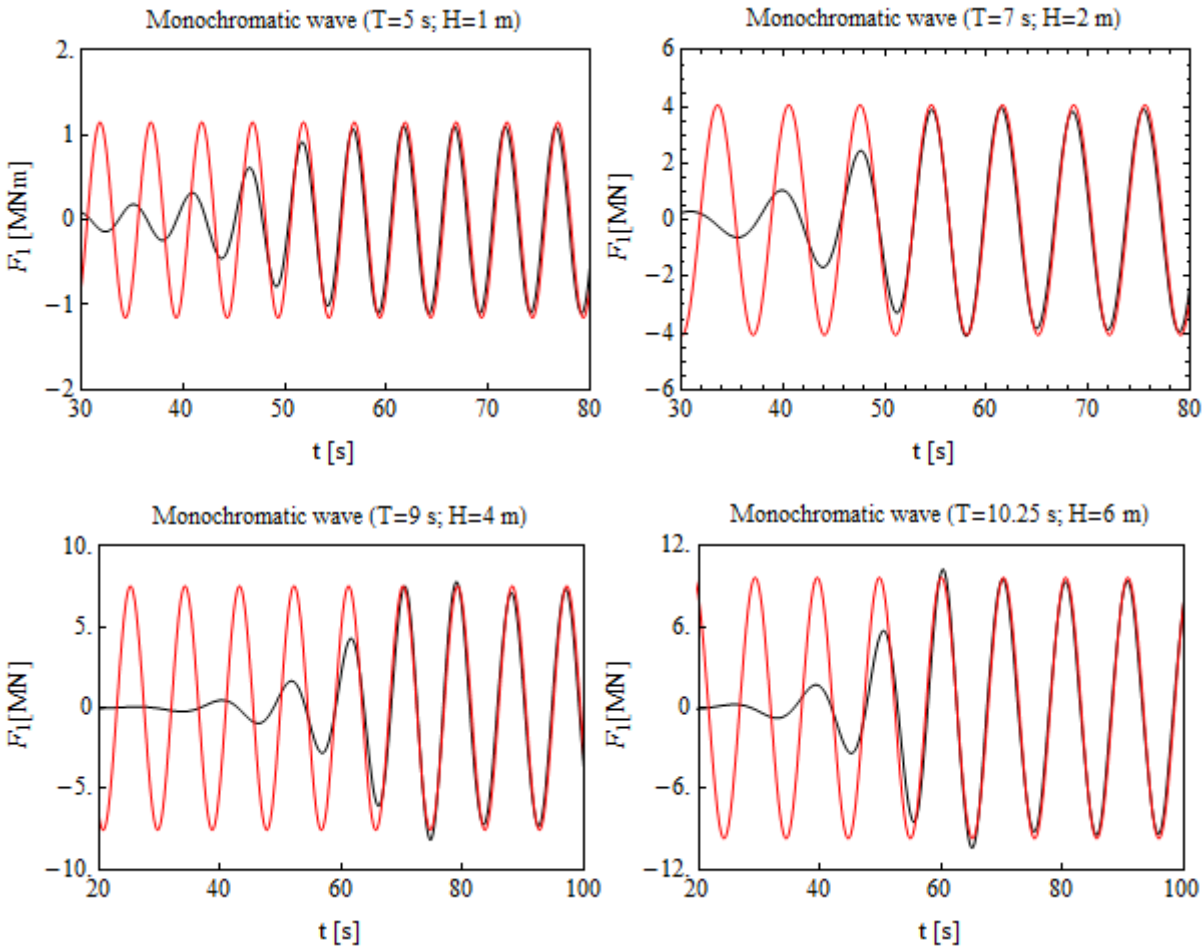

Figure 12 Comparison of linearised OXPOT results (black) to first-order WAMIT results (red) for the surge excitation forces for the four regular waves described in Table 1.

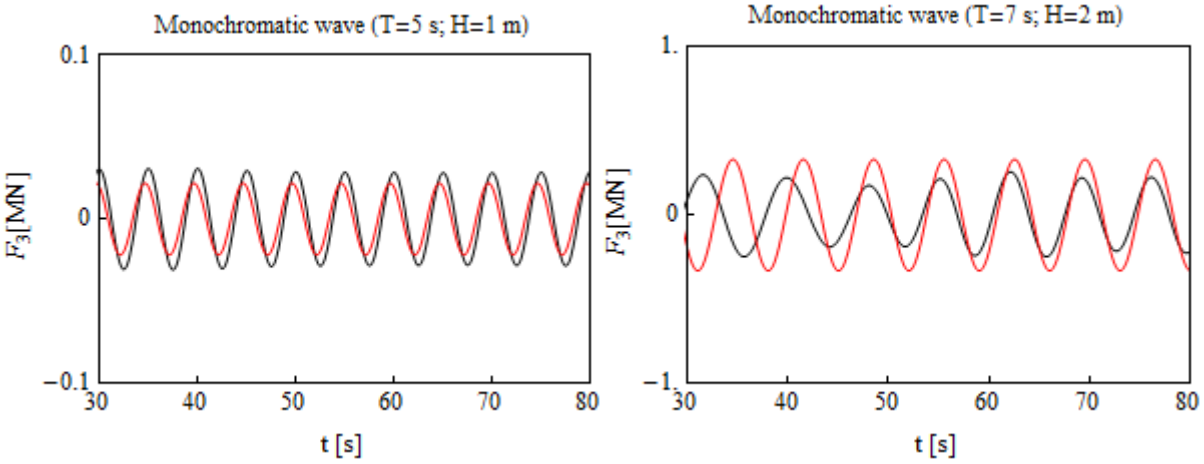

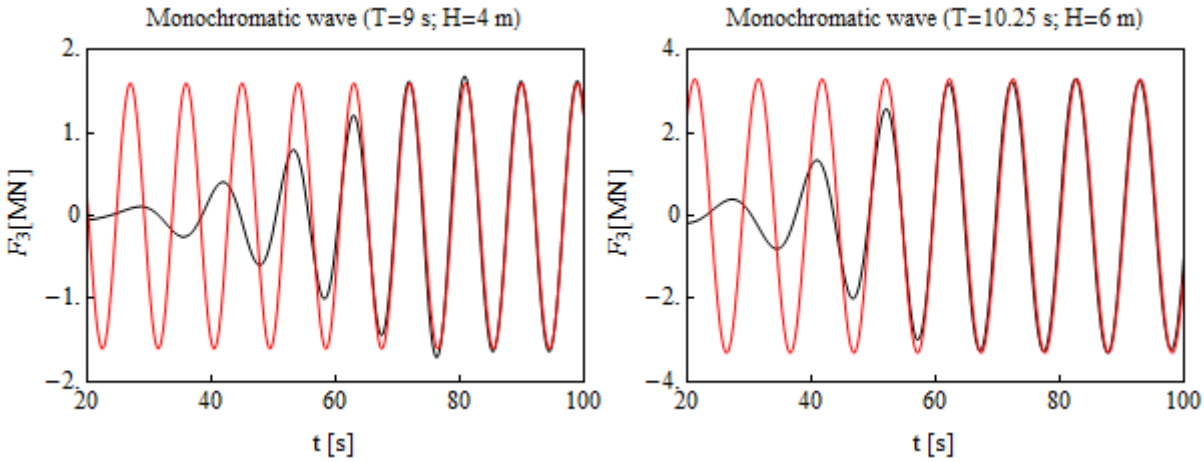

Figure 13: Comparison of linearised OXPOT results (black) and first order WAMIT results (red) for excitation heave forces for the four regular waves whose properties are described in Table 1.

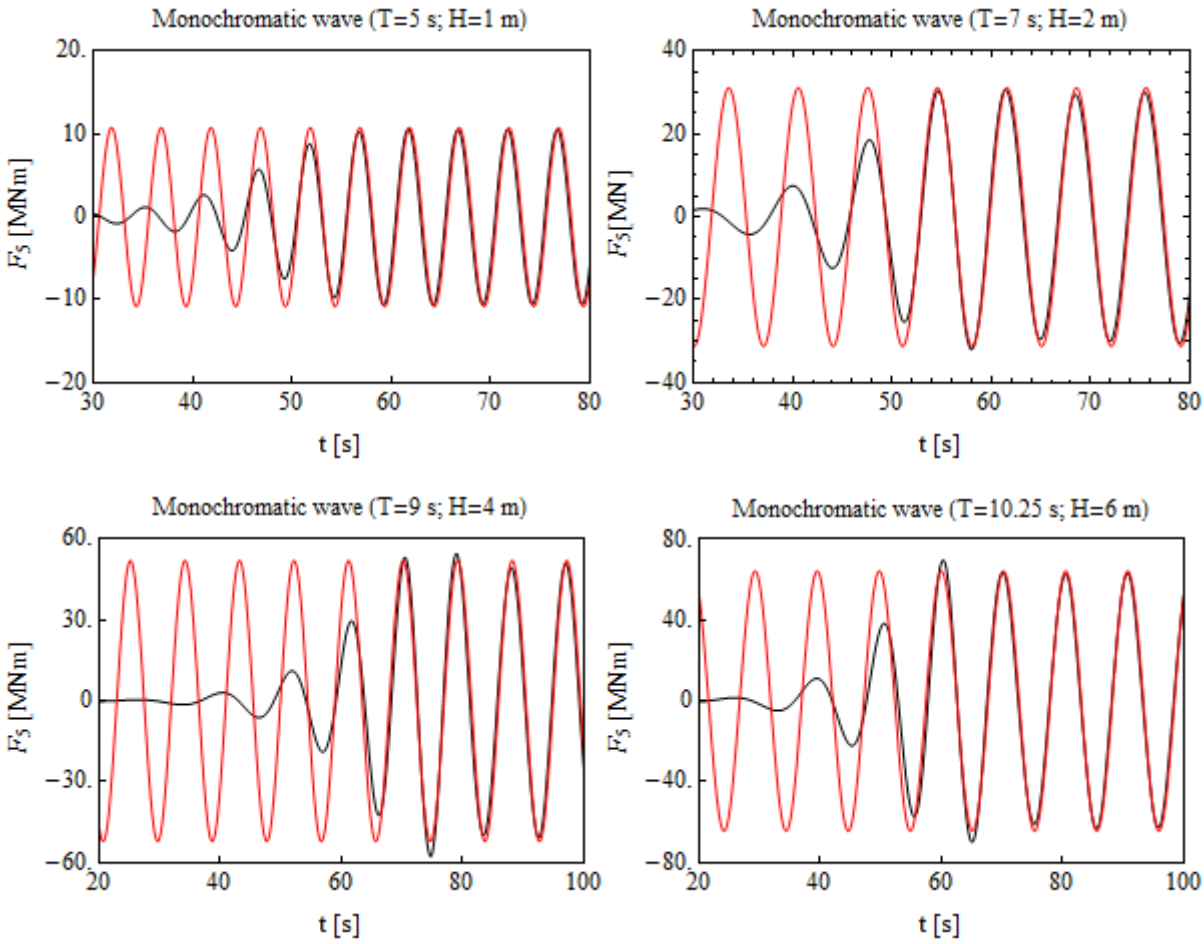

Figure 14: Comparison of linearised OXPOT results (black) and first order WAMIT results (red) for the pitch excitation forces for the four regular waves whose properties are described in Table 1

4.2.2 Heave response of body to incident waves

The most important mode of motion to be considered, in the context of power take-off and future experimental investigations, is the heave mode. Therefore, the response of the body to incident waves was constrained to the heave mode only in the following simulations so as to isolate the interaction from the other body dynamics that would otherwise be excited. As discussed in section 4.1.3, the natural resonance of the body plays an important role in the motion of the body after excitation. Side-wall reflections will also affect the results, however, for the simulations involving the short period incident waves the difference in the time-domain and frequency-domain results are too large to be explained by side-wall reflections and are more likely due to the resonant body motion. Therefore, without very long simulations it is difficult to obtain a good agreement between the transient (time-domain) and steady state (frequency-domain) results.

To assess the properties of the resonance for this particular body geometry a simulation of the release of the body from an initial displacement was conducted and the frequency and decay rate of the oscillations were measured. In terms of the complex frequency description the resonance was located at $\omega_0 - i\varepsilon \simeq 1.76 - i\ 0.026$, where the analysis has been conducted on the non-dimensional problem. This frequency is very close to the non-dimensional frequency of the $T = 10.25\ s$ incident waves so that large forces and displacements may occur when the body is excited by such a wave. More importantly, the decay constant is significantly smaller than in the test cylinder case and hence the oscillations will tend to persist in any simulations of moderate length (up to 20 periods). In particular, the time taken for the oscillation amplitude to decay by $1/\varepsilon$ is approximately 110 seconds so that for the $T = 10.25$ s waves more than ten periods must elapse before significant decay occurs and for the shortest period ($T = 5\ s$) waves 20 periods must elapse. The difference in decay rate between the current cylinder and the test cylinder is due to the larger radius and shorter draft of the test cylinder – when it oscillates it is more effective at radiating waves and hence energy than the more slender cylinder of longer draft which is currently under consideration. Therefore, the decay in the motion for the shorter, wider cylinder will occur more rapidly.

The linearised heave motions for the four incident waves are compared to the first order WAMIT results for the four regular incident waves in Figure 15. The effect of the natural resonance of the body can be observed in all cases and particularly for the near-resonant case $T = 10.25\ s$ where the heave oscillation amplitude grows in time. However, the comparison between the linearised OXPOT and linear WAMIT results is made more difficult by the presence of the transient resonant oscillation as it contributes significantly in most cases. For the incident wave with a period of 7 s the natural body resonance is excited but not as much as in the subsequent longer period cases and a relatively good agreement can be observed in the heave motion amplitudes. The variations in the amplitude and phase of the oscillations are due to the interaction of the resonant and forced (incident wave) mode contributions. For the incident wave of period 9 s, the variations in the amplitude are also evident – the oscillation amplitude increases and decreases over the duration of the simulation. If the simulation time was longer the amplitudes would increase over the subsequent periods in the same manner as beating interference pattern due to the interference of two modes of similar frequencies. In the final incident wave case ($T = 10.25\ s, H = 6\ m$) the incident wave frequency is approximately equal to the body resonance so that significant growth of the amplitude of the oscillations occurs for the duration of the simulation. This amplitude growth will eventually cease as

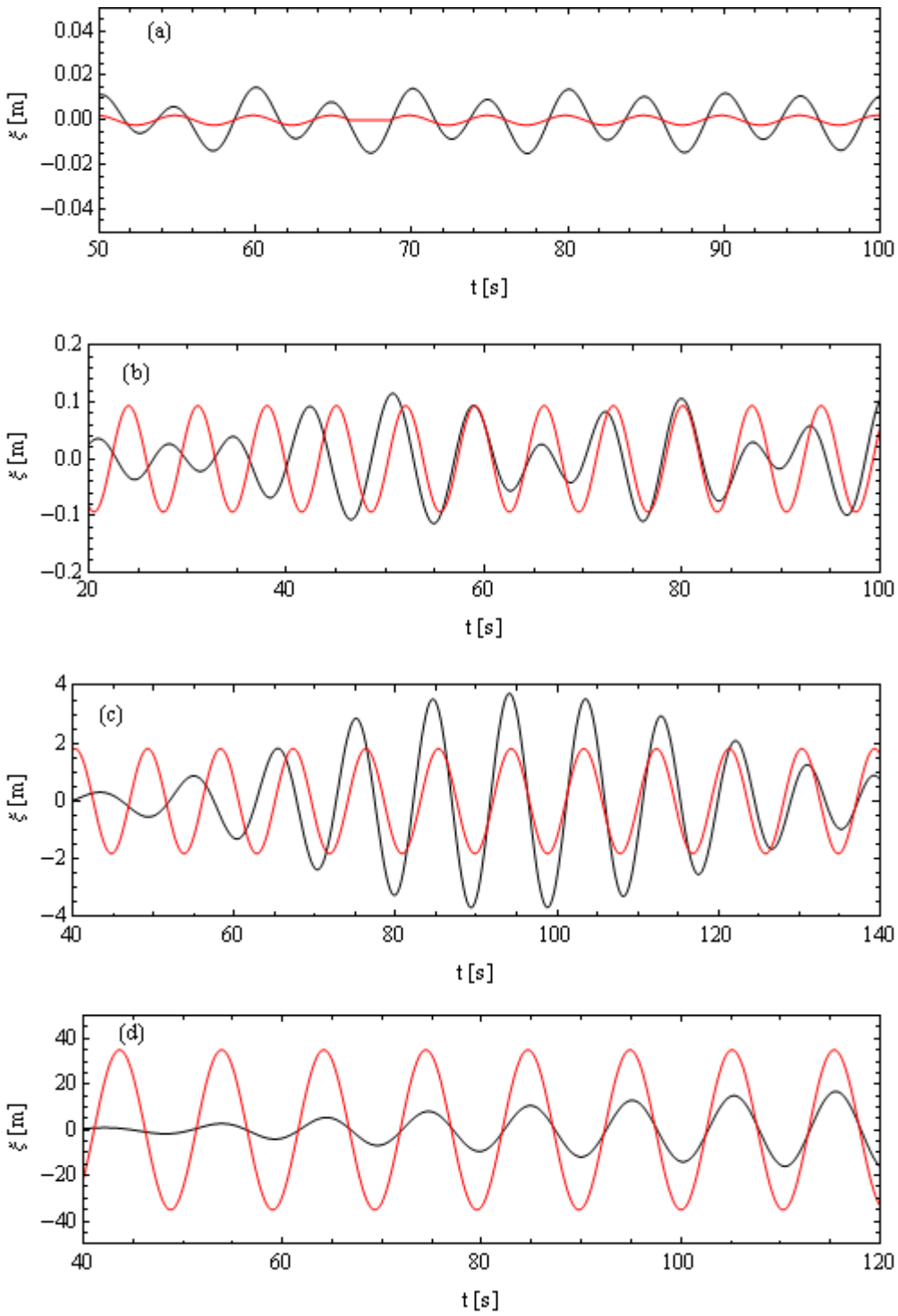

Figure 15: Heave displacement of a cylinder free to respond to incident waves in heave only for waves (a) ($T = 5\ s, H = 1\ m$), (b) ($T = 7\ s, H = 2\ m$), (c) ($T = 9\ s, H = 4\ m$), (d) ($T = 10.25\ s, H = 6\ m$) as computed by OXPOT (black) and from the WAMIT results of WG1 WP1 D8 (red).

the transient decays leaving a steady state oscillation. It is difficult to estimate the amplitude that would be reached in the OXPOT computations as non-linear effects will become significant for such large body motion.

4.2.3 Fully unconstrained motions of the cylinder

The fully nonlinear response of a single cylinder in regular waves was also simulated. The motions in surge, heave and pitch are presented for the four regular waves of interest identified previously. The agreement is reasonably good in heave as identified previously; however, the agreement between the linearised OXPOT results for the surge and pitch motions compared to WAMIT results is limited. One point worth mentioning is that the simulation of the unconstrained response of the cylinder to the regular waves of period 10.25 seconds (close to the natural resonance of the body) experienced convergence problems as the simulation progressed due to the increasing motions of the cylinder. In all cases, the fully nonlinear surge motion involved an increasing difference-frequency term corresponding to the drift motion of the cylinder down the tank parallel to the direction of wave incidence. The mesh is automatically regridded at every time step so OXPOT is capable of simulating such drift motions. Problems can arise however if the cylinder approaches one end of the subdomain in which it is situated. The drift motions were observed to be larger for the incident waves of larger amplitude.

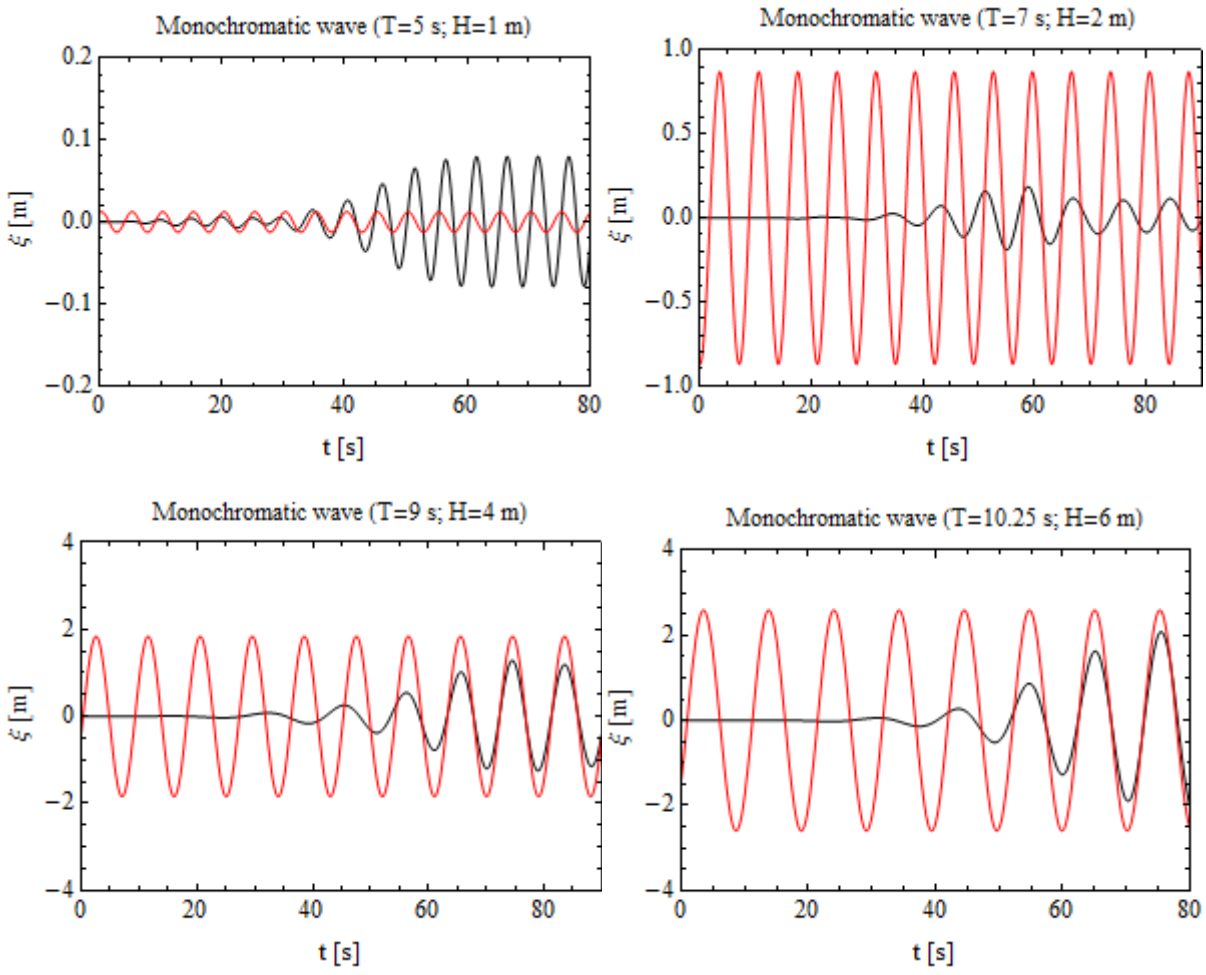

Figure 16: Unconstrained linear response in surge of a single floating truncated cylinder to regular incident waves as computed by OXPOT (black) and compared to the frequency domain results of WG1 WP1 D8 results (red) for the four key incident waves.

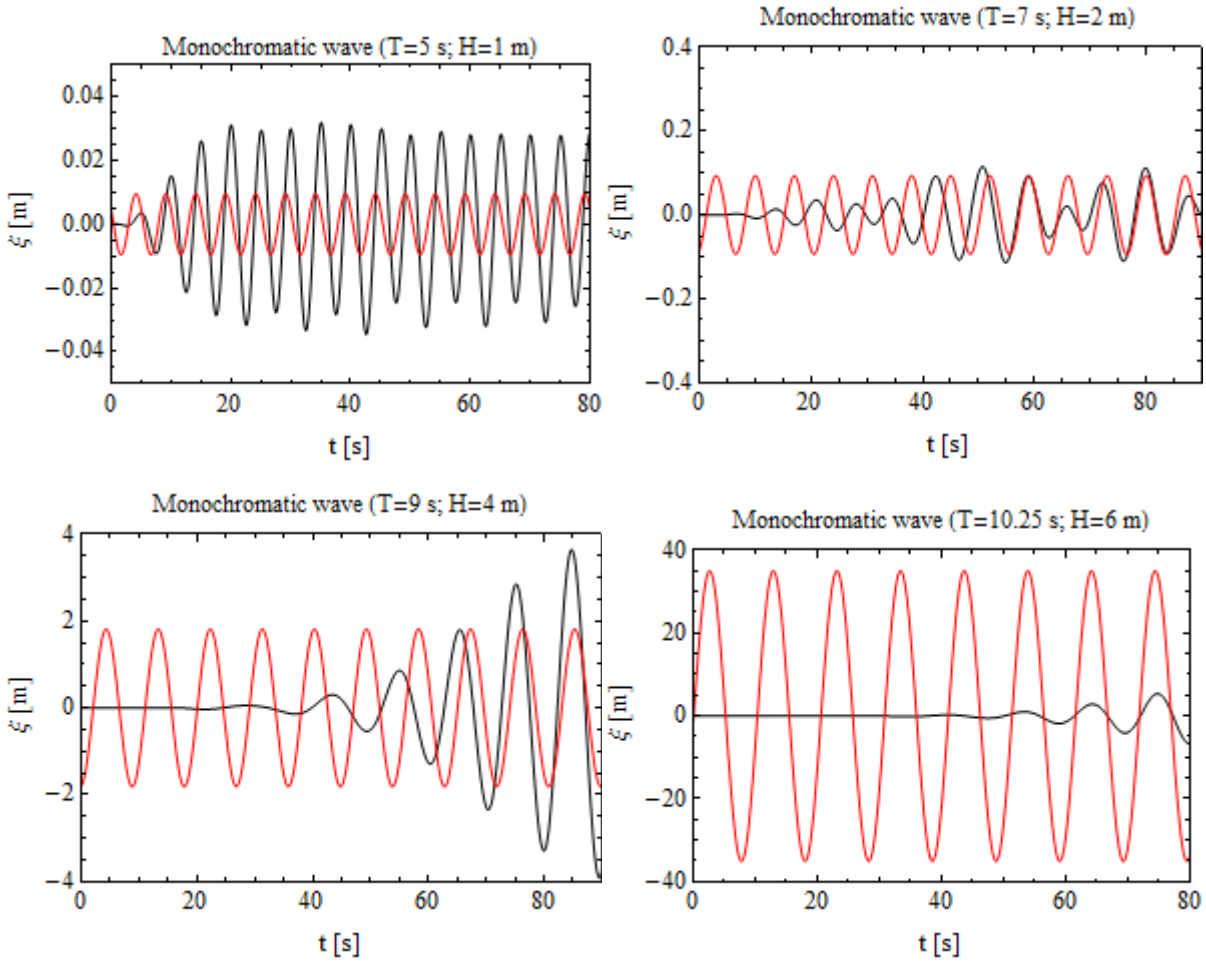

Figure 17: Unconstrained linear response in heave of a single floating truncated cylinder to regular incident waves as computed by OXPOT (black) and compared to the frequency domain results of WG1 WP1 D8 results (red) for the four key incident waves.

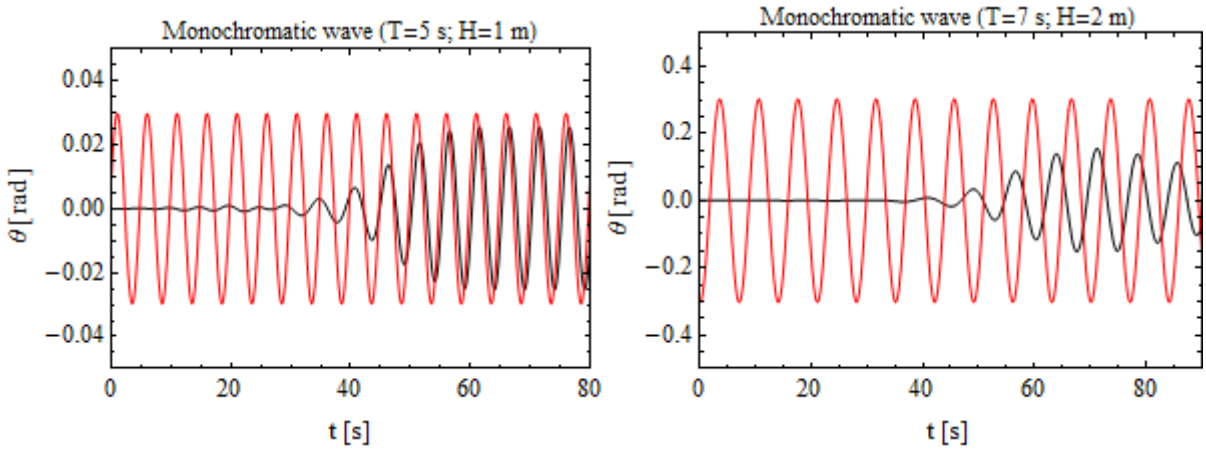

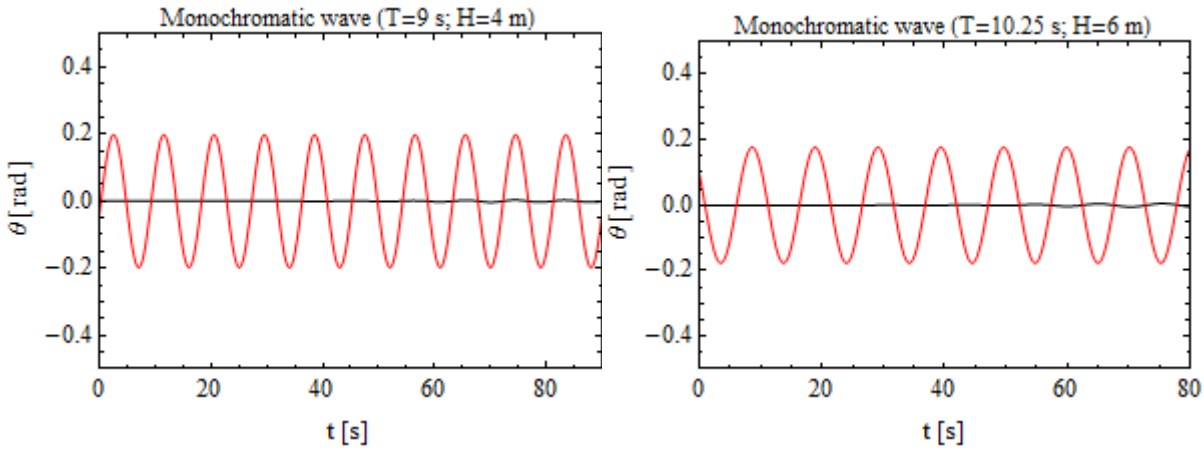

Figure 18: Unconstrained linear response in pitch of a single floating truncated cylinder to regular incident waves as computed by OXPOT (black) and from the frequency-domain results of WG1 WP1 D8 (red) for the four key regular incident waves.

4.3 Summary of linear analysis

In this section it has been shown that OXPOT is capable of successfully simulating the linear component of wave-structure interactions within the fully nonlinear hydrodynamic simulations. The agreement of the OXPOT and WAMIT results for the diffraction problem is excellent, particularly for the surge and pitch forces, for all four incident waves identified as the key comparison cases in WG1 WP1 D8. The heave force computations do not agree quite as well but this is a consequence of the reflections that occur due to the presence of the side walls near the cylinder. The effect of these reflections on the force computations was clearly demonstrated as part of an independent verification of the code. It was also shown how increasing the width of the computational domains mitigates this problem; however, the simulations become much more computationally expensive as a consequence of this increase in domain size.

The response of the body in heave to incident waves has also been simulated and the motion of the body, as expected for a time-domain code, consists of a mode due to the incident wave forcing and a decaying free vibration mode due to the excitation of the natural resonance of the body. The presence of this resonant term makes comparisons of the OXPOT results to the frequency-domain results more difficult because frequency domain results only describe the oscillations due to the wave incidence. The unconstrained motion of the body in surge, heave and pitch was also modelled with qualified success.

5 SINGLE TRUNCATED CYLINDER SIMULATIONS – A SECOND ORDER ANALYSIS

To obtain the second order forces from the OXPOT simulations we sum the forces that arise in two numerical simulations run with incident waves that are π out of phase. The resultant force will be

$$F^{(2)}(t) = F^{(0)} + A^2 F^{(2)}(t) + \cdots \tag{20}$$

and assuming the $O(A^4)$ term is negligible this gives us the second-order sum and difference frequency terms $F^{(2)}(t)$ and $F^{(0)}$, respectively. To obtain the sum-frequency component it is necessary to subtract the slowly varying (or in a regular wave-field the mean) term $F^{(0)}$ from the total second-order force. This difference frequency term will arise as a positive or negative force around which the sum frequency oscillates. For example, the second-order pitch moment for the $(T = 7s, H = 2\ m)$ wave is shown in Figure 19 (a) where towards the end of the simulation there is a mean second-order force which is positive. In the OXPOT simulations it was typical to observe variations in the mean value – a long wave oscillation – but it is still possible to obtain an approximation for the second-order difference frequency term by taking the average value of the force oscillations over the approximately steady-state part of the interaction corresponding to the time interval $(60\ s, 90\ s\ )$ in Figure 19 (a). In this case, the mean value of the second order oscillations is $F_5^{(0)} = 1.05\ MNm$. In a similar manner to the first order force comparisons, a comparison between the second-order force results from WG1 WP1 D8 was sought. A visual comparison of the second-order sum frequency pitch moment from WG1 WP1 D8 and as computed by OXPOT is shown in Figure 19 (b) over the time interval $(60\ s, 90\ s)$. There is a large disparity in the results and the agreement between the second-order difference-frequency force computations is not significantly better: the results from D8 give a value of $F_5^{(0)} = 0.85\ MNm$.

The second order surge and heave comparisons do not yield good agreement either, in fact in the surge case the OXPOT sum-frequency results are much smaller than those predicted in WG1 WP1 D8 as is shown in Figure 20. It is clear that the difference is not merely a constant factor because the differences for surge, heave and pitch all vary in magnitude. With similar results arising from the other incident wave calculations, it was decided to test the OXPOT computations against existing results.

5.1 Independent second order OXPOT comparisons

The truncated cylinder problem is a computationally challenging problem because of the presence of a sharp corner at the bottom of the cylinder. In physical flows, the corner tends to give rise to flow separation while in mathematical terms there is an associated singularity in the Euler equations. In numerical computations, this singularity can generate numerical instability and so convergence of the solution is slower than in the case of a simpler structure such as a bottom mounted cylinder. In the literature of water wave interactions there many more results at second order for the loads on a bottom mounted cylinder in waves. Therefore, it was decided to investigate the second order computations in OXPOT in the context of a bottom mounted cylinder diffraction problem.

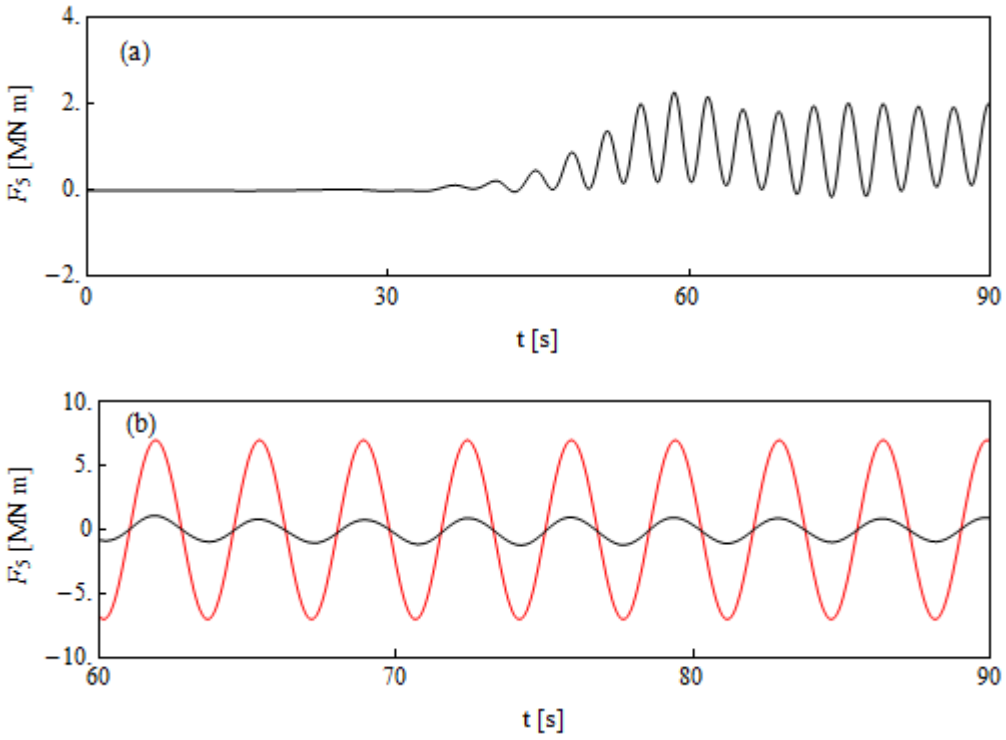

Figure 19: Second-order pitch excitation moment for the incident wave $(T = 7\ s, H = 2\ m)$ as computed by OXPOT (black) (a) over the total simulation range and (b) compared to the results from WG1 WP1 D8 (red) over the steady state interval.

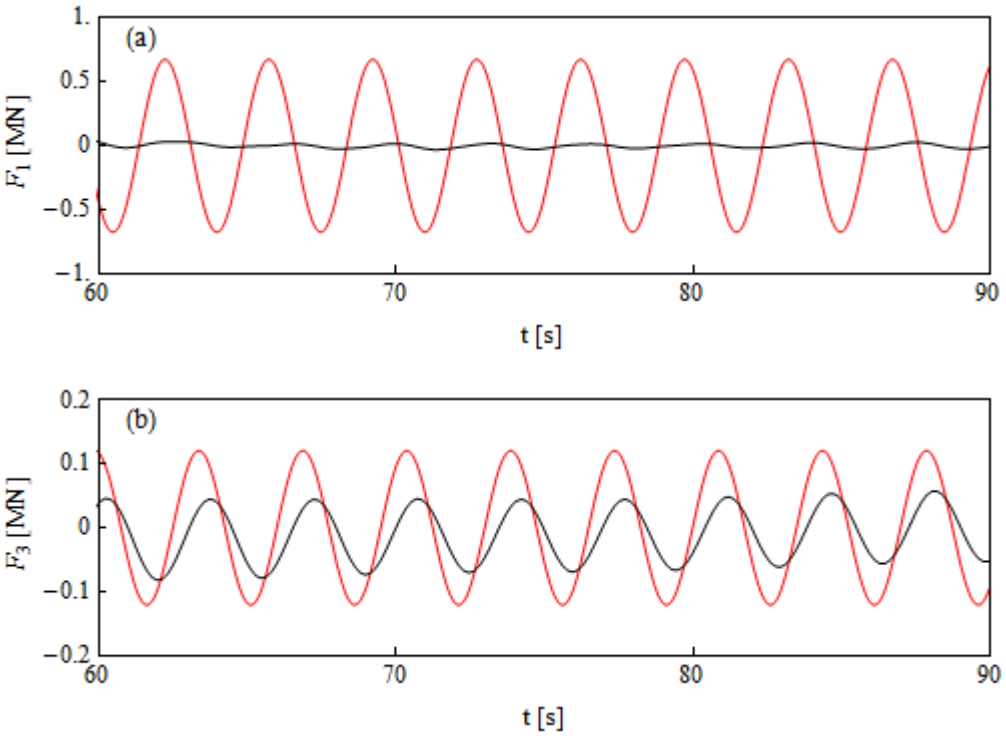

Figure 20: Sum-frequency excitation forces for (a) surge and (b) pitch as computed by OXPOT (black) and compared to D8 results (red) for the incident wave $(T = 7\ s, H = 2\ m)$.

(Zang, et al., 2010) and (Zang & Taylor, 2010) describe an experiment performed at DHI in the large coastal basin to measure the loads on a bottom mounted cylinder due to non-linear wave impact for the case of localised incident wave groups. The advantage of using compact focussed wave groups to investigate hydrodynamic loads is twofold: over the duration of the interaction no extraneous effects due to the presence of side-walls and absorbing beaches will interfere with the results and also it is possible, by careful control of the phase of the wave generated, to extract the harmonic structure of the loading on the cylinder. This phase control approach is the experimental implementation of the method used to extract the linear and second-order forces in the OXPOT simulations: namely to generate two experiments with the incident waves π out of phase so that the first and second order forces can be obtained by combination of the signals. Higher order forces were obtained by digital filtering of the odd and even harmonics but the first and second order terms only are considered here.

In the experimental setup, the cylinder was placed 7.8 metres from the wavemaker paddles in equilibrium in a tank of length 35 metres and width 25 metres. The depth of the water was 0.505 metres and the radius of the cylinder 0.125m. The computational domain for the OXPOT simulation (the numerical wave tank) was by necessity significantly narrower by comparison and due to the presence of an effective damping layer it was possible to use a shorter model of the experimental tank. A comparison of the experimental and numerical simulation configurations is given in Table 8. The compact focussed wave group was a New Wave type wave group (see section 4.4 of WG1 WP1 D7 for details) with a JONSWAP spectral shape of peak frequency $0.61\ Hz$ and a peak enhancement γ coefficient of 3.3.

To simulate the interaction between such a compact focussed wave group and a bottom mounted cylinder, it was first necessary to ensure that the incident wave generated by the piston wavemaker in the numerical simulation was similar to that generated by the piston paddle array in the experimental setup. Therefore, a wave propagation simulation was conducted with the free-surface elevation computed at the position where the cylinder was to be placed (the focus point) and at other positions near the focus. The results were then compared to the corresponding experimental measurements. The computational domain was discretised as follows: the total domain was divided into 8 subdomains of length 1.75 and width 1.5 with 12 elements and 10 elements in the horizontal direction on the side walls and subdomain interfaces, respectively. The number of elements in the vertical direction was 6 so that on the side walls (interfaces) there were a total of 84 (70) elements. The meshing corresponded to approximately 13 elements per second order wave-length assuming the length of side of a free-surface element was similar to that on the side wall. The simulation results and experimental measurements are compared at two different points in the wave tank – the first at the focus point and the second one metre upstream of this focus – in Figure 21. Although there is some slight disparity between the two signals around the troughs and crests either side of the central crest, the difference was considered to be sufficiently small for the diffraction interaction to be simulated using the same piston paddle motion for wave generation.

The interaction problem involved a cylinder of radius $r = 0.125$m diffracting a compact focussed wave group of peak wavelength 1.97m and so the cylinder is, in relative terms, slender. Therefore, the meshing of the cylinder could be relatively coarse; the cylinder circumference was divided into 6 intervals and 6 vertical elements were placed in each interval so that the cylinder was meshed by 36 quadrilateral elements. The rows of element were clustered towards the top of the cylinder. On the

Quantity	Experimental	Numerical
Depth	$0.505m$	0.505
Width	$25m$	1.5
Length	$35m$	14
Cylinder –Paddle Distance	$7.8m$	7.8
Cylinder Diameter	$0.25m$	0.25

Table 8: Numerical and experimental wave tank cylinder characteristics.

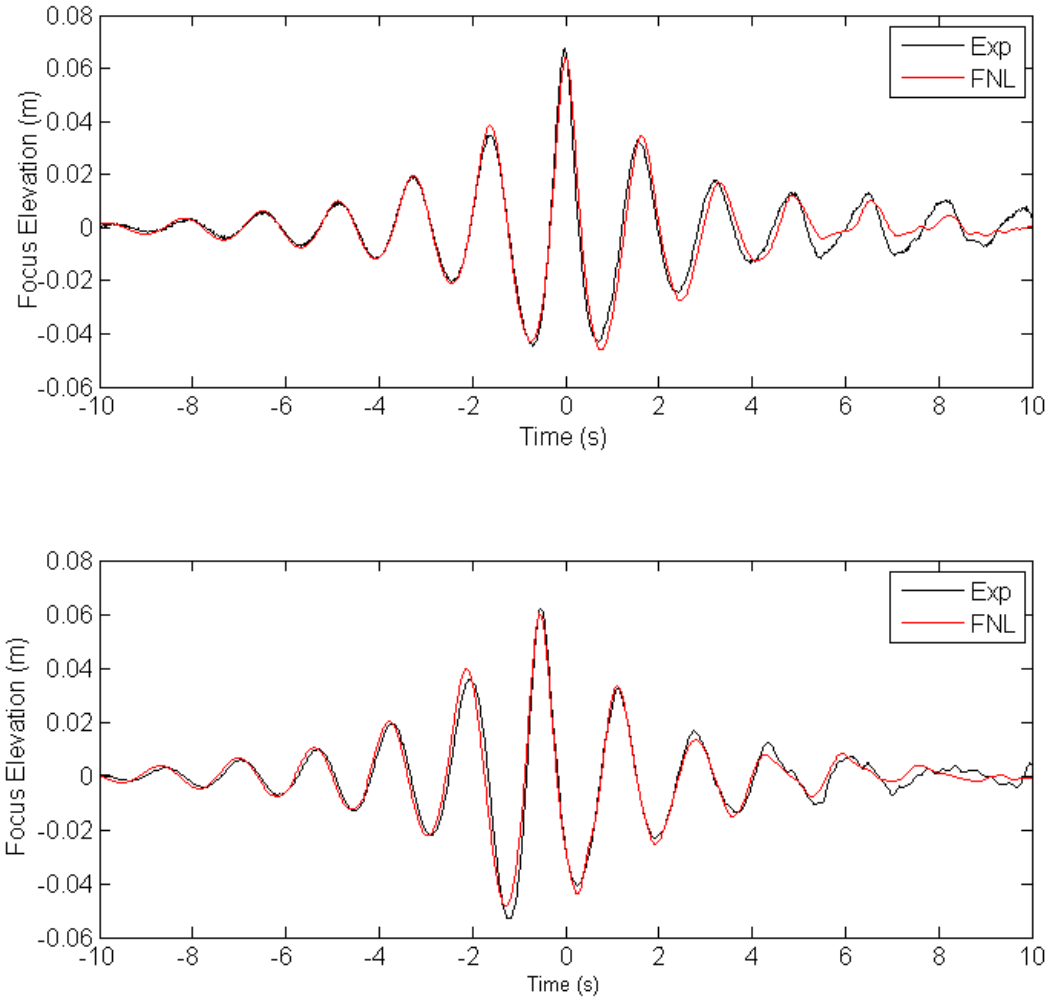

Figure 21: Comparison of the free-surface elevation at (a) the focus point and (b) one metre upstream of the focus as computed by OXPOT (red) and measured in the experiment (black).

horizontal plane, the triangular free-surface elements immediately around the cylinder had a length of side of approximately $\pi r/6 \simeq 0.065$ which was approximately 48 elements per first-order wavelength and 15 elements per second order wavelength. In total, there were 3336 elements on the computational domain boundary with an associated set of 9461 nodes. The simulation time was specified to be 30 seconds with a time increment of 0.01s and the total computational time was approximately 120 hours.

The simulation results, after the first and second order harmonics have been extracted, are compared to the corresponding harmonics extracted from the experimental data in Figure 22. The agreement is very satisfactory at both first and second order although the agreement is slightly better in the case of the first order results. Nevertheless, the magnitude and phase of the second-order sum frequency force time history is very similar and the overall trend of the interaction is predicted extremely well. These results provide compelling evidence that OXPOT is capable of accurately predicting the non-linear dynamics in a diffraction interaction. However, the case of diffraction by a bottom mounted cylinder is much simpler in terms of flow complexity than the corresponding problem for a truncated cylinder. More extensive second order investigations are necessary to understand the second order truncated cylinder problem and this will inevitably result in a further increase in computational times.

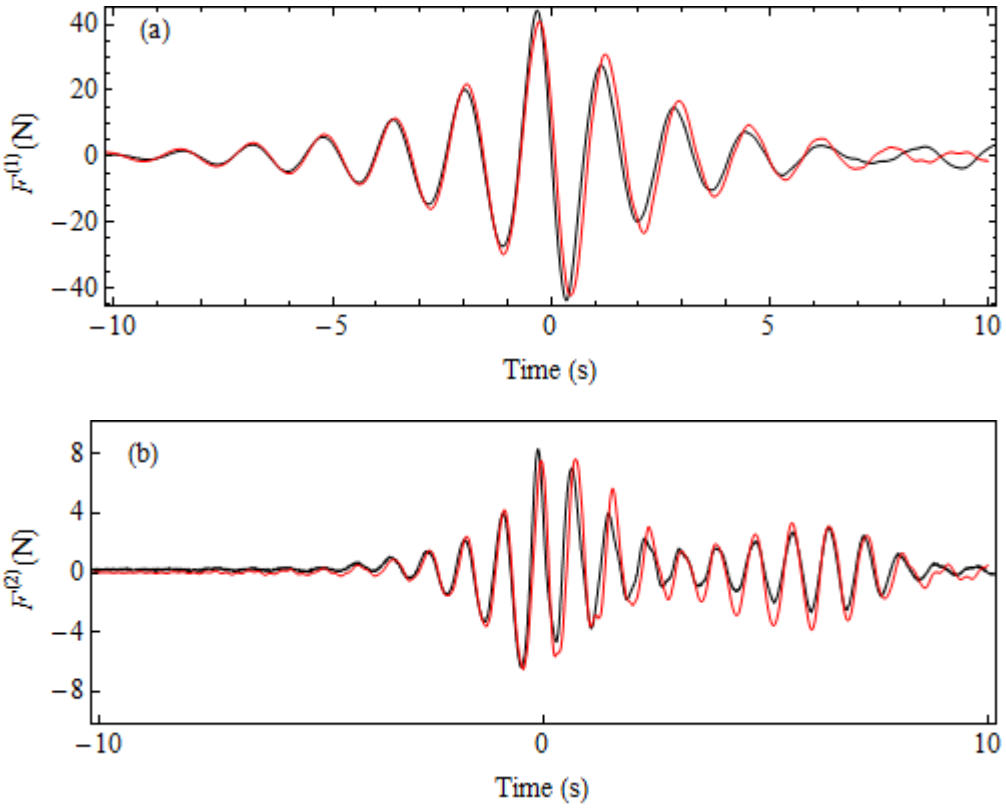

Figure 22: Comparison of numerical (red) and experimental (black) results for (a) linear and (b) second-order sum frequency surge forces on the bottom mounted cylinder.

Simulation	First order force $\boldsymbol{F^{(1)}[N]}$	Second order force $\boldsymbol{F^{(2)}[N]}$
WAMIT	$-2.13 - i\ 44.32$	$-3.65 - i\ 7.75$
DIFFRACT	$-2.14 - i\ 44.16$	$-3.70 - i7.83$

Table 9: Comparison of frequency domain results for the regular wave diffraction by the bottom mounted cylinder at the peak focussed wave frequency $0.61\ Hz$.

Although comparing OXPOT and second order results directly is of most relevance, the existence of data from a frequency-domain code developed in Oxford, known as DIFFRACT, for this problem allowed a cross comparison of results with the WAMIT second-order approach used in WG1 WP1 D8. Therefore, first-order and second-order WAMIT results were generated in the same manner as in WG1 WP1 D8 by GH and passed to the University of Oxford for comparison with the existing DIFFRACT results for the case of regular wave diffraction by the cylinder described above at the peak frequency $f_0 = 0.61\ Hz$. The results for both the first and second order forces are shown in Table 9 and the agreement is excellent. Therefore, in the case of the bottom mounted cylinder, OXPOT is consistent with experimental data and the second order frequency-domain method used in WG1 WP1 D8 is consistent with in-house frequency-domain data available to us.

A regular wave diffraction simulation involving weakly nonlinear waves interacting with a bottom mounted cylinder was also investigated in order to examine in more detail the differences that might arise between the nonlinear time domain results and the frequency domain results. In this problem the incident wave and cylinder are described in non-dimensional terms and so the density ρ, gravitational acceleration g and the water depth h are assumed to be unity. The wave is specified to have a wavenumber parameter $kh = 4.0$, corresponding to a non-dimensional frequency $\omega = 1.99395$ and period $T \simeq \pi$, and is generated by a piston motion of the leftmost wall of displacement amplitude $a_p = 0.01h$. This wave is weakly nonlinear and, from the linear theory (7), has an amplitude of approximately $A = 0.01988$ (with a corresponding nonlinearity parameter $H/\lambda = 0.0253$ or $kA = 0.0795$). The cylinder, of radius $r = 0.2h$, is located a distance $5.25h$ from the undisturbed piston wavemaker in a numerical wave tank of total length $9.0h$ and width $2.0h$. The sidewalls in each subdomain have 12 elements in the horizontal x-direction and the interfaces have 16 elements in the horizontal y-direction with 6 elements in the vertical z-direction on all boundary walls. There are 374 triangular elements on the free-surface in all subdomains apart from the subdomain containing the body where there are 572. The circumference of the body was divided into 16 intervals and each interval had 6 vertical elements. The horizontal extent of mesh elements at the body is approximately 0.04 corresponding to 40 (10) elements per first- (second-) order wavelength. In total there are 4022 elements distributed on the computational domain with a corresponding set of 10891 nodes; a plot of the free-surface and body meshes are shown in Figure 23. Furthermore, a summary of the mesh properties is provided in Table 10. The interaction was simulated for 18 wave periods with a time step of $0.025T$ and took 70 hours to complete.

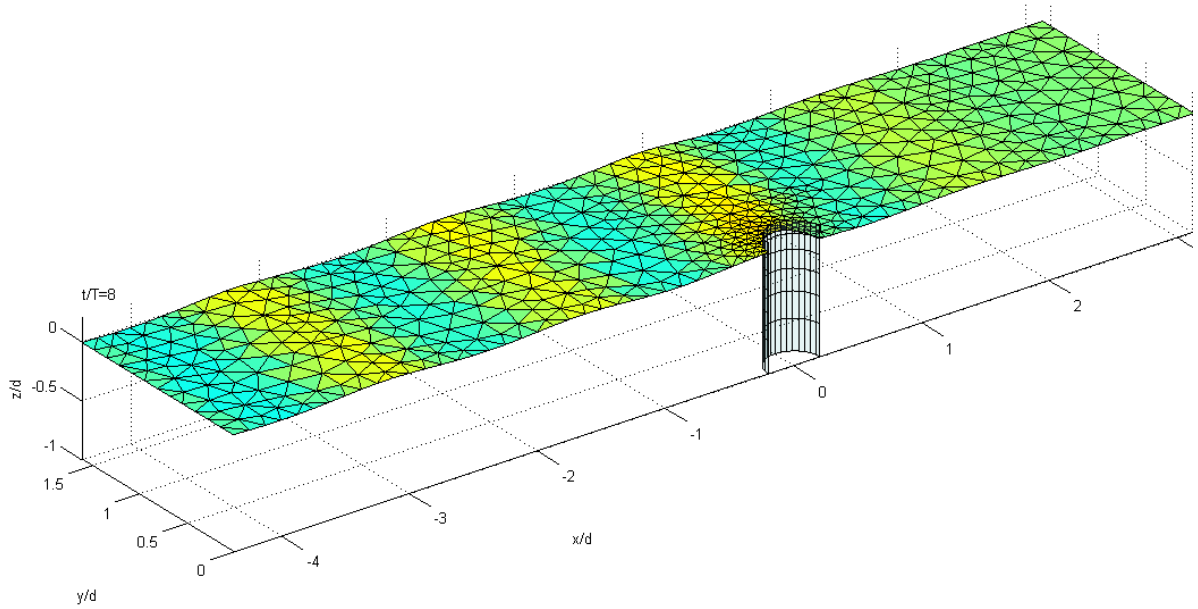

Figure 23: Unstructured free-surface mesh and structured cylinder mesh for the diffraction problem involving a bottom mounted cylinder of radius $0.2h$.

The first order surge excitation force results for OXPOT are compared to existing data from DIFFRACT in Figure 24 (a). The agreement is good and a measurement of the steady state amplitude between $t/T = 10$ and $t/T = 18$ gives a surge force amplitude of $F_1 = 5.0 \pm 0.1$ compared to DIFFRACT value of 5.205. So, although the agreement is good it should be noted that there is a 4% difference between the mean OXPOT force and the DIFFRACT force. The second order sum-frequency surge force OXPOT results are compared to the corresponding DIFFRACT results in Figure 24 (b). Notice that the mean second-order force component has been subtracted from the total second order force to enable the comparison of the sum frequency terms. The OXPOT second order sum-frequency force agrees quite well with the DIFFRACT computations although there are some significant unsteady motions around $t/T = 10$ and $t/T = 16$. Given that the magnitude of the second order force is much smaller than that at first order it is not surprising that this sum-frequency force does not settle to a steady state in the same manner as the first order force. Furthermore, it takes several cycles for the transient motions at the wave front to settle down and any such transient effects are likely to be magnified at second order. The mean second order force on the interval $(10T, 18T)$, where the second order response has become an almost steady oscillation, was computed to be $F^{(0)} = 0.59$ while the second order difference-frequency force computed by DIFFRACT was $F^{(0)} = 0.67$. This is indicative of the reasonably satisfactory agreement between the time-domain fully non-linear simulation and the weakly non-linear frequency domain computations.

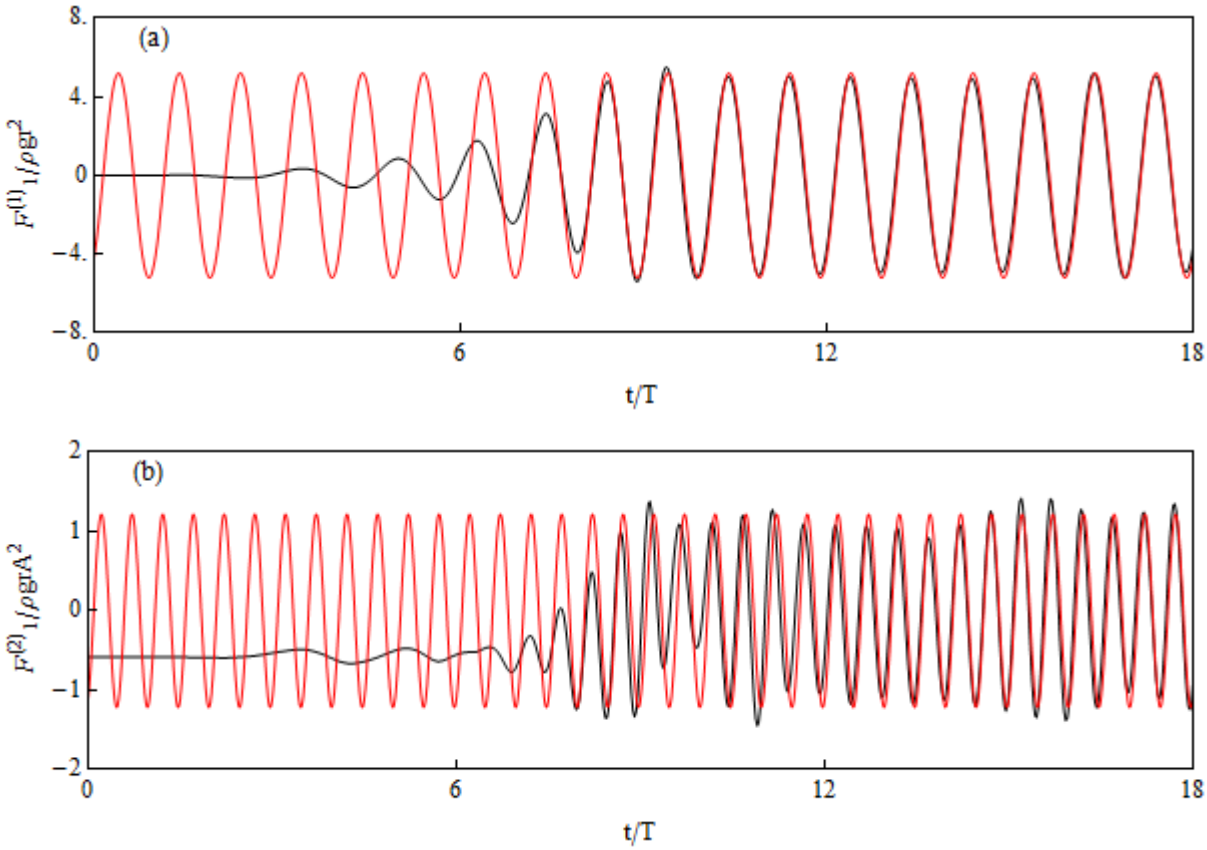

Figure 24: Comparison of non-dimensional surge excitation forces as computed by OXPOT (black) and DIFFRACT (red) in (a) first-order and (b) second order sum-frequency.

It should be mentioned that for the regular wave diffraction problem involving a bottom mounted cylinder (described above) a simulation involving a coarser mesh was also used. However, the domain itself was also smaller so it is more difficult to assess the effect of the mesh density on the results. Nevertheless, a summary of the main mesh properties for the two simulations is provided in Table 10. Both domains were divided into six subdomains and the number of vertical elements was held constant. However, in the simulation with the smaller computational domain (simulation 2 in Table 10), the cylinder was discretised into 48 elements with 8 intervals on the circumference as opposed to 16 intervals on the circumference for simulation 2 described previously. Furthermore, the number of free-surface elements per unit free-surface area was approximately 130 in the simulation with the finer body mesh and 90 in the simulation featuring the coarse mesh. The second order sum-frequency forces are compared to the DIFFRACT results in Figure 25 and although the force is on average larger than that shown in Figure 24(b) for the previous simulation, the trend of variations in time of the force is very similar in both cases. Furthermore, the mean second-order difference frequency term is 0.57 as compared to 0.59 in the previous simulation. Although it is not possible to discern whether convergence of the second-order solution has definitely occurred, the similarity in the responses for a doubling of the mesh fineness on the body indicates that the results presented in Figure 24 are an accurate representation of the second-order forces.

Simulation	Comp. Domain		Intervals		Body mesh		Free-surface	
	(L, L_{SUB})	W	n_x	n_y	n_{CIRCUM}	n_z	Elements	Nodes
1	(9.0,1.5)	2.0	12	16	16	6	2342	5044
2	(7.5,1.25)	1.6	10	12	8	6	1098	2472

Table 10: Mesh properties for the simulations of the regular wave diffraction by a bottom mounted cylinder.

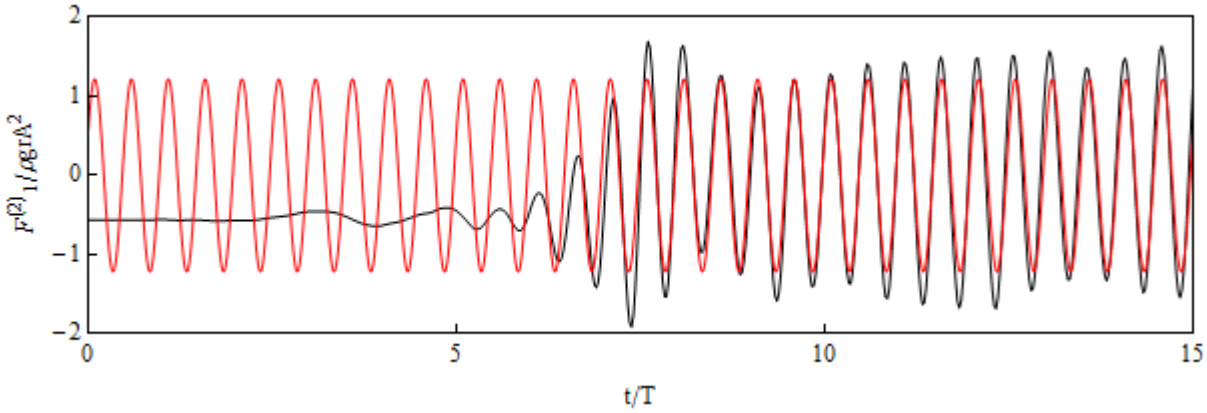

Figure 25: Second order sum-frequency excitation force as computed by OXPOT (black) and WAMIT (red) for the coarsely meshed cylinder referred to as simulation 2 in Table 10.

From these two case-studies involving experimental and numerical comparison it can be seen that, for the case of a bottom mounted cylinder, OXPOT is generating accurate second order forces. However, there are a number of issues that are worth considering. Firstly, the OXPOT simulation of the diffraction experiment models the second order physics of the interaction quite accurately and this provides a strong validation of OXPOT. However, the context in which this simulation was conducted must be considered. As stated previously, the problem of a compact focussed wave group being diffracted by a bottom mounted cylinder is very suitable for experimental investigation because it yields 'clean' data due to the short time-scale of the interaction – no reflections from side walls interfere during the interaction. The same principle applies to the OXPOT simulations so the focussed wave group experiment provides a good opportunity to properly assess the accuracy of the simulations. In regular wave simulations, the force computations are affected by side wall reflections and it is not always straightforward to compare to open-water frequency domain results. In the second order case the computations are also very sensitive to disturbances from transient or reflected waves. Therefore, OXPOT produces comparatively better results when simulating transient phenomena such as focussed wave groups.

The second factor to consider, which has already been alluded to at the start of this section on second-order forces, is that these simulations involve bottom mounted cylinders and the wave motion which arises from incident wave diffraction by such cylinders is less complex than that occurring in truncated cylinder diffraction problems. Therefore, in the simulation of truncated diffraction problems finer body meshes may be necessary including more vertical elements on the body and also higher mesh densities around the cylinder. Unfortunately, this leads to large computational times but a convergence investigation similar to that conducted for first-order excitation forces on the test cylinder in section 4.1.2 would be useful. It should be noted that in the

simulation of the experiment, the horizontal extent of the elements on the cylinder and surrounding free-surface is such that there are approximately 15 elements per second-order wavelength. In the regular wave diffraction problem there are 10 elements per second-order wavelength. These were typical values for the truncated cylinder problem but may need to be increased to describe the more complex motion around the truncated cylinder.

5.2 Summary of second-order force computational issues

A summary of the second order forces investigation is given here to highlight important observations and to suggest some actions to resolve the uncertainties that have arisen. The OXPOT second-order computations differ significantly from the results in WG1 WP1 D8 as illustrated in Figure 19 (b) and Figure 20. Although the results are presented here for the one incident wave ($T = 7\ s, H = 2\ m$) only, these were a typical representation of the second order force comparisons for the other incident wave cases. In general, the OXPOT results under-estimate the results from WG1 WP1 D8 by more than a factor of 2. Given the disagreement between the second order excitation forces and the occurrence of the transient resonant body mode in the first order motions, the second order OXPOT motions have not been compared to the frequency domain results from WG1 WP1 D8. Before such comparisons can be made the current disagreement between the results must be resolved. The following investigations may be necessary to achieve such a resolution:

- the convergence of the second-order solution for the truncated cylinder simulations should be investigated – longer computational times than in the bottom mounted cylinder simulations can be expected and have been the reason for delays on this course of action;
- a comparison of the OXPOT computations for the second-order excitation forces on a truncated cylinder to an independent set of results – for example (Abul-Azm & Williams, 1988) contains a solution for the hydrodynamic loading on a stationary truncated cylinder up to second-order in wave steepness;
- the bottom mounted cylinder investigation could be extended to include the cases described in the analytical solution by (Eatock Taylor & Hung, 1987);

By following some of these courses of action, it should be possible to understand and resolve the cause of the current disagreement between the OXPOT results and the second order frequency-domain forces provided in WG1 WP1 D8.

However, it should also be emphasised that a very important confirmation of the capability of OXPOT to accurately model nonlinear hydrodynamics has been obtained by simulating the diffraction experiment conducted by (Zang, et al., 2010). The agreement between the numerical results and experimental measurements is remarkably good and this bodes well for the validation studies involving comparison with experimental results that are to be conducted later in the project. The experimental work to be done by QUB in WG2 WP2 will feature rounded cylinders and not truncated cylinders. The absence of sharp corners at the bottom surface of the cylinder should result in a reduction in vortex shedding at the cylinder bottom and this more laminar flow should be easier for OXPOT to simulate. In computational terms the numerical solution for the rounded cylinder interactions should converge faster than for interactions involving the truncated cylinder.

6 VERIFICATION OF TWO-BODY ARRAY INTERACTIONS

The most complex interaction to be considered here involves the diffraction of an incident wave by an array of four truncated cylinders (fixed and allowed to respond in heave). In order to ensure that the generalised multiple body form of the code yields valid results it was considered prudent, as an intermediate step, to investigate two body problems. In particular, the existence of linear frequency-domain solutions for two body problems (see (Matsui & Tamaki, 1981)) provided a good opportunity to validate OXPOT against analytical results. Therefore, in a similar manner to the single body analysis, the excitation and radiation problems were considered for the case of two truncated cylinders. As a preliminary step, the diffraction of an incident wave by a pair of bottom mounted cylinders is also simulated (the bottom mounted cylinder simulations are less computationally expensive).

6.1 Diffraction by a pair of bottom mounted cylinders

(Matsui & Tamaki, 1981) reproduce the excitation forces on a pair of bottom mounted cylinders based on the analytical work of (Ohkusu, 1972) over a large range of frequencies. In order to verify the force computations in the multiple body version of OXPOT, four different diffraction problems were simulated involving regular waves of different frequencies. These (non-dimensional) frequencies were chosen to be similar to the frequencies of the four incident waves identified as key cases in WG1 WP1 D8.

In this diffraction problem, two bottom mounted cylinders of radius a are present in water of depth $h = 5a$ and are aligned along the incident wave direction with the cylinder axes five radii apart. The excitation forces on the cylinders in regular waves were computed using the general method for multiple cylinders described by (Evans & Porter, 1997) over the range of wavenumbers from $ka = 0.1$ to $ka = 2.0$ for comparison with OXPOT. In the OXPOT simulations, the cylinder was chosen to have a radius of $a = 0.2$ so that, as usual, the water depth was unity. Similarly, the acceleration due to gravity and density were chosen to be unity also. The wave-tank specifications were dependent on the incident wavelength – the four incident wavenumbers considered were $ka = 0.5, 0.6, 0.8, 1.0$ corresponding to the wavelengths $\lambda \simeq 2.51, 2.10, 1.57, 1.26$. In all cases the amplitude of the wavemaker displacement was chosen to be 0.001 thus generating effectively linear waves. The dimensions of the numerical wave tank for each simulation are shown in Table 11 along with the total number of elements N_E and nodes N on the boundary. The wave forces on each body were then computed using the auxiliary function method (described in WG1 WP1 D7) and compared to the frequency domain results.

The comparison of the OXPOT results to the frequency-domain exciting force amplitudes required the identification of the time at which the diffraction interaction reaches an approximate steady state. By measuring the maxima and minima of the exciting force oscillations during the steady state an estimate for the exciting force amplitude could be obtained. The oscillation of the exciting forces on the two bodies during the simulation is shown for the incident wave of wavenumber $ka = 0.8$ in Figure 26 while a snapshot of the free-surface during this simulation is shown in Figure 27. Note that cylinder labelled 1 (2) refers to the more upstream (downstream) of the cylinders. In Figure 26, the system is close to steady state from $t/T = 12.0$ onwards and it is in this range that the maxima and minima of the exciting forces on both cylinders are measured. Due to reflections from the computational boundaries, particularly the side wall, the surge exciting force signals have some local variations in time. For a single truncated cylinder it was noted that the side-wall reflections did not

affect the surge force results due to symmetry. However, when two cylinders are present the diffracted waves from cylinder 1 which are reflected by the side wall are not symmetric with respect to cylinder 2 (and vice versa) and so a net surge force can be exerted on the cylinders. Intuitively it is expected that the surge force due to reflections will be larger on cylinder 2, initially at least, as the waves arrive at cylinder 1 first. The mean time-domain amplitudes as computed by OXPOT are compared to the analytical frequency-domain results in Figure 28.

ka	λ	Half-width (W)	Length (L)	N_E	N
0.5	2.51	4.0	15.0	2892	8018
0.6	2.10	3.2	12.0	2702	7448
0.8	1.57	2.5	10.0	2926	8080
1.0	1.25	1.75	7.5	2788	6780

Table 11: The numerical wave tank dimensions and the total number of elements and nodes for different incident wavenumbers.

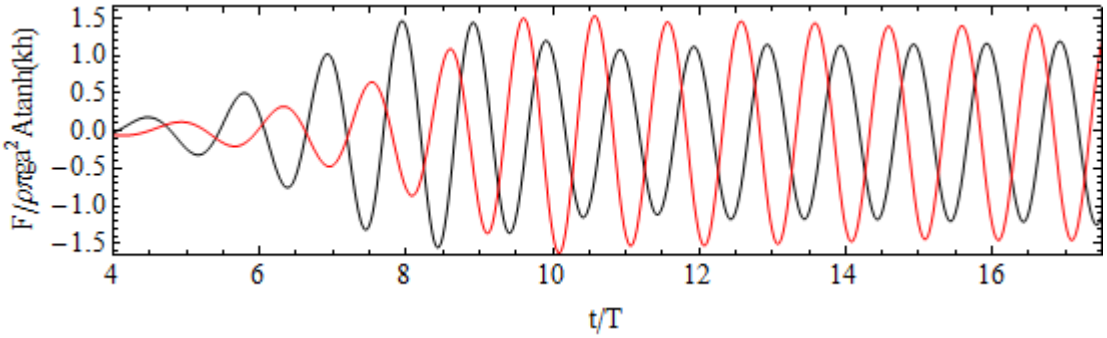

Figure 26: Variation of the exciting force on cylinder 1 (black) and cylinder 2 (red) with time for the incident wave of wavenumber ka=0.8.

6.1.1 Effects of side wall reflections on computations

The agreement between the OXPOT and linear frequency-domain is quite satisfactory as shown in Figure 28. However, these simulations involved domains with significant half widths – in all cases the domain widths were greater than one wavelength. However, for the simulation involving the incident wave of wavenumber parameter $ka = 0.8$ ($\lambda = 1.57$) a previous simulation had been conducted in a numerical wave tank of half-width $W = 1.5$, that is a width just less than one wavelength. On computing the excitation forces for the two bottom-mounted cylinders, the OXPOT value for the force on the second cylinder was found to be significantly larger than the linear frequency domain prediction. An analysis of the simulation showed that a component of the waves scattered by the first cylinder was being reflected from the side wall and impinging upon the downstream cylinder. However, by increasing the width of the numerical wave tank a significant improvement in the OXPOT estimate for the excitation force was observed. To illustrate the influence of the domain width on the computed forces, the forces on cylinder 1 and cylinder 2 from both simulations are shown in Figure 29. The difference between the excitation forces on cylinder 2 for the two tank widths is significant and a decrease in the mean non-dimensional force amplitude from $F_2 = 1.57$ to $F_2 = 1.46$ over the steady state section of the oscillation was observed.

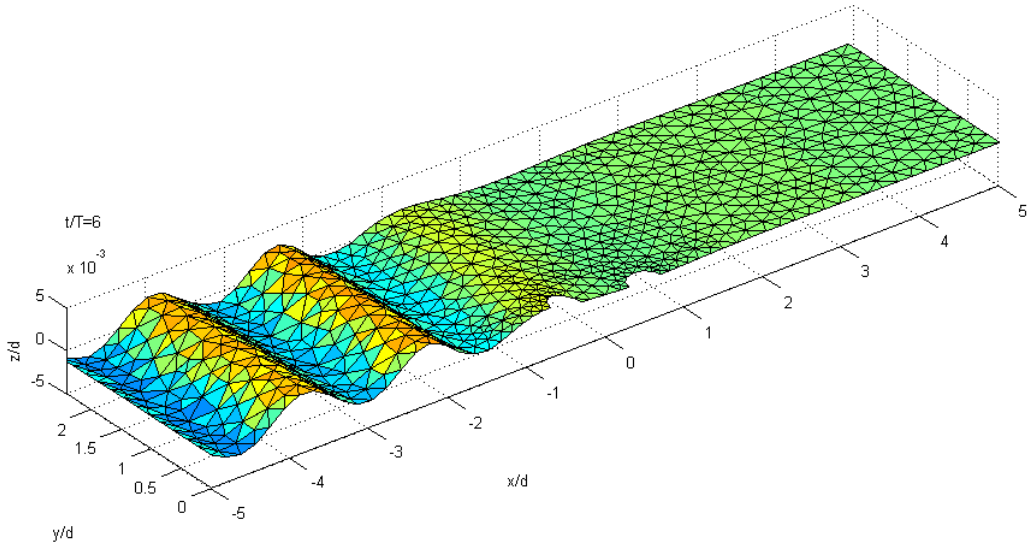

Figure 27: Free surface elevation 6 periods into the diffraction simulation with the incident wave of wavenumber ka=0.8.

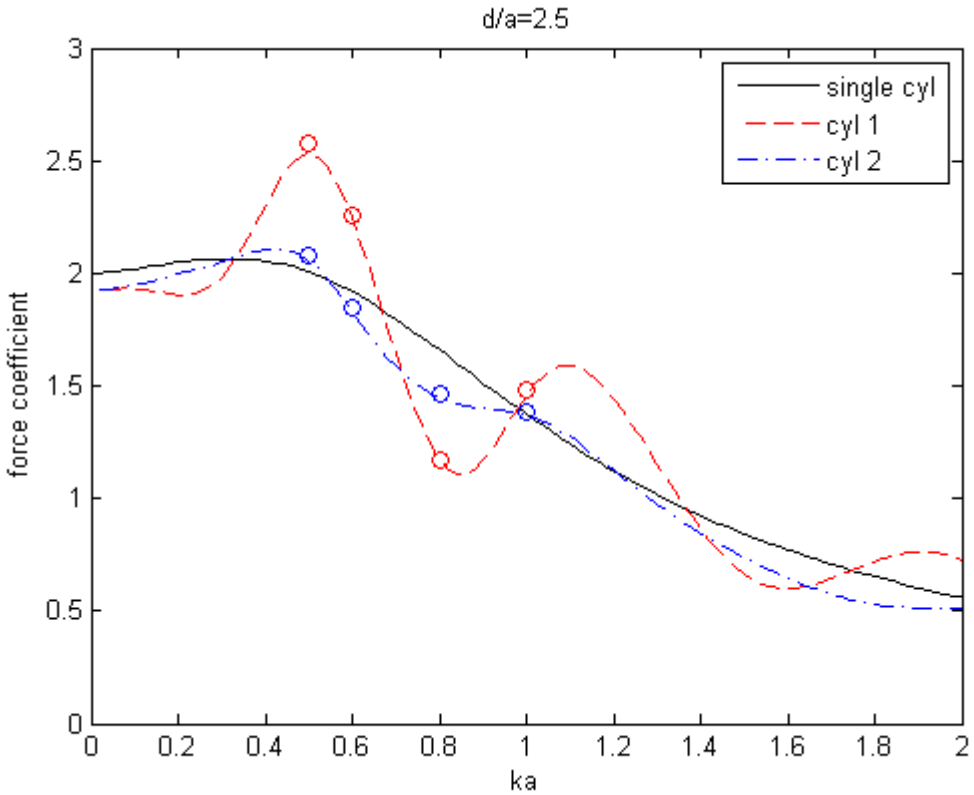

Figure 28: Comparison of exciting force computations from OXPOT (circles) for the four incident wave frequencies to the corresponding analytical frequency domain results (dashed lines).

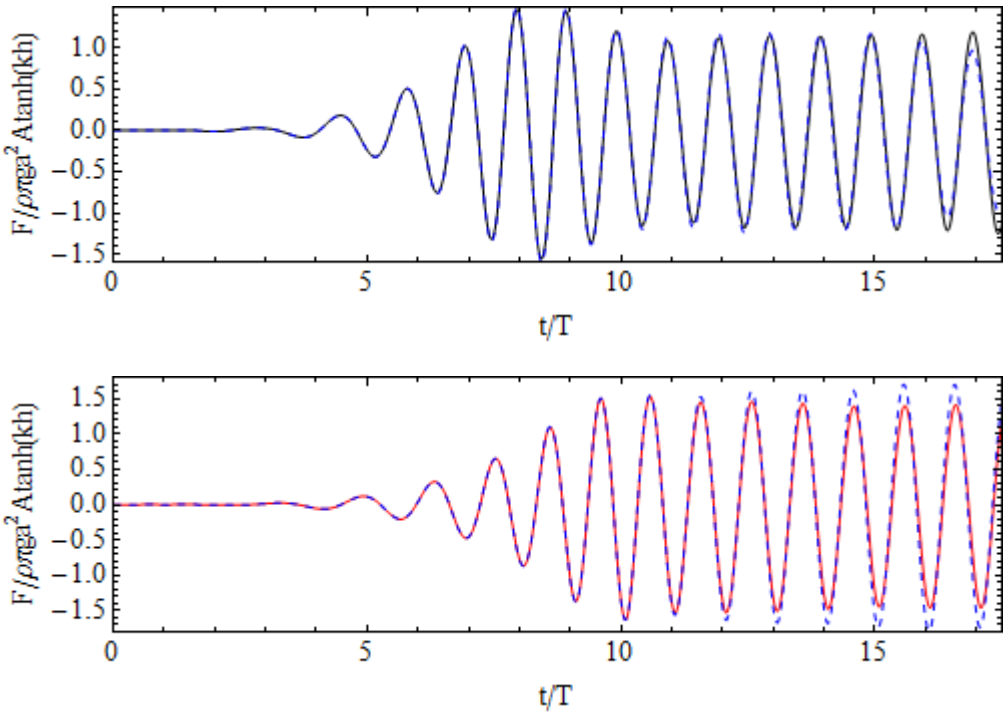

Figure 29: Comparison of excitation forces on cylinder 1 (black) and cylinder 2 (red) for wave tank half-width of W=2.5 and for a wave tank half-width of W=1.5 (blue).

It is clear that side wall reflections can be quite important in the diffraction simulations and this must be borne in mind when interpreting the results for the array of four cylinders. However, the effects can be mitigated with a wider tank (with a consequent increase in computational time) and also by avoiding tank widths close to an integer or integer and a half multiple of the wavelength. The smaller tank width in this case was almost one wavelength and this can result in the occurrence of sloshing modes in the numerical wave tank. As observed in the single body investigations, a domain half-width of at least one wavelength is necessary to avoid artificial reflections.

6.2 Radiation forces in an array of two cylinders

In a similar fashion to the single body verifications, the two body radiation problem was simulated using OXPOT and compared to the radiation force coefficients presented by (Matsui & Tamaki, 1981). In the two body radiation problem, one of the cylinders is forced to heave or surge and the radiation forces on the cylinder radiating the waves and on the fixed neighbouring cylinder are computed. No pitch motion is considered as these results are not available in the paper by (Matsui & Tamaki, 1981). The computational domain in these simulations is significantly smaller than in the excitation force problems because it is possible to implement an artificial damping layer around the total boundary of the domain to minimise reflections. With these reflections minimised it was expected that the agreement between the OXPOT computations and the linear frequency-domain results would better than in the subsequent diffraction study involving truncated cylinders. The radiation problem is described next.

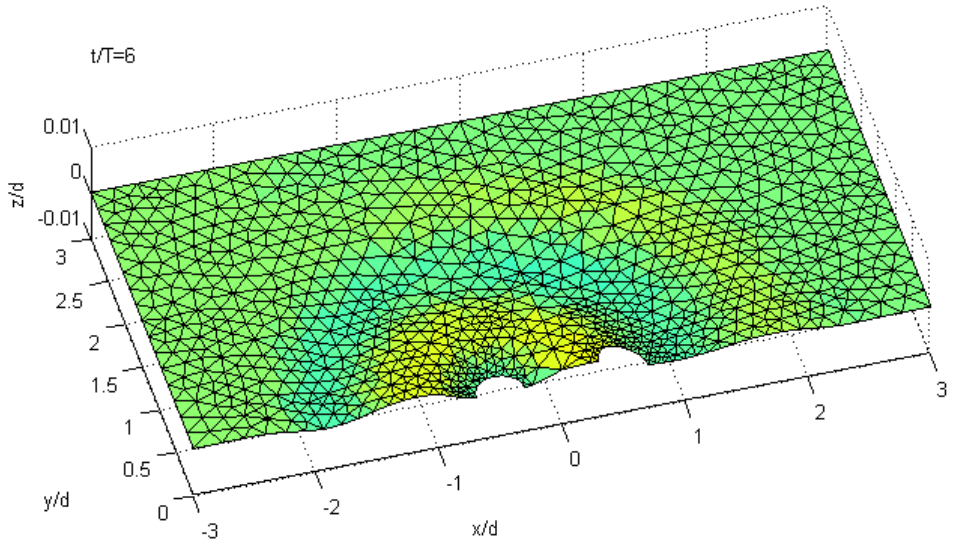

Figure 30: Free-surface mesh for heave radiation simulation after 5 periods have elapsed.

Two vertical truncated cylinders of radius a, draft $a/2$ and a distance $5a$ apart are initially at rest in water of depth $10a$. One cylinder is then forced to oscillate in heave or surge and the forces exerted by the radiated waves on the radiating cylinder and on the adjacent cylinder are measured. These radiation forces are compared with results obtained from the frequency domain analytical solution of this radiation problem given by (Matsui & Tamaki, 1981) using a generalisation of Equations (15) and (16) for the multi-body case. An existing set of frequency domain results generated using DIFFRACT were also available and the comparison between the OXPOT simulation and these results is shown next, followed by a table summarising the comparisons to the analytical results of (Matsui & Tamaki, 1981).

In the radiation problem for which there existed DIFFRACT results, one cylinder is forced to oscillate in heave at the frequency corresponding to $ka = 0.8$ while the other is held fixed. The computational domain is divided into two square subdomains of side length $L_{SUB} = 3.0$ and each subdomain contains a cylinder located at $(x, y) = (\pm 2.5a, 0.0)$ where cylinder C_1 is positioned in the left subdomain . Only one half of the computational domain is modelled due to the symmetry along $y = 0$. On each wall there are 16 horizontal intervals with 6 vertical elements in each interval yielding a total of 96 quadrilateral elements on each side wall and on the subdomain interface. The free-surface in each subdomain is meshed using a set of 1991 triangular elements and the truncated cylinder mesh comprised 60 quadrilateral elements on the curved surface and 94 triangular elements on the truncated surface. In total there were 2796 elements and 6816 nodes distributed on the computational boundary. An illustration of a typical free-surface mesh is provided in Figure 30. The total simulation time is $8T$ and the time step size is $0.025T$, where T is the oscillation period, and the computational time was approximately 65 hours. It should be noted that the artificial damping layer is specified to begin at $\sqrt{x^2 + y^2} = L_{SUB} - \lambda$, where λ is the wavelength of the oscillation, and extends outwards to the domain boundaries so although the total domain is

rectangular the area inside the damping layer is semi-circular. The displacement amplitude of the heave motions is specified to be $a_c = 0.01$.

The heave forces on the oscillating and fixed cylinder and the surge force on the fixed cylinder are compared to the DIFFRACT frequency-domain results in Figure 31 . The agreement is very good in all cases although there is a slight underestimation of the heave force on the fixed cylinder due to the heave oscillations of the other cylinder. The error is less than 1% for the heave reaction force on the heaving cylinder and for the surge force on the fixed cylinder but approximately 7% for the heave force on the fixed cylinder. The heave force computation for the fixed cylinder is quite sensitive because the generation and propagation of the waves by the motion of the oscillating cylinder must be simulated accurately and the interaction of these waves with the truncated surface of the fixed cylinder must also be simulated accurately. Improvements in the accuracy will likely require an increase in the mesh fineness both on the free-surface and on the body. Nevertheless, this test case illustrates the capabilities of OXPOT in multiple body problems featuring truncated cylinders.

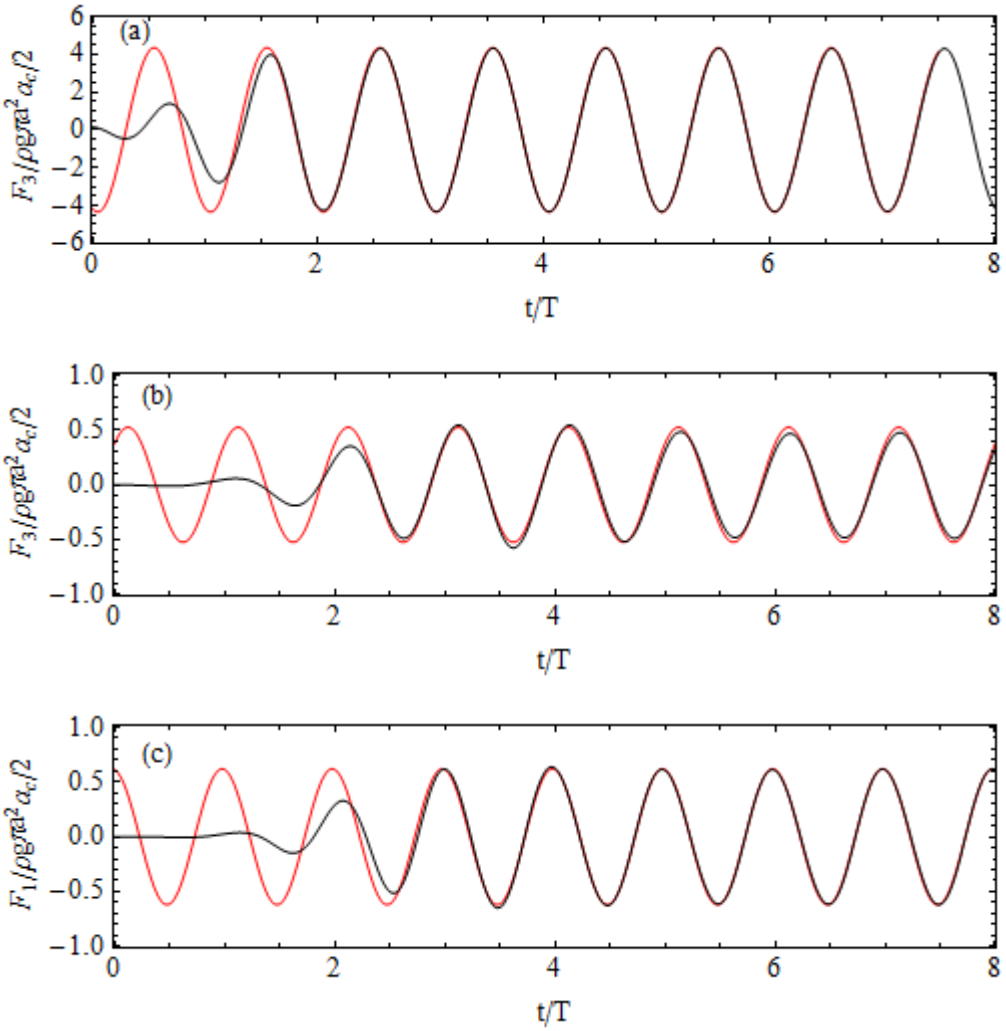

Figure 31: Radiation forces comparisons between OXPOT (black) and DIFFRACT (red) results for (a) the heave reaction force on the oscillating cylinder, (b) the heave interaction force on the fixed cylinder and (c) the surge interaction force on the fixed cylinder.

The other radiation simulations considered were for the heave and surge oscillations of displacement amplitude a_c of one truncated cylinder located a distance $5a$ from an identical cylinder that is fixed at the frequencies corresponding to $ka = 0.5$ and 1.0. The domain and mesh specifications are summarised in Table 12 and the comparison of the non-dimensional forces $\tilde{F} = F/(\rho g \pi a^2 a_c/2\ \ )$ as computed by OXPOT with the results of (Matsui & Tamaki, 1981) (denoted "Frequency") are shown in Table 13. In this table, the notation "Heave C_1" denotes the heave oscillations of cylinder 1 at the frequency corresponding to the wavenumber parameter specified immediately afterwards. There is an error interval associated with the analytical frequency domain results because the data was obtained from graphical representations of the forces. The agreement between the results is very similar to the previous heave radiation case.

ka	Domain Geometry		Intervals on side-walls			Body mesh		Total	
	(L, L_{SUB})	W	n_x	n_y	n_z	n_{CIRCUM}	n_z	Elements	Nodes
0.5	(5.0,2.5)	2.5	18	16	6	8	6	2706	6674
1.0	(10,5.0)	5.0	15	15	6	12	6	2226	5662

Table 12: Summary of mesh configuration for the two cylinder array radiation problem at two different frequencies.

Radiation Problem	Source of data	Cylinder 1		Cylinder 2	
		$\widetilde{F}_1$	$\widetilde{F}_3$	$\widetilde{F}_1$	$\widetilde{F}_3$
Heave C_1, $ka = 0.5$	OXPOT	$-$	2.98 ± 0.02	0.33 ± 0.02	0.53 ± 0.01
	Frequency	$-$	2.96 ± 0.05	0.34 ± 0.03	0.50 ± 0.03
Heave C_1, $ka = 1.0$	OXPOT	$-$	5.17 ± 0.02	0.80 ± 0.01	0.50 ± 0.01
	Frequency	$-$	5.15 ± 0.05	0.78 ± 0.03	0.47 ± 0.03
Surge C_1, $ka = 0.5$	OXPOT	1.45 ± 0.01	$-$	0.23 ± 0.02	0.34 ± 0.02
	Frequency	1.46 ± 0.03	$-$	0.21 ± 0.02	0.34 ± 0.02
Surge C_1, $ka = 1.0$	OXPOT	3.23 ± 0.03	$-$	1.24 ± 0.01	0.77 ± 0.01
	Frequency	3.26 ± 0.05	$-$	1.25 ± 0.05	0.78 ± 0.03
Diffraction, $ka = 0.8$	OXPOT	1.15 ± 0.03	1.41 ± 0.09	1.15 ± 0.05	0.95 ± 0.03
	DIFFRACT	1.18	1.33	1.16	1.0

Table 13: Heave and surge forces on the truncated cylinders due the forced oscillation of cylinder 1 and also for the diffraction of an incident wave the cylinder array.

6.3 Excitation problem for two truncated cylinders

The final two body verification simulation was for regular wave diffraction by two truncated cylinders. The incident wave amplitude is specified to be very small so that only the linear dynamics are considered for comparison with frequency domain results (existing DIFFRACT data). The cylinder configuration is identical to that for the radiation problems outlined above, i.e. two cylinders of radius a, draft $a/2$ spaced a distance $5a$ apart. The computational domain and boundary mesh specifications are as follows. The problem is specified in non-dimensional terms so $\rho = g = h = 1.0$ so the domain depth is 1.0, the domain length is $L = 9.0$, the domain width is $W = 1.25$ and the cylinder radius is $a = 0.2$. This domain is divided equally into 6 subdomains and the cylinders are

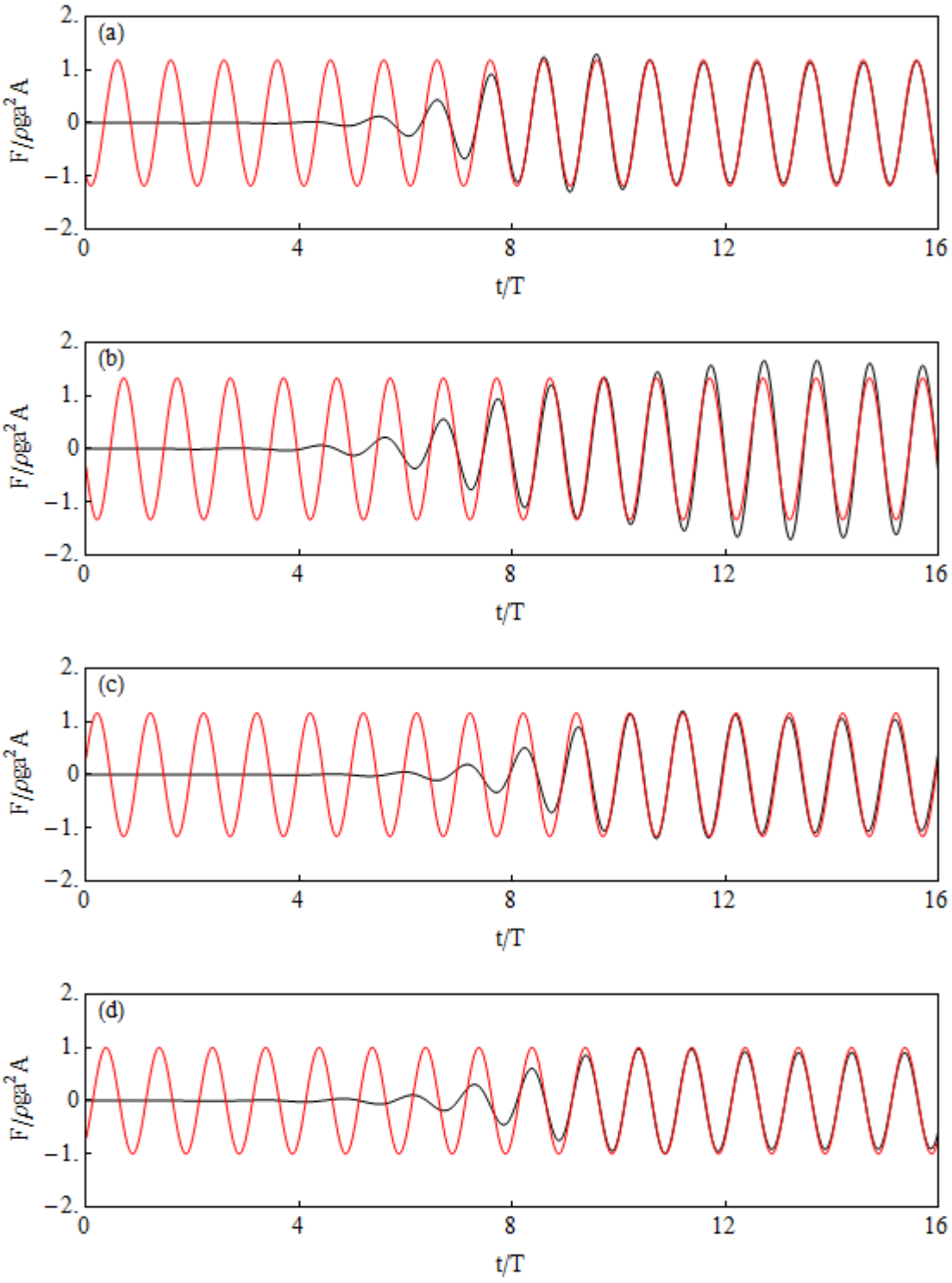

Figure 32: Excitation forces on cylinder 1 in surge (a) and heave (b) and on cylinder 2 in surge (c) and heave (d) as computed by OXPOT (black) and DIFFRACT (red).

located in the third and fourth subdomains at $x = -2.5a$ and $x = 2.5a$ and due to symmetry only the $y \geq 0$ half of the domain is modelled. The piston wavemaker is prescribed to move with a displacement amplitude of $a_p = 0.001$ and a frequency $\omega = 2.0$.

The side walls of each subdomain are divided into 10 intervals with 6 vertical quadrilateral elements in each interval giving a total of 60 elements. The interfaces, piston wavemaker and end wall are divided into 12 intervals and have 6 vertical elements also. The free-surface mesh in the subdomains not containing a cylinder consists of 272 triangular elements while in the subdomains containing the cylinders there are 404 elements so the mesh density is increased around the cylinders. The cylinders have 72 quadrilateral elements on the curved surface and 67 triangular elements on the truncated surface. In total there are 3302 elements and 8898 nodes distributed on the domain boundary. The simulation time is $15T$ and for a time step of $0.025T$ the computation takes 50 hours.

The surge and heave forces computed by OXPOT are non-dimensionalised and compared to the DIFFRACT results in Figure 32. The agreement is very good for the surge forces on both cylinders but for the heave force on cylinder 1 there is a significant divergence from the frequency domain results around $t/T = 12$. Given that there is generally a good agreement for the other force computations and that the domain width is less than a wavelength it is reasonable to attribute this difference to side-wall reflections. The force amplitudes quoted in Table 13 for the surge mode and heave mode on cylinder 2 measured from $t = 10T$ to $t = 14T$ where the oscillations are uniform in amplitude and reflection effects are minimal. For the heave force on cylinder 1 only the three periods between and $t = 9T$ and $t = 12T$ are used to compute the amplitude.

7 FOUR CYLINDER ARRAY SIMULATIONS

The final set of simulations feature an array of four truncated cylinders in regular waves. Data for the excitation forces and unconstrained body motions was computed previously in WG1 WP1 D8 and an attempt is made to validate the four-cylinder array OXPOT simulations in a similar manner to the single body case. Two sets of simulations were conducted, one set investigating the diffraction of regular waves by the array of cylinders and the other investigating the heave response of the cylinders to the incident wave. In the experimental tests that will take place as part of WG2 WP2, for which cross-comparisons will be made with OXPOT, the cylinder is free to move in heave only. Therefore, the heave motion of the cylinders is the most important mode to investigate and so, although full validations with the results of WG1 WP1 D8 would be useful, it was decided to restrict the cylinder motions to heave.

The array configuration is depicted in Figure 33 – there are four truncated cylinders of radius a, draft $2a$ spaced a distance $6a$ (three diameters) apart which diffract an incident wave which arrives at an angle of incidence β. As in the single cylinder case, the non-dimensional radius is $a = 0.125$ in water of depth unity. The incident waves are considered to be incident from $\beta = 0$ in the simulations that follow and in this case the symmetry about this incident wave direction can be exploited. Therefore, only one half of the domain is modelled in the simulations and the forces on and motions of cylinders 1 and 2 only are considered because the forces on and responses of cylinder 4 and 3 are symmetric to cylinder 1 and 2, respectively, about $y = 0$.

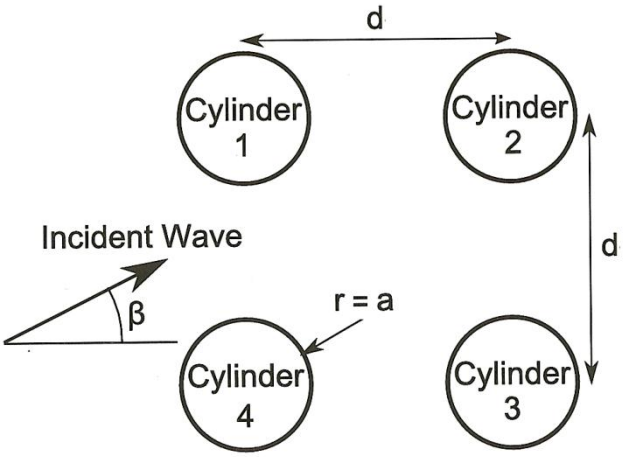

Figure 33: Four cylinder array configuration for cylinders of radius a spaced a distance $d = 6a$ apart.

However, compared to the two body simulations considered previously this is a significantly more complex problem requiring a larger domain because cylinders 1 and 2 must be a distance $3a$ from the wall of symmetry and so the total width of the numerical wave tank must increase to ensure the side wall is not too close to the cylinders. Furthermore, complex free-surface motions will occur between the cylinders and the wall of symmetry and the mesh in this region must be reasonably fine to accurately model these motions. It has been mentioned in the single cylinder investigations that it is preferable to have at least one wavelength between the cylinders and the side wall. Also, in relation to the wave propagation problems it was discussed how the number of elements per wavelength on the free-surface is generally held constant so that if the domain size must be increased due to a larger wavelength then the number of elements still remains the same. However, if the domain width must be at least $\lambda + 3a$ (so the distance from the centre of the cylinder to the side wall is one wavelength) then the larger the cylinder radius a is relative to the wavelength λ the more elements that must be introduced to the domain. For example, for a dimensionless wavelength $\lambda \simeq 2.0$ (corresponding to the wave $T = 10.25s$) and cylinder radius $a = 0.125$ the relative increase in the domain width due to the presence of the cylinders is just $3a/2 \simeq 20\%$ and so a 20% increase in the number of elements is necessary on the free-surface relative to the single body case. However, for the incident wave of period $T = 5$s the dimensionless wavelength is $\lambda \simeq 0.5$ and the relative increase in the domain width due to the presence of a cylinder at a distance $3a$ from the wall of symmetry $3a/0.5 \simeq 75\%$ and so a 75% increase in the number of elements on the free-surface compared to the single cylinder case is necessary. This results in a significant increase in the computational time and hence this particular incident wave was not considered and the focus is on one array configuration and a set of simulations with the incident waves of period $(T = 7s,\ T = 9s,\ T = 10.25s)$ from Table 1 were conducted.

Therefore, it was necessary to implement some reductions in mesh fineness to obtain reasonable computational run times. Compared to the single body simulations, there were less nodes distributed on the cylinders, e.g. on the half cylinder in the single body simulation for the waves of period 9 seconds the circumference is divided by 12 intervals whereas in the four body simulation (where a full cylinder circumference must be discretised) there only 20 intervals. Similarly, it was

necessary to reduce the density of triangular elements on the free-surface. The typical number of nodes distributed on the computational domain boundary is between 11000 and 12000 nodes which, for simulation times of $15T$ and a time-step size of $0.025T$, result in a computational runtime of 120 hours.

The free-surface meshes for the incident wave of period $T = 10.25s$ and period $T = 7s$ are shown in Figure 34 and Figure 35, respectively. The size of the computational domains and the mesh characteristics for the three waves considered here are compiled and presented in Table 14. It has been assumed that all the side walls and interfaces have 6 elements in the vertical direction as usual and the number of quadrilateral elements on the curved surface is presented as the multiplication of the intervals on the circumference and the number of vertical elements. The domain sizes are not as standardised as in the case of the single body because it was necessary to minimise the number of nodes used while ensuring the density of the unstructured free-surface mesh changed relatively slowly in space. (Mesh distortion whereby triangular elements involving one large interior angle tend to cause instabilities and this type of element can arise when the mesh fineness changes rapidly over a short distance. This tends to happen when a finely meshed body is located near a coarsely meshed wall). Note that the computational domain for the $T = 9s$ wave is quite narrow relative to the other cases and has the least number of elements and nodes – similar to the single cylinder simulations.

Wave (T, H)	**Comp. Domain**		**Subdomain intervals**		**Body elements**		**Total**	
	(L, L_{SUB})	W	n_x	n_y	N_{CURVE}	N_{TRUNC}	**Elements**	**Nodes**
$(7s, 2m)$	(4.5,0.75)	1.5	15	8	(24×6)	182	4384	12050
$(9s, 4m)$	(9.0,1.5)	1.5	12	10	(20×6)	178	4156	11046
$(10.25s, 6m)$	(9.9,2.5)	2.5	16	10	(14×6)	112	4476	12358

Table 14: Computational domain specifications and computational domain boundary discretisation properties for the three incident waves considered.

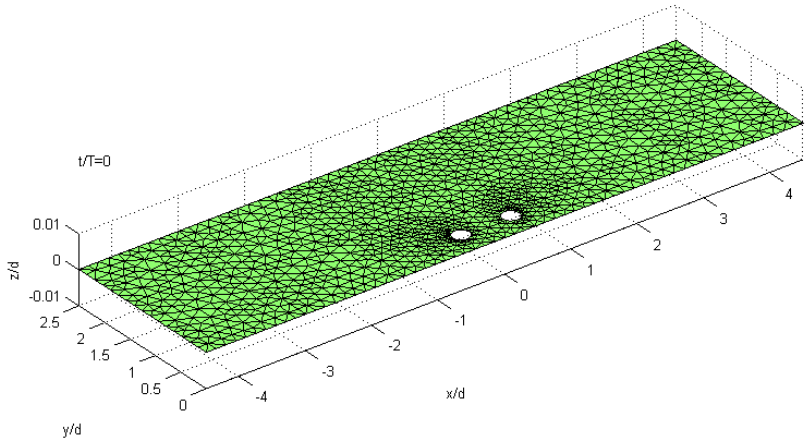

Figure 34: Free-surface mesh for the four body diffraction problem for the incident wave ($T = 10.25s, H = 6m$) which has a non-dimensional wavelength of $\lambda \simeq 2.0$.

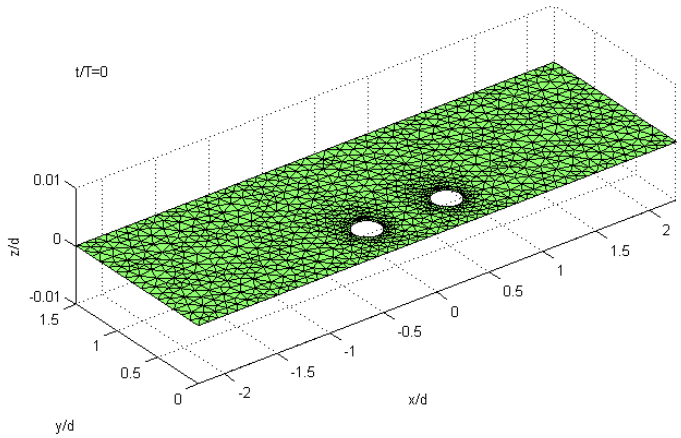

Figure 35: Free-surface mesh for the four body diffraction problem for the incident wave ($T = 7s, H = 2m$) which has a non-dimensional wavelength of $\lambda \simeq 0.95$.

7.1 Excitation Forces

The linearised excitation forces on cylinder 1 and 2 in the array depicted in Figure 33 are shown next for the three incident wave cases under consideration. For this array configuration, the surge, heave and pitch forces on cylinder 4 are identical to cylinder 1 and the sway and roll forces on cylinder 4 are in the opposite direction to those on cylinder 1 (this is equally true for the forces on cylinder 3 relative to those on cylinder 2). The OXPOT computations are compared to the frequency-domain results from WG1 WP1 D8 in Figure 36-38 in order to assess the accuracy of the OXPOT results relative to the single body results

It can generally be observed that the surge, heave and pitch results are closer to the frequency-domain results than the forces in sway and roll. The forces in the latter modes are generated only through the diffraction of the incident waves by the cylinders and the subsequent reflection of these waves by the wall of symmetry. Therefore, the accuracy of these forces depends strongly on the meshing around the cylinders and the walls. In the case of the ($T = 9s, H = 4m$) incident wave, the sway and roll excitation force results for cylinder 1 are very similar to the frequency domain results. However, the same computational results for cylinder 2 are quite 'noisy' and do not stay in phase with the frequency domain predictions. The noise in the sway and roll force computations could be due to a lack mesh density between the cylinders and the walls – the waves may not be resolved properly. The sway and roll forces are small relative to surge and pitch and hence are more susceptible to noise due to lack of mesh fineness. Furthermore, these forces are not directly due to the incident wave like the surge, heave and pitch forces, rather they are generated by the diffraction of the incident wave and subsequent reflection of this diffracted wave by the wall of symmetry. Such an interaction will certainly be more susceptible to numerical error. In addition to comparing the OXPOT force computations to the frequency-domain results graphically, the steady state amplitudes of the OXPOT simulations are also tabulated in Table 15 to Table 17 and compared to results of WG1 WP1 D8. In some cases, where the force oscillations do not reach a steady state, no OXPOT entry is given.

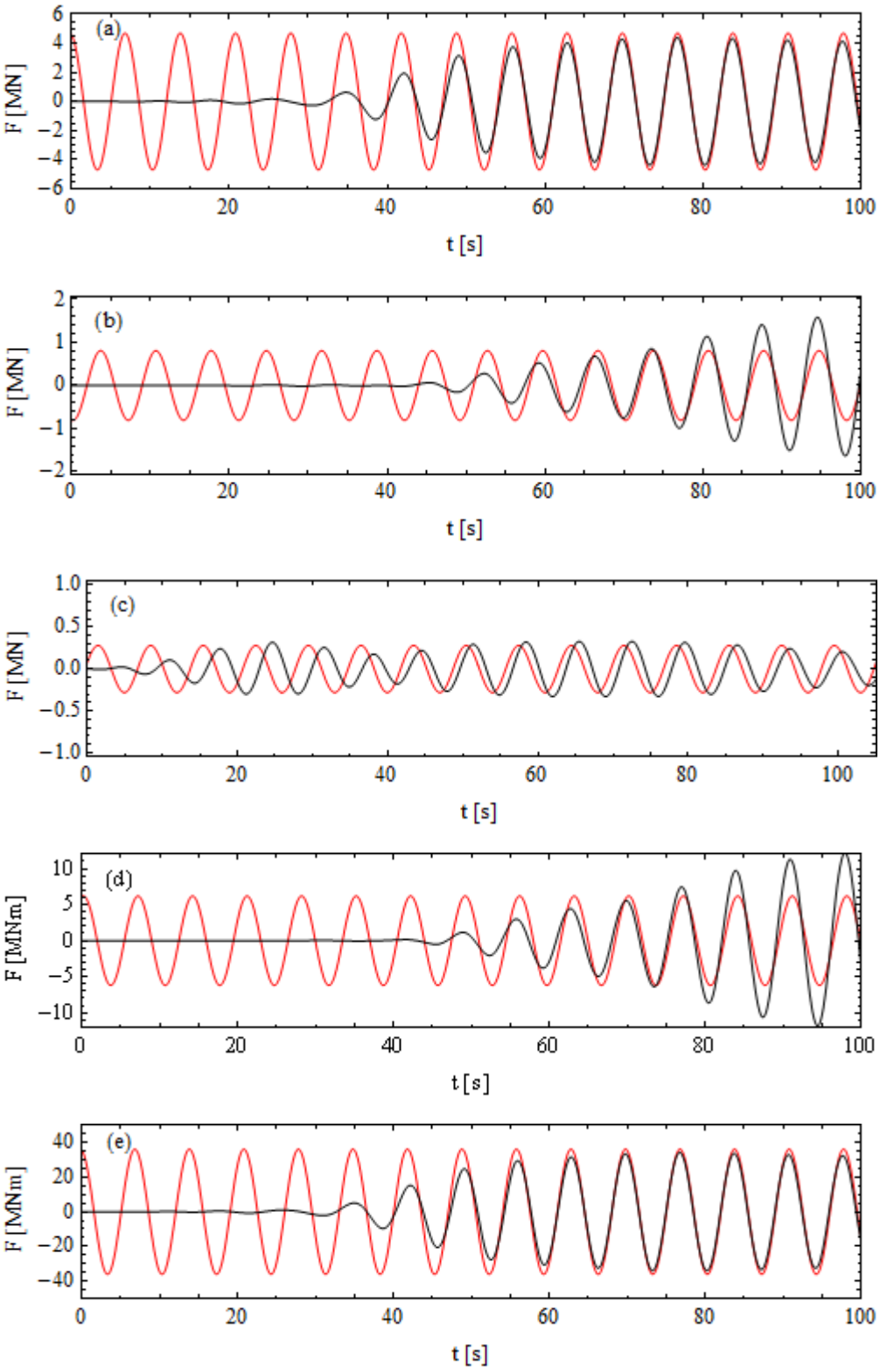

Figure 36: Comparison of linearised OXPOT results (black) for the excitation forces on cylinder 1 in (a) surge, (b) sway, (c) heave, (d) roll and (e) pitch to the corresponding linear WG1 WP1 D8 results for the incident wave ($T = 7s, H = 2m$).

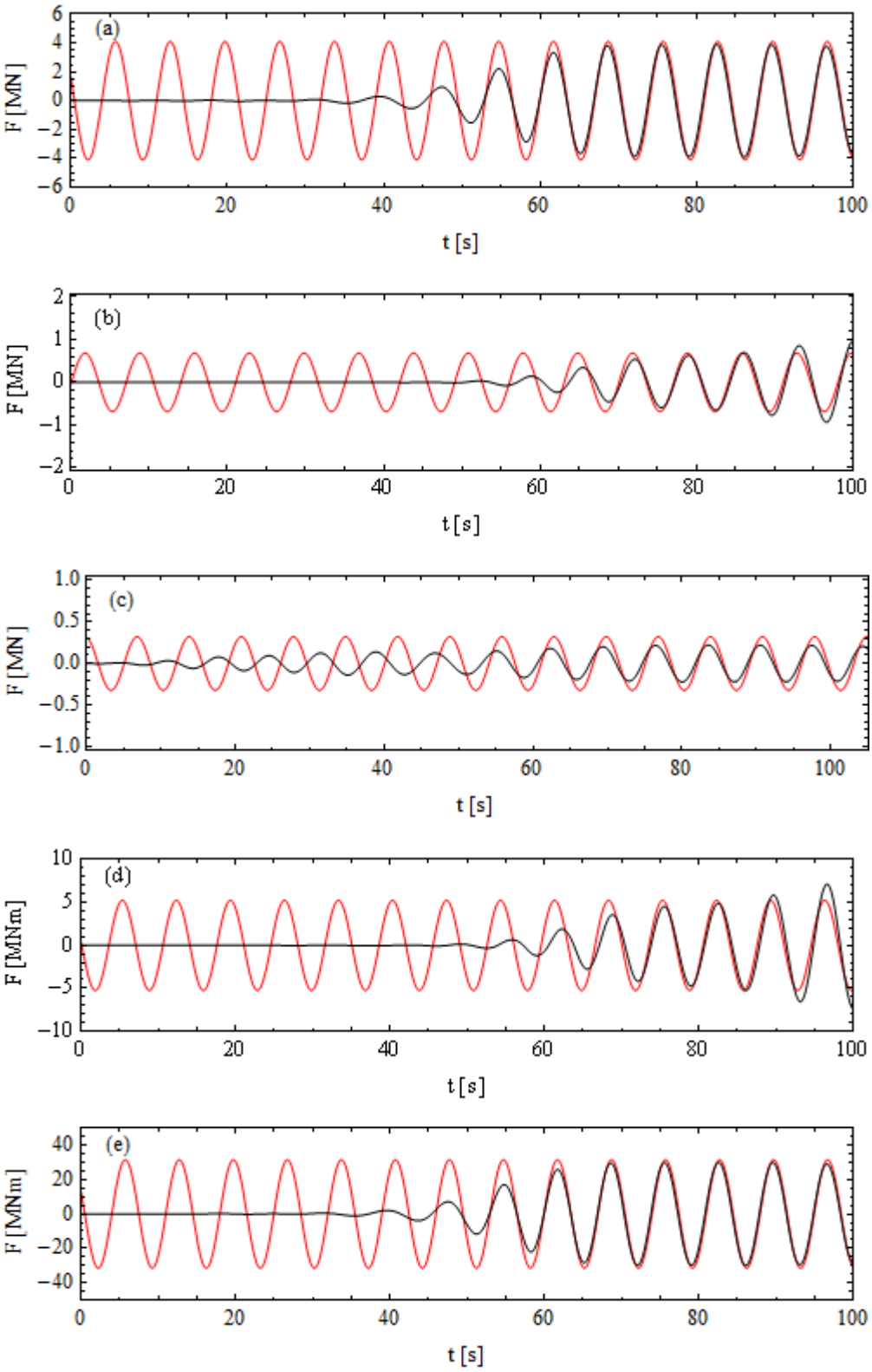

Figure 37: Comparison of linearised OXPOT results (black) for the excitation forces on cylinder 2 in (a) surge, (b) sway, (c) heave, (d) roll and (e) pitch to the corresponding linear WG1 WP1 D8 results for the incident wave ($T = 7s, H = 2m$).

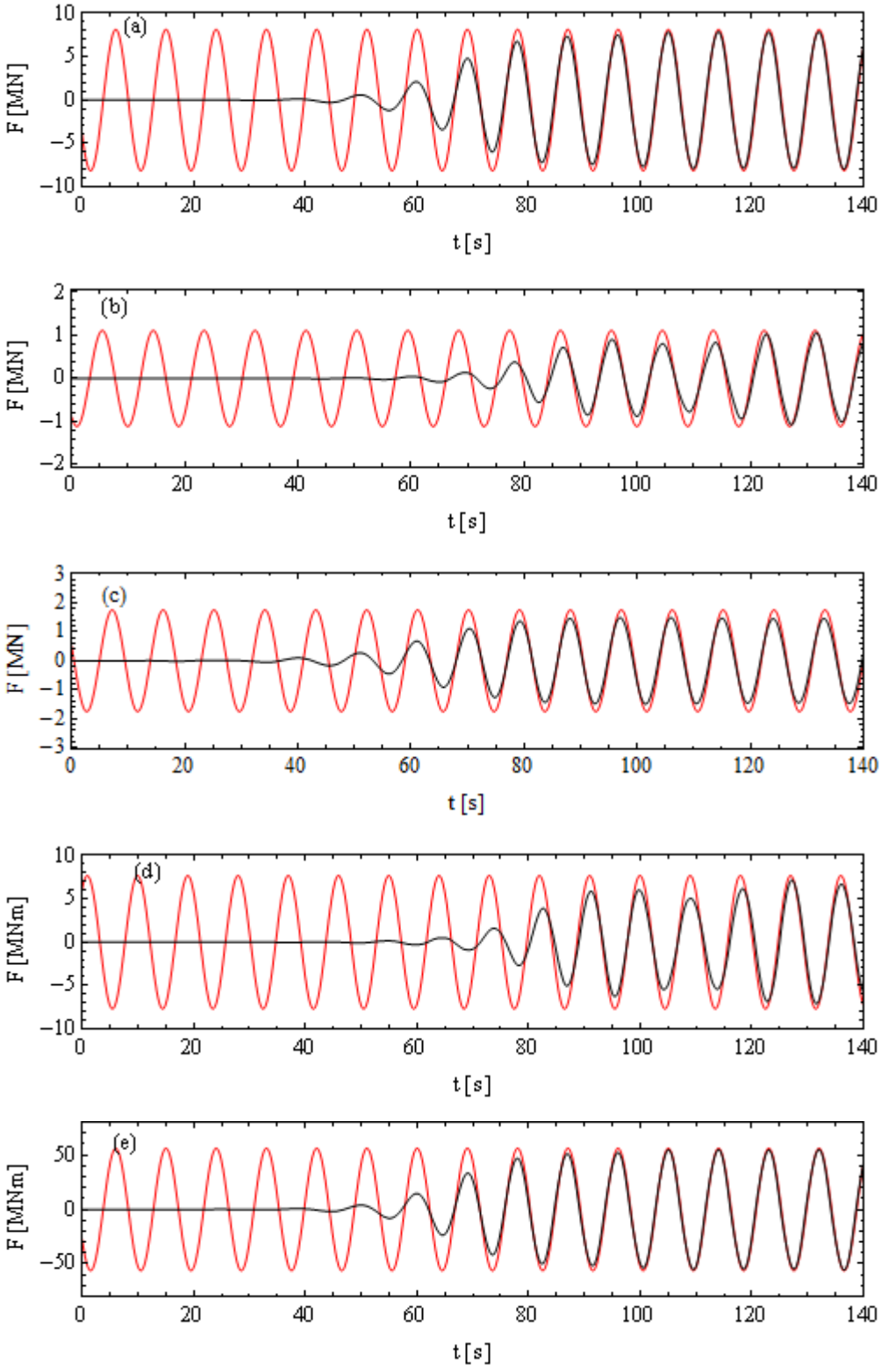

Figure 38: Comparison of linearised OXPOT results (black) for the excitation forces on cylinder 1 in (a) surge, (b) sway, (c) heave, (d) roll and (e) pitch to the corresponding linear WG1 WP1 D8 results for the incident wave ($T = 9s, H = 4m$).

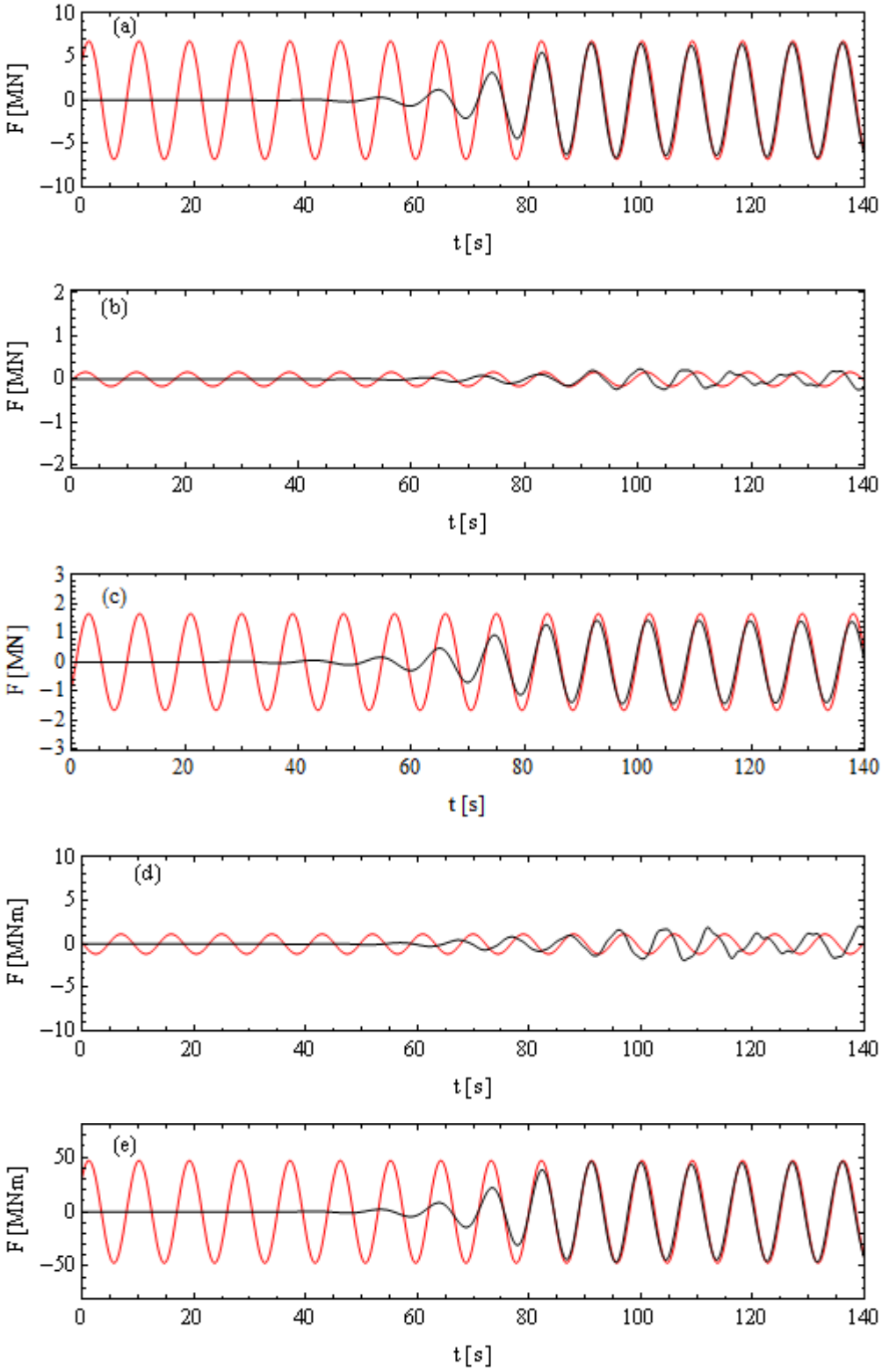

Figure 39: Comparison of linearised OXPOT results (black) for the excitation forces on cylinder 2 in (a) surge, (b) sway, (c) heave, (d) roll and (e) pitch to the corresponding linear WG1 WP1 D8 results for the incident wave ($T = 9s, H = 4m$).

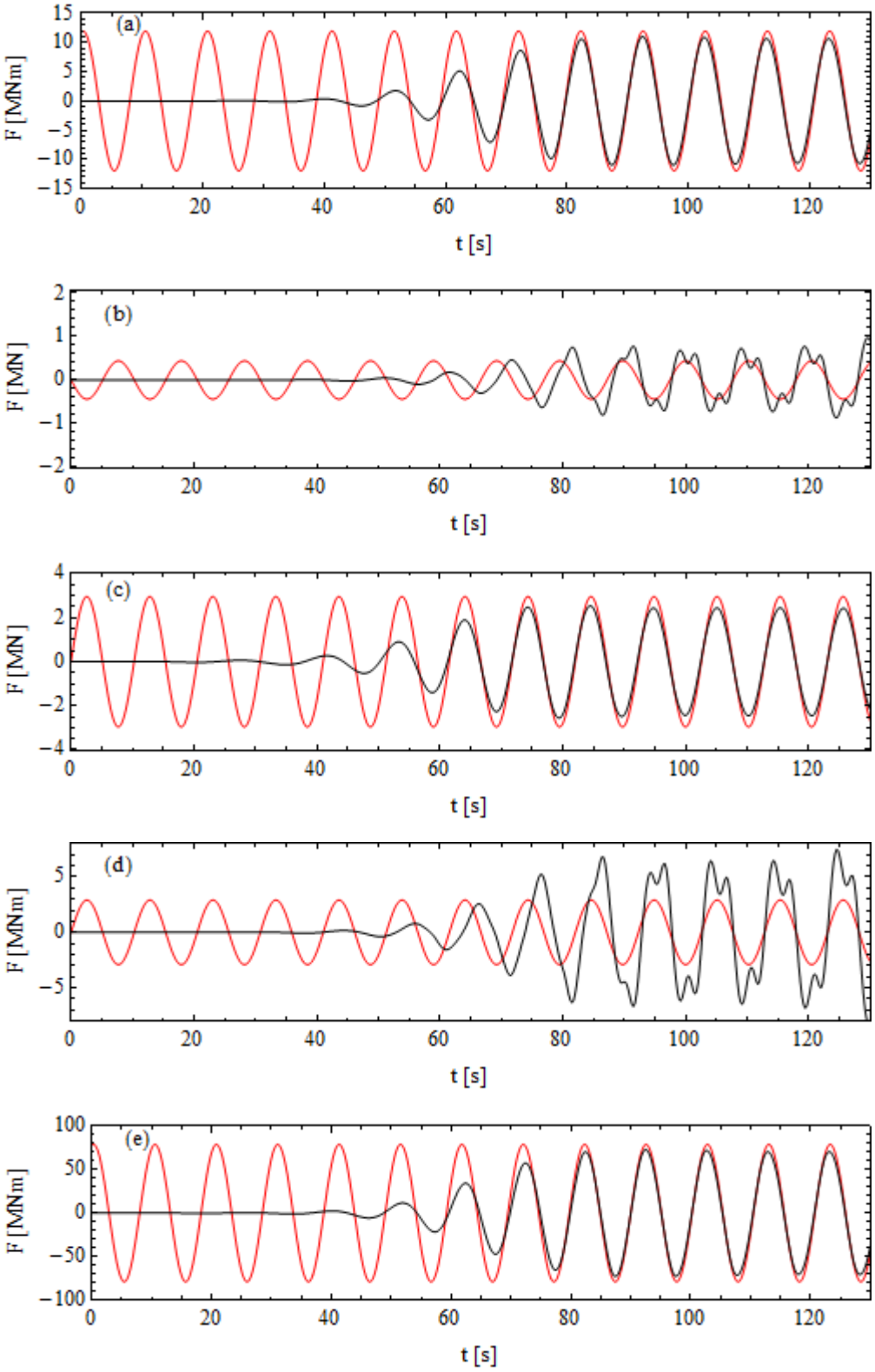

Figure 40: Comparison of linearised OXPOT results (black) for the excitation forces on cylinder 1 in (a) surge, (b) sway, (c) heave, (d) roll and (e) pitch to the corresponding linear WG1 WP1 D8 results for the incident wave ($T = 10.25s, H = 6m$).

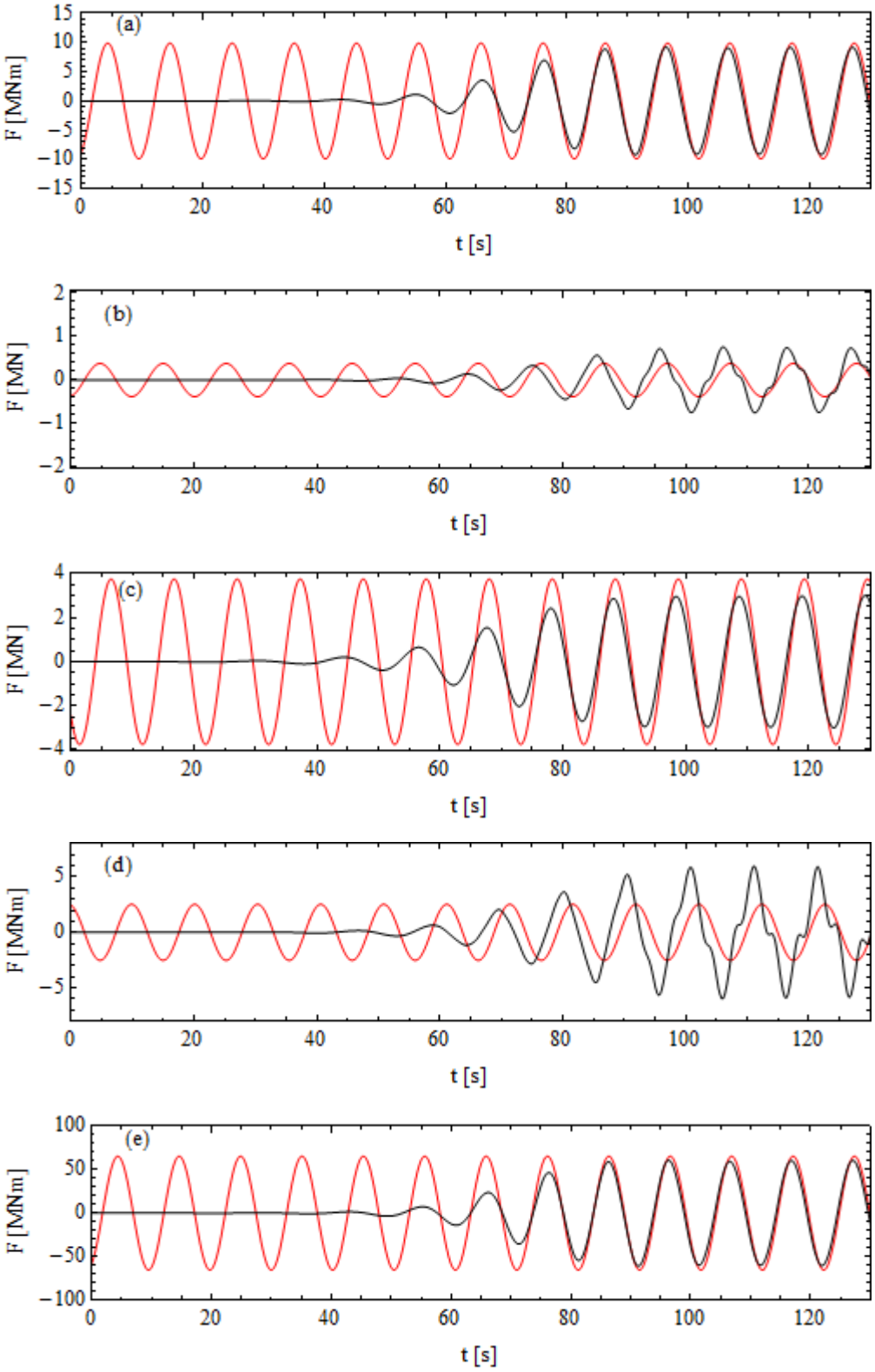

Figure 41: Comparison of linearised OXPOT results (black) for the excitation forces on cylinder 2 in (a) surge, (b) sway, (c) heave, (d) roll and (e) pitch to the corresponding linear WG1 WP1 D8 results for the incident wave ($T = 10.25s, H = 6m$).

In the $(T = 7s, H = 2m)$ simulation, the heave force on cylinder 1 as computed by OXPOT differs slightly in phase from the frequency-domain results. However, this is quite similar to the single body results and by resolving this issue in the single body case the difference here should also be explained. It may be a mesh related problem or it may be necessary to analyse the effect of moving the cylinder further from the wavemaker because the heave force on cylinder 2 as computed by OXPOT is in phase with the frequency domain result. Another noticeable divergence between the fully non-linear time-domain results and the frequency domain results is the increase in the sway and roll force amplitudes on cylinder 1 and 2 towards the end of the simulation. This effect is most noticeable on cylinder 1 but it is clear a similar increase in amplitude begins to occur for cylinder 2 also for $t > 90$s. It is difficult to isolate the exact cause of this increase because the diffracted wave disturbance cannot be isolated from the incident wave in a straightforward manner when plotting the free-surface wave elevation. The most likely explanation is that it is a side-wall reflection effect although it may be also related to the sloshing/trapping of waves within the array. The simulation of the diffraction of a focussed wave group might indicate whether any trapping occurs because in that case the persistence of any oscillations after the incident wave has passed will be clear.

Some unusual behaviour is observed in the sway and surge forces exerted on cylinder 1 and 2 in simulation of the diffraction by the array of the incident wave $(T = 10.25s, H = 6m)$. In both cases, there are higher order frequencies superposed on the linear component. For cylinder 1 this effect is more marked and it can be observed here that the linear component is in phase with the linear frequency-domain result. These higher order frequency contributions arise in the 'linearised' OXPOT result because, in fact, the method used to obtain the linear component by summing the forces measured on the body for incident waves π out of phase includes all odd powers of the amplitude A and not just the linear term. In the cases where A is small the linear term only contributes but in this case the wave amplitude in the vicinity of the cylinders is sufficiently large to add third order contributions to the force. In the case of the diffraction interaction the higher order term could be due to high frequency sloshing modes being trapped within the array.

Mode	**Force on cylinder 1**		**Force on cylinder 2**	
	OXPOT	**WG1 WP1 D8**	**OXPOT**	**WG WP1 D8**
Surge	4.22 ± 0.04	4.70	3.80 ± 0.10	4.10
Sway	$-$	0.81	$-$	0.68
Heave	0.31 ± 0.02	0.28	0.22 ± 0.02	0.32
Roll	$-$	6.2	$-$	5.3
Pitch	32.6 ± 0.3	36.1	29.1 ± 0.1	31.5

Table 15: Comparison of OXPOT results and WG1 WP1 D8 results for the excitation forces on the cylinders in the incident wave $(T = 7s, H = 2m)$. The units of force for the translational modes are mega-Newtons $[M\ N]$ and for the rotational modes are mega Newton-metres $[MNm]$.

Mode	Force on cylinder 1		Force on cylinder 2	
	OXPOT	WG1 WP1 D8	OXPOT	WG WP1 D8
Surge	7.83 ± 0.02	8.15	3.80 ± 0.10	6.80
Sway	0.9 ± 0.1	1.11	$-$	0.08
Heave	1.48 ± 0.01	1.76	0.22 ± 0.02	1.67
Roll	6.2 ± 0.7	7.7	$-$	1.14
Pitch	54.8 ± 0.6	56.2	44.3 ± 0.7	47.0

Table 16: Comparison of OXPOT results and WG1 WP1 D8 results for the excitation forces on the cylinders in the incident wave ($T = 9s, H = 4m$). The units of force for the translational modes and rotational modes are mega-Newtons $[M\ N]$ and mega Newton-metres $[MNm]$ respectively.

Mode	Force on cylinder 1		Force on cylinder 2	
	OXPOT	WG1 WP1 D8	OXPOT	WG WP1 D8
Surge	10.8 ± 0.2	11.9	9.16 ± 0.05	9.88
Sway	$-$	0.44	$-$	0.12
Heave	2.44 ± 0.03	2.96	3.00 ± 0.02	3.75
Roll	$-$	2.91	$-$	2.52
Pitch	72.0 ± 1.0	79.1	60.5 ± 0.5	65.5

Table 17: Comparison of OXPOT results and WG1 WP1 D8 results for the excitation forces on the cylinders in the incident wave ($T = 10.25s, H = 6m$). The units of force for the translational modes and rotational modes are mega-Newtons $[M\ N]$ and mega Newton-metres $[MNm]$ respectively.

7.1.1 Second order forces

The second order forces on the cylinders in the square array configuration depicted in Figure 33 are briefly analysed for the ($T = 7s, H = 2m$) case. The problems regarding second order force comparisons for a single body have been discussed already and it is clear that these problems are also present for the diffraction by an array of cylinders. The second -order excitation forces on cylinder 1 are shown in Figure 42 and are representative of the results for cylinder 2 also. The time interval over which the second order forces are analysed is shorter than in the first-order analysis because the second order forces are slower to build up to a relatively steady oscillation. It is evident from these plots that OXPOT underestimates the second-order force significantly compared to the frequency-domain results just as in the single body case. The OXPOT results for the incident wave ($T = 9s, H = 4m$) are slightly better and in some of the cylinder 1 modes the difference to the frequency-domain results is less than a factor of 2. The OXPOT results for the second order forces for the longest incident wave ($T = 10.25s, H = 6m$) are significantly smaller (an order of magnitude less) than the frequency domain results. Therefore, it is clear that there is not a lot of consistency in the second order force comparisons and further investigation is required in combination with the single cylinder second order force investigations.

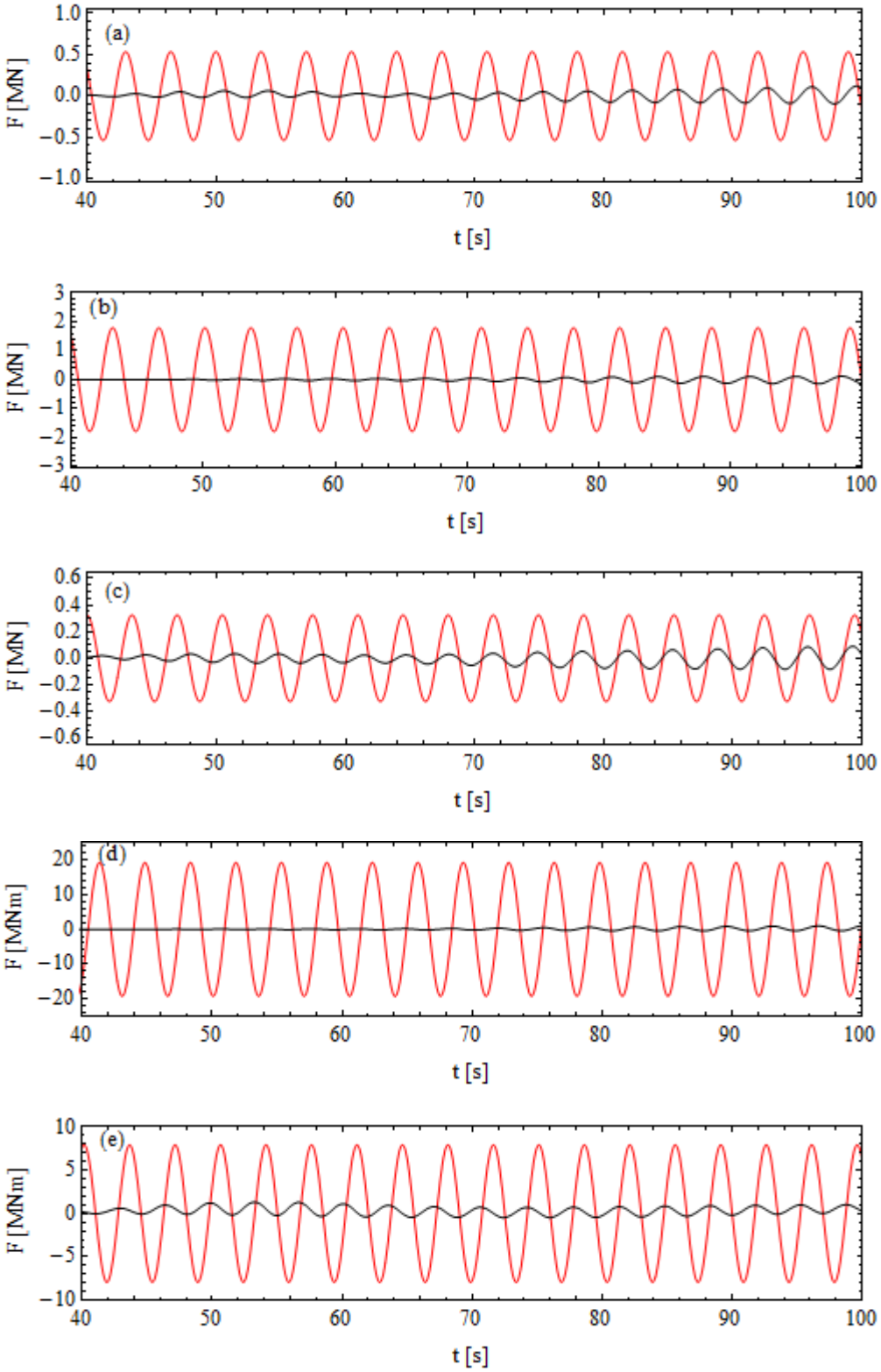

Figure 42: Comparison of second order OXPOT results (black) for the excitation forces on cylinder 1 in (a) surge, (b) sway, (c) heave, (d) roll and (e) pitch to the corresponding linear WG1 WP1 D8 results for the incident wave ($T = 7s, H = 2m$).

7.1.2 Heave motions

The responses of the cylinders in heave to the incident waves of periods $T = 7s$, $T = 9s$ and $T = 10.25s$ were also computed using OXPOT. These motions consist of the forced incident wave component and the resonant component just as in the single body case. Reflected and diffracted waves from the other cylinders will affect the motion of cylinder 1 but the properties of the motion are very similar to that of the single body case. The nonlinear component of the results was observed to be very small in all cases and any differences between the nonlinear OXPOT results and the linear WG1 WP1 D8 results are due to linear transient effects in the time-domain (OXPOT) model or side-wall reflections. The motion of cylinder 2 depends on how much transmission (past cylinder 1) of the incident wave occurs and in particular is dependent on the cylinder size relative to the incident wavelength and the inter-cylinder spacing. The fully nonlinear heave motions for cylinder 1 and cylinder 2 are shown in Figure 43 and Figure 44, respectively, for the three incident waves considered in this section.

For the incident wave of period 7 seconds, the motion of cylinder 2 is tending to settle to a steady-state oscillation amplitude that is significantly smaller than that of cylinder 1. The transient resonant motion is still excited and yields relatively large oscillation amplitudes at $t = 50s$ and $t = 80s$; however, the underlying oscillation at the incident wave frequency is much smaller than in the case of cylinder 1. This is due to a combination of 'sheltering' by cylinder 1, i.e. cylinder 1 diffracts the incident wave to such an extent that a significant proportion of the incident wave energy doesn't reach cylinder 2, and the influence of the array spacing. Such sheltering effects are more likely to occur for the shorter wavelength waves where the cylinder radius is relatively large – in this case $ka \simeq 0.8$. The spacing of the cylinders also influences the proportion of energy reaching the cylinder.

In the case of the incident wave of period 9 seconds the amplitudes of both cylinder motions is of the same magnitude and the response of cylinder 2 has identical characteristics to the response of cylinder 1. The incident wavelength in this case is 150% larger than the previous case ($ka \simeq 0.5$). Therefore, diffraction effects are still important and it may be that the inter-cylinder spacing is more favourable for the transmission of the incident wave to cylinder 2. For the final incident wave case considered ($T = 10.25s, H = 6m$), the motions of the cylinders are tending to increase even at the end of the OXPOT simulation because the incident wave frequency is approximately equal to the cylinder's natural resonant frequency. However, comparing the frequency domain forces it can be seen that the steady-state motion of cylinder 2 is approximately a third smaller than that of cylinder 2. This can be attributed to the fact that resonant excitation of the cylinder motion occurs and cylinder 1 will take some of the energy from the incident wave front and radiate it through its motion; however, these radiated waves effectively dissipate the energy throughout the wave tank and so less of the incident wave energy arrives at cylinder 2.

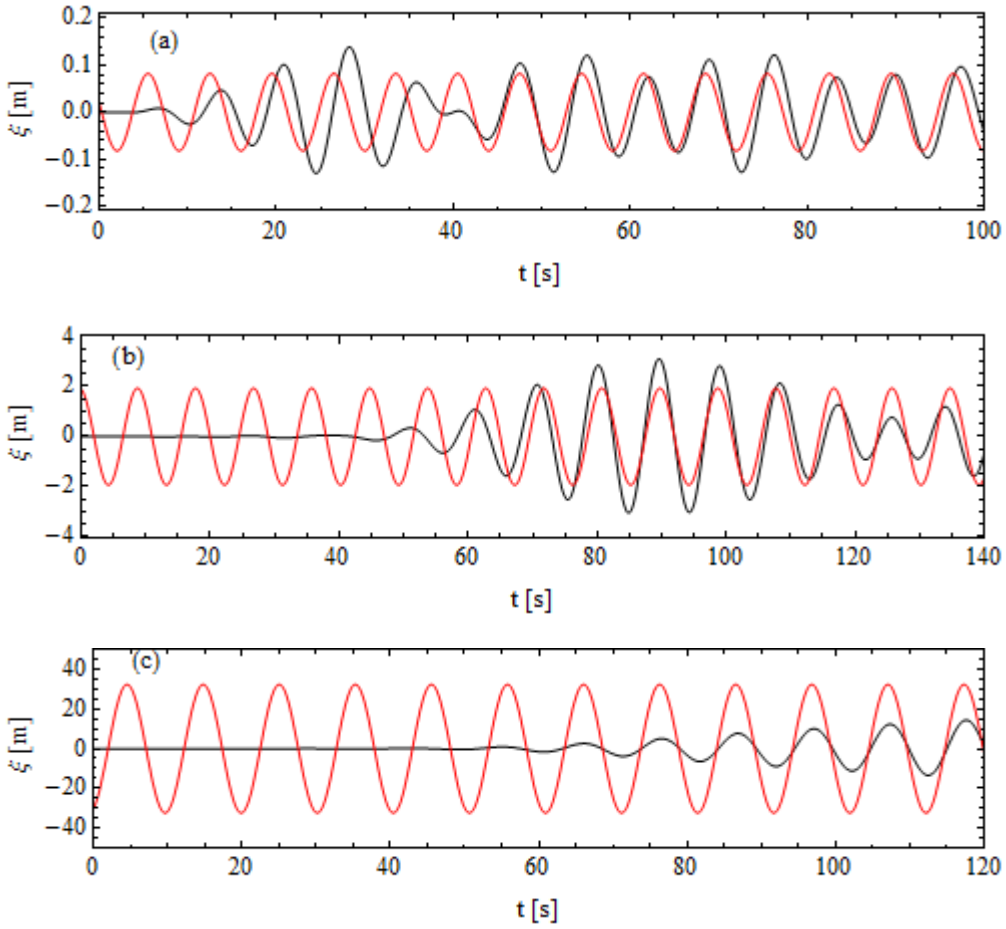

Figure 43: Fully nonlinear heave motion of cylinder 1 as computed by OXPOT (black) compared to the linear results from WG1 WP1 D8 (red) for the incident wave (a) $(T = 7s, H = 2m)$, (b) $(T = 9s, H = 4m)$ and (c) $(T = 10.25, H = 6m)$.

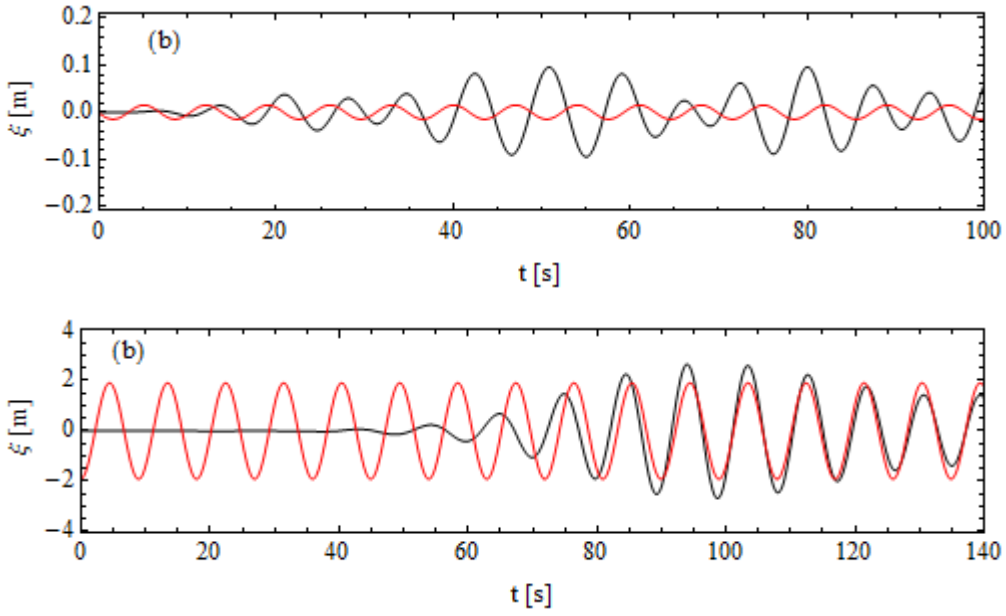

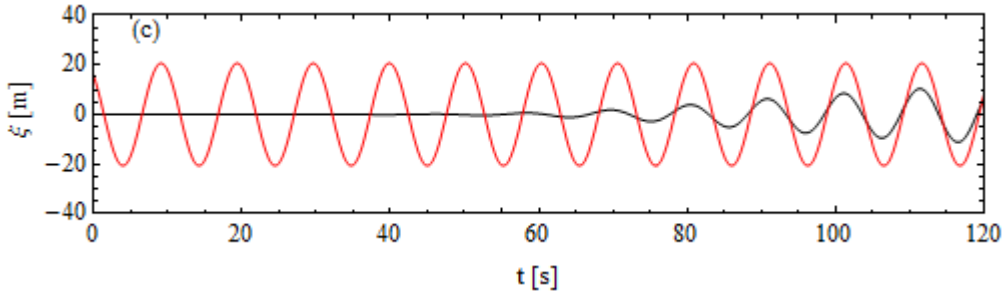

Figure 44: Fully nonlinear heave motion of cylinder 2 as computed by OXPOT (black) compared to the linear results from WG1 WP1 D8 (red) for the incident wave (a) $(T = 7s, H = 2m)$, (b) $(T = 9s, H = 4m)$ and (c) $(T = 10.25, H = 6m)$.

7.2 Summary of four body investigation

This four body investigation, while relatively preliminary, has shown that OXPOT is capable of simulating the interaction of waves with a small array of cylinders. However, at the moment the computational times are prohibitively large and have significantly reduced the breadth of the fully nonlinear investigation into the interaction of the incident waves with the array. Attempts to parallelise sections of the code have already been made and work on implementing this parellelisation will continue in the near future in order to reduce the computational times. Substantial reductions in computational time are envisaged because the simulations involve domain decomposition (whereby solutions are obtained in each subdomain separately and matched on the interfaces) which is suitable for parallel code architecture. If this parallelisation can be implemented then it will be more straightforward to consider the oblique incident wave case corresponding to $\beta = 45°$ in Figure 33 and the five-diameter spacing which require larger computational domains than the $\beta = 0°$ case for the three-diameter spacing. Currently, simulations with these array configurations will take at least one week of computational time for approximately 15 periods of simulation. Therefore, once parallelisation has been achieved it will be possible to investigate the effect of increasing the cylinder spacing on the excitation forces and motions of the body and how the variation in the incident wave direction affects the dynamics of the cylinders.

Simulations involving the rounded cylinder geometries must also be conducted in order to provide an understanding of what will be observed in the QUB experimental work as part of WG2 WP2. The investigations into the truncated cylinder array will be relevant to the experimental work in particular for the diffraction of the incident wave. The heave motions and heave forces may change considerably due to the rounding of the cylinder end and the change in mass of the cylinder so it will be necessary to compare the results. The agreement observed in the linear comparisons combined with the success of OXPOT in simulating small-scale experiments indicates that realistic nonlinear simulations of small arrays with OXPOT are definitely possible although not without challenges.

Regarding the nonlinear effects, further investigation into the $(T = 10.25, H = 6m)$ excitation interaction are necessary to isolate the higher order frequency terms. As stated previously, a simulation involving a focussed wave group could be effective in understanding whether the motion of the free-surface between the cylinders is significantly contributing to the sway and roll forces. More nonlinear waves might also be simulated given that the key incident wave cases identified for

the single body investigation are not strongly nonlinear. In particular, it would be interesting to consider the effect on nonlinearities on near-trapping interactions.

8 CONCLUSIONS AND FUTURE WORK

This report presents the results of the fully nonlinear simulations of the interaction of a single truncated cylinder with regular incident waves. The linear and second-order excitation forces and linear responses are compared to the frequency-domain (WAMIT) results computed with WAMIT in WG1 WP1 D8. Furthermore, the fully nonlinear simulations of the interaction of regular incident waves with four cylinders are also described and the results for the excitation forces on the cylinders and the fully uncontrolled heave responses of the cylinders are presented.

In the OXPOT simulations, the total hydrodynamic force exerted on the bodies and the fully nonlinear response (if the cylinder is free to move) are computed along with the full motion of the free-surface. To obtain the linear and second order components it is necessary to employ the method described by (Zang, et al., 2006) and (Zang, et al., 2010) among others whereby the fully nonlinear forces and responses (and other hydrodynamic quantities) for two interactions involving incident waves that are π out of phase are combined in order to obtain the odd and even Stokes' expansion terms. For weakly nonlinear interactions, higher order amplitude terms are negligible and the linear and second-order terms dominate. Application of this method allows the comparisons of the linearised and second-order components of the nonlinear forces and responses to the linear and second-order frequency domain results in WG1 WP1 D8. To obtain the excitation forces and responses it is necessary to run two different sets of simulations because the excitation force cannot be separated from contributions due to the motions of the cylinders in the fully nonlinear interactions.

The comparisons between the linearised excitation forces obtained from OXPOT and the linear frequency-domain results from D8 yield a very good agreement for the single truncated cylinder case. The surge and pitch forces are particularly close to the WAMIT results and the heave force OXPOT results also compare well although the effects of side wall reflections and issues with convergence at the bottom surface compromise the results slightly in some cases. At second-order the comparisons do not fare as well and there is significant disagreement between the OXPOT and WG1 WP1 D8 results. However, it has been shown that OXPOT is capable of accurately modelling the second-order hydrodynamics in other diffraction case studies and so the cause of the uncertainty in the second-order forces is most likely due to difficulties with the truncated cylinder geometry. The uncontrolled response of the cylinder in regular waves is also seen to agree quite well in the linear comparisons. The excitation of the resonant mode oscillations of the body makes comparisons in heave more difficult as this response is transient and is not described by the steady state (frequency-domain results). The resonant mode for the particular geometry considered is very lightly damped and does not decay significantly during the simulations.

The results for the fully nonlinear simulations of the interactions of the array of four cylinders with regular waves are also presented and comparisons of the linear component of excitation forces on the cylinders and the uncontrolled responses of the cylinders with the linear data presented in WG1 WP1 D8 are also provided. The agreement between the excitation force results is good and some interesting third-order contributions are also observed in some of the OXPOT results. The

comparisons of the uncontrolled heave responses as computed by OXPOT to the frequency-domain results are very similar to the single cylinder case so that the transient resonant responses contribute significantly to the total motion.

To complement the analyses involving the truncated cylinder geometry specified in WG1 WP1 D8 some further fully nonlinear hydrodynamic investigations were conducted for the bodies of different geometries and the results of these investigations are presented here. For the single body case, a standard cylinder geometry analysed in previous linear frequency domain literature was considered and the results of diffraction, radiation and heave response simulations are compared to the linear analytical results. The investigation of the diffraction simulations illustrates the significant effect that side-wall reflections can have on the force computations. A simulation of the diffraction of a compact focussed wave group by a bottom mounted cylinder was also conducted and the comparisons with the data from the experiment which the simulation models are presented here. The agreement at first and second order is shown to be excellent and provides compelling evidence of the capability of OXPOT in modelling nonlinear hydrodynamics.

The simulations presented in this report highlight the computationally intensive nature of the OXPOT tool in modelling nonlinear hydrodynamic interactions. However, the simulation of the experimental investigation of diffraction also highlights the significant capabilities of OXPOT in modelling the physics of nonlinear interactions. The four body simulations are also seen to be quite successful. Therefore, it can be concluded that OXPOT is certainly capable of modelling realistic wave interactions involving small arrays of cylinders despite the computational challenges inherent in the fully nonlinear approach.

The next steps involved in the modelling of the performance of point absorber wave energy converters (WECs) require the introduction of control and power take-off (PTO) to the fully nonlinear simulations. In WG1 WP1 D10 simulations of the responses of controlled axisymmetric devices in regular waves will be performed and in addition an assessment of linear and nonlinear PTOs will also be made. The effect of different control strategies on device performance will also be investigated. Both single body and square four-body array configurations in regular waves will be considered. In the deliverables to follow, the responses and performance of axisymmetric devices in irregular seas will be reported on. In relation to the issues raised in this report, investigations into the uncertainties in the second order forces will also continue. Finally, in preparation for the comparisons with the experiments in WG2 conducted by QUB that will form WG1 WP1 D13 the interactions involving a single rounded vertical cylinder and four-unit arrays of such cylinders will be simulated in a similar manner to the simulations reported here.

REFERENCES

Abul-Azm, A. G. & Williams, A. N., 1988. Second-order diffraction loads on truncated cylinders. *Journal of Waterway, Port, Coastal and Ocean Engineering,* 114(4), pp. 436-455.

Bai, W. & Eatock Taylor, R., 2006. Higher-order boundary element simulation of fully nonlinear wave radiation by oscillatiing vertical cylinders. *Applied Ocean Research,* Volume 28, pp. 247-265.

Bai, W. & Eatock Taylor, R., 2007. Numerical simulation of fully nonlinear regular and focused wave diffraction around a vertical cylinder using domain decomposition. *Applied Ocean Research,* Volume 29, pp. 55-71.

Bai, W. & Eatock Taylor, R., 2009. Fully nonlinear simulation of wave interaction with fixed and floating flared structures. *Ocean Engineering,* Volume 36, pp. 223-236.

Eatock Taylor, R. & Hung, S. M., 1987. Second order diffraction forces on a vertical cylinder in regular waves. *Applied Ocean Research,* 9(1), pp. 19-30.

Evans, D. V. & Porter, R., 1997. Near-trapping of water-waves by circular arrays of vertical cylinders. *Applied Ocean Research,* Volume 19, pp. 83-89.

Jonathan, P. & Taylor, P. H., 1997. On irregular, nonlinear waves in a spread sea. *Journal of Offshore Mechanics and Arctic Engineering,* Volume 119, pp. 37-41.

Maskell, S. J. & Ursell, F., 1970. The transient motion of a floating body. *Journal of Fluid Mechancis,* pp. 303-313.

Matsui, T. & Tamaki, T., 1981. *Hydrodynamic interaction between groups of vertical axisymmetric bodies floating in waves.* Trondheim, International Symposium on Hydrodynamics in Ocean Engineering, pp. 817-836.

McIver, P., 2005. Complex resonances in the water-wave problem for a floating structure. *Journal of Fluid Mechanics,* Volume 536, pp. 424-443.

Ohkusu, M., 1972. Wave Action on Groups of Vertical Cylinder Circular Cylinders. *Journal of the Society of Naval Architects of Japan,* Volume 131, pp. 53-64.

Ursell, F., 1964. The decay of the free motion of a floating body. *Journal of Fluid Mechanics,* pp. 305-319.

Wu, G. X. & Eatock Taylor, R., 1996. *Transient motion of a floating bodyin steep water waves.* Hamburg, Proceedings of Eleventh International Workshop on Water Waves and Floating Bodies.

Yeung, R. W., 1981. Added mass and damping of a vertical cylinder in finite depth waters. *Applied Ocean Research,* 3(3), pp. 119-133.

Zang, J. et al., 2006. Second order wave diffraction around a fixed ship-shaped body in unidirectional steep waves. *Journal of Offshore Mechanics and Arctic Engineering,* Volume 128, pp. 89-100.

Zang, J. & Taylor, P. H., 2010. *Steep wave and breaking wave impact on offshore wind turbine foundations - ringing revisited.* Harbin, Proceedings of the 25th International Workshop on Water Waves and Floating Bodies.

Zang, J. et al., 2010. *Experimental study of non-linear wave impact on offshore wind turbine foundations.* s.l., Proceedings on the Third International Conference on the Application of Physical Modelling to Port and Coastal Protection.